



Virginia Commonwealth University
VCU Scholars Compass

Theses and Dissertations

Graduate School

2023

Mechanistic insight into traumatic brain injury induced neuronal membrane disruption: Cathepsin B relocalization and a NeuN negative cortical neuron subpopulation

Martina L. Hernandez
Virginia Commonwealth University

Follow this and additional works at: <https://scholarscompass.vcu.edu/etd>



Part of the [Molecular and Cellular Neuroscience Commons](#)

© Martina L. Hernandez

Downloaded from

<https://scholarscompass.vcu.edu/etd/7488>

This Dissertation is brought to you for free and open access by the Graduate School at VCU Scholars Compass. It has been accepted for inclusion in Theses and Dissertations by an authorized administrator of VCU Scholars Compass. For more information, please contact libcompass@vcu.edu.

Mechanistic insight into traumatic brain injury induced neuronal membrane disruption: Cathepsin B relocalization and a NeuN negative cortical neuron subpopulation

A dissertation submitted in partial fulfillment of the requirements for the degree of Doctor of
Philosophy in Neuroscience at Virginia Commonwealth University

By

Martina L. Hernandez
B.S. Virginia Commonwealth University, 2017

Advisor: Audrey D. Lafrenaye, Ph.D.
Assistant Professor
Department of Anatomy and Neurobiology

Virginia Commonwealth University
Richmond, Virginia
August 2023

Acknowledgements

I would like to extend my deepest gratitude to my mentor and science role model, Dr. Audrey Lafrenaye. She helped me take my first steps in science, always encouraging me, especially when I doubted myself. Audrey always accommodated my needs as a trainee and person to help me reach this stepping stone in my career. Because of her and mentors like her, I would like to earnestly continue in academic science, training our next generation of scientists and health professionals. Thank you for letting me be your first graduate student, it was a true delight to work with and learn from you.

I am also grateful to my committee members for their genuine support and impact on my scientific development. Particularly, Dr. Jeff Dupree, who was not only my committee member for my graduate training but gave me my first opportunity to gain research experience as an undergraduate student. As for Dr. Carmen Sato-Bigbee, thank you for all the best scientific inquiries that furthered my scope of understanding in my project as well as science and for all your guidance in writing my fellowship award. Thank you to Dr. Dong Sun for her additional expertise in neurotrauma and neural progenitor cells. Also, a thanks to Dr. Phil Gerk for his insight on pharmacological interventions and verification that the main component of my project would be feasible. I also appreciate Dr. Gretchen Neigh and Dr. Kelly Harell, for taking the time to participate in my training. Thank you, Dr. John Bigbee for running the Neuroscience Graduate Program. I have met some amazing scientists in this program.

Next, I would be remiss if I did not include the people I worked with directly in Lafrenaya (Lafrenaye Lab). Karen Gorse, thank you for helping me through some troubleshooting and lending an ear when I needed to complain. You are my lab mom. Amanda Logan-Wesley, I have only known you for some months, however, you were vital to helping me complete this work in addition to Karen. Thank you to all the mentees who helped me with my project, it was an honor to work with and train you.

People I have worked with at VCU: Lynn Davis, Susan Walker, Amanda Furman, Gladys Shaw, Ph.D. ,The microscopy core at VCU: Fran White and especially former EM specialist Judy Williamson and her successor Terry Smith.

I also extremely appreciate Dr. Sarah Golding and Dr. Joyce Lloyd and the rest of those who direct IMSD, the program that allowed me to delve into a research career fully. Thank you to SREB and their partnership with VCU Graduate School for the support and professional development. Much obliged to the DSPAN program that supported my F99/K00 award and the directors, Dr. Lauren Ullrich and Dr. Michelle Jones-London.

Endless gratitude to my siblings, Altaire and Rosalia, who have lived with me through grad school and still tolerate me. I also would like to thank my best friend since the 6th grade, Becky Marshall and other family. Thank you all for putting up with my nerdiness and crankiness all of these years. Shoutout to the “lab” members of the Crossmodal Podcast, reminding me that there are cool wonders outside of the microcosm of my graduate school work.

Lastly, there aren't words that convey my gratitude for Dr. Nicole “Nico” Ekanem, who asked the best questions in journal club, started the Crossmodal Podcast, and was my lab neighbor on the 11th floor of Sanger Hall. I am proud to call you my partner and best friend.

© Martina L. Hernandez 2023
All Rights Reserved

Table of Contents

Mechanistic insight into traumatic brain injury induced neuronal membrane disruption: Cathepsin B relocation and a NeuN negative cortical neuron subpopulation

Introduction.....	3
What is a TBI?	3
Intracranial Hypertension.....	5
Membranes	6
Why study membrane disruption?.....	6
In vitro Membrane disruption in TBI	7
In vivo Membrane disruption TBI	8
NeuN	11
Chapter 1: Neuronal Membrane Disruption Occurs Late Following Diffuse Brain Trauma in Rats and Involves a Subpopulation of NeuN Negative Cortical Neurons.....	13
Abstract.....	13
Methods.....	16
Surgical preparation and injury induction.....	17
Tracer infusion.....	18
Tissue processing.....	19
Western blotting	19
Membrane Disruption Analysis	20
Glial Analysis.....	21
TUNEL Analysis	22
Preparation of tissue for light microscopy for neuronal quantification.....	23
Ultrastructural assessment of membrane disrupted neurons	23
Statistical analysis	24
Results.....	25
Chronic membrane disruption is associated with a transient shift toward a NeuN negative phenotype.....	26
NeuN negative membrane disrupted cells are not glia.....	26
Cortical NeuN protein expression does not change following TBI.....	26
Late membrane disruption is not associated with cell death/loss post-CFPI	27
The lateral neocortex contains a subpopulation of NeuN negative neurons regardless of injury	28
Discussion	28
Methods.....	43
Animals.....	43
Surgical preparation and injury induction.....	43
Tracer infusion.....	45
Tissue processing.....	45
Western blotting	46
Immunohistological Analyses	47
Statistical analysis	48
Results.....	49
There are no changes in protein quantity for Doublecortin and cFos following TBI.....	49
NeuN cells are half immunopositive for Doublecortin and all cFos cells contain NeuN.....	49
Chapter 3: Cathepsin B Relocalization in Late Membrane Disrupted Neurons Following Diffuse Brain Injury in Rats	57
Abstract.....	57
Introduction.....	58

Materials and Methods	60
Animals.....	60
Surgical preparation and injury induction.....	60
Tracer infusion.....	62
Tissue processing.....	62
Western blotting.....	63
Cellular Cathepsin B Localization Analysis.....	64
Quantification of Cathepsin B Activity.....	65
Ultrastructural assessment of Cathepsin B localization.....	65
Statistical analysis.....	66
Results	67
Protein expression of Cathepsin B or its proteolytic activity was unchanged following CFPI.....	67
Cathepsin B re-localizes from lysosomes to cytosol in disrupted neurons at 2 and 4 weeks following central fluid percussion injury.....	68
Cathepsin B re-localization and neuronal membrane disruption are associated with reductions in cellular and nuclear area.....	69
Discussion	72
<i>Chapter 4: The effects of ICP and Cathepsin B inhibition on the Membrane Disrupted Population</i>	85
Introduction	85
Materials and Methods	87
Animals.....	87
Surgical preparation and injury induction.....	88
Drug Preparation and Treatment Administration.....	89
Tracer infusion.....	89
Tissue processing.....	90
Quantification of Cathepsin B Activity.....	91
Western blotting.....	92
Membrane Disruption and Total Cell Count Analysis.....	93
Cellular Cathepsin B Localization Analysis.....	94
Whisker Nuisance Task.....	95
Statistics.....	96
Results	96
Cathepsin B activity was decreased in the left and right cortex 2w post-injury with concurrent CA-074Me administration.....	96
Protein expression of Cathepsin B and other signaling partners; Bak, Bcl-XL, and AIF.....	97
Neuronal membrane disruption stays consistent between injury and treatment groups.....	99
Total cell count does not change at 2w post-injury with ICP elevation or administration of CA-074Me.....	100
Cathepsin B re-localizes from lysosomes to cytosol in disrupted neurons at 2 weeks following central fluid percussion injury.....	100
Injury with intracranial pressure increases somatosensory sensitivity that is reduced with CA-074Me.....	102
Discussion	102
<i>Discussion and Conclusions</i>	117
Two Phases of Membrane Disruption; Potential for Resealing?	121
Future Directions.....	123
Guess Who? (NeuN Negative Membrane Disrupted Subpopulation)	123
Mechanisms in membrane disruption: Cathepsin B or not to be?	125

Figure List

Figure 1.1.	TBI-induced membrane disruption occurs biphasically and involves a NeuN negative subpopulation.	34
Figure 1.2.	Glia do not appear to be membrane disrupted following CFPI.	35-35
Figure 1.3.	Expression of NeuN did not change in the lateral neocortex after TBI.	37
Figure 1.4.	There is no indication of cell death in the lateral neocortex following CFPI.	38
Figure 1.5.	Neurons sustaining membrane disruption weeks post-injury display few signs of ultrastructural damage indicative of cell death.	39-40
Figure 1.6.	There is a consistent NeuN- subpopulation in layers V and VI of the lateral neocortex.	41
Figure 2.1.	Doublecortin (DCX) Protein Quantities after TBI were unchanged from sham.	52
Figure 2.2.	About 40% of DCX positive cells are NeuN positive.	53
Figure 2.3.	cFos expression after TBI were unchanged from sham.	54
Figure 2.4.	cFos positive cells are NeuN-positive, and only half of cFos positive cells are membrane disrupted.	55-56
Figure 3.1.	There were no differences in the expression of Cathepsin B (Cath-B) or Cath-B signaling proteins 6hr to 4w post-CFPI compared to sham.	77-78
Figure 3.2.	Cathepsin B activity does not significantly change following injury.	79
Figure 3.3.	Representative confocal images at 6h, 1w, 2w, and 4w of immunolabeled Cathepsin B (red) in the lateral neocortex following CFPI	80-81
Figure 3.4.	Qualitative ultrastructural confirmation of Cathepsin B redistribution outside of lysosomes following CFPI.	82-83
Figure 3.5.	Membrane disruption and Cathepsin B mislocalization affect cell morphology.	84
Figure 4.1.	Cathepsin B Activity significantly decreases in the left and right lateral neocortex following 2w administration of CA-074Me compared to 10% DMSO (vehicle).	106
Figure 4.2.	Cathepsin B expression does not change with injury group or treatment.	107
Figure 4.3.	Protein quantification of Bcl-XL revealed no differences in the protein quantity regardless of group.	108 109
Figure 4.4.	Bak protein levels were unchanged regardless of injury or treatment group.	
Figure 4.5.	There were no alterations of the protein quantity in AIF for the injury groups or treatment groups	110
Figure 4.6.	Representative images of membrane disruption after sham, TBI, or TBI+ 20 mmHg ICP elevation with 10% DMSO (vehicle) or CA-074Me (Cath B inhibitor)	113
Figure 4.7.	There are no significant changes in membrane disruption between injury and treatment groups.	115
Figure 4.8.	The total number of cells not affected by injury manipulation, even with ICP elevation and treatment in the lateral neocortex layers V and VI.	116
Figure 4.9.	Representative fluorescent images of injured (sham, TBI, TBI +20mmHg ICP) and treatment groups (10% DMSO (vehicle) and CA074Me.	117
Figure 4.10.	Percentage (%) of Punctate Cathepsin B presented in a bar graph.	118
Figure 4.11	Somatosensory sensitivity was affected by injury and further with secondary ICP elevation.	119

Abbreviations

°C	degrees Celcius
%	percent
AIF	apoptosis initiating factor
ANOVA	analysis of variance
APC/CC-1	Adenomatous polyposis Coli
Bcl2/XL	B-cell lymphoma 2 (Bcl-2)/Bcl-XL
BSA	bovine serum albumin
CA-074Me	L-3- <i>trans</i> -(Propylcarbamoyl)oxirane-2-carbonyl]-L-isoleucyl-L-proline Methyl Ester
Cath B	Cathepsin B
CCI	Controlled Cortical Impact
CFPI or mFPI	central (midline) fluid percussion injury
d	days
DAB	Diaminobenzidine
DAG	diacylglycerol
DAPI	4',6-diamidino-2-phenylindole
DCX	Doublecortin
DMSO	Dimethylsulfoxide
DNA	deoxyribonucleic acid
DTT	dithiothreitol
EDTA	Ethylenediaminetetraacetic acid
EM	electron microscopy
GFAP	Glial Fibular Activation Protein
h	Hour(s)
H&E	Hemotoxylin and Eosin
HRP	horseradish peroxidase
Iba-1	Ionized Calcium Binding Adaptor Protein -1
ICP	Intracranial Pressure
ICV	Intracerebroventricular
IP	Intraperitoneal
IV	intravenous
kDa	kilo Daltons
LFPI	Lateral Fluid Percussion Injury
mL	milliliter
mm	millimeter
mM	millimolar
min	Minute(s)
NeuN/Rbfox3	Neuronal Nuclei/ RNA Binding Fox-3
NGS	Normal goat serum
NHS	Normal horse serum
nM	nanomolar
PA	Phosphatidic acid
PBBI	penetrating ballistic-like brain injury
PBS	Phosphate buffered saline
PIP2	phosphatidylinositol 4,5-bisphosphate
PIP3	phosphatidylinositol (3,4,5)-triphosphate
PI	Propidium Iodide
PKC	Protein kinase C
PS	phosphotidylserine

RNA	Ribonucleic Acid
TBI	Traumatic Brain Injury
TUNEL	Terminal dUTP Nick End Labeling
w	Week(s)
ZFR-AMC	Z-Phe-Arg-7-amino-4-(trifluoromethyl) coumarin
μL	microliter
μM	micromolar
μm	micron

Abstract

Traumatic brain injury (TBI) is a mechanical insult to the head that leads to brain damage and, in turn, causes long-term sensory, motor, cognitive, and affective dysfunction. Diffuse pathologies seen following such injury are associated with these life-altering outcomes that impact the daily lives of TBI survivors. The diffuse pathology that this body of work focuses on is neuronal membrane disruption; it is characterized by increased permeability of the neuron's plasma membrane. Moreover, our lab had previously found that membrane disruption is exacerbated with intracranial pressure (ICP) elevation. We set out to measure the duration of membrane disruption following injury with ICP elevation. Still, we needed to define the duration of membrane disruption after TBI as the lone insult. The histological findings indicate that membrane disruption occurs in a biphasic trajectory, sub-acute (6h to 3d) and late (2w-4w). Interestingly, not all of these membrane disrupted neurons are labeled with the neuronal marker NeuN. These cells were included in the quantification, which revealed that membrane disrupted NeuN- cells increase at 2w. We followed this lead with NeuN protein quantification, glial assessments, cell death evaluations and analysis of the total cell population. NeuN protein levels were not changing, and they were not glia either. We interrogated the tissue for cell death using a DNA damage sensitive assay as well as quantification of the total cell population to evaluate for cell loss; cells are not dying and overall NeuN negative population is not changing. However, there is a consistent population of NeuN negative cells in the lateral neocortex of rats. Following this study, we wanted to identify this NeuN- membrane disrupted subpopulation. We posited the NeuN negative membrane disrupted subpopulation as adapting an immature profile; we used immature/early markers, Doublecortin and cFos in cellular and molecular analyses. Overall, we found that this NeuN- membrane disrupted subpopulation could not be identified in an immature state using those markers. Simultaneously, there is no cohesive molecular mechanism for late membrane disruption. Previous data from our lab exhibited Cathepsin B, a lysosomal protease relocalized

into the cytosol 6h post-injury. We set out to further elaborate the dynamics of Cathepsin B following TBI from 6h-4w. Cathepsin B protein levels and activity in the lateral neocortex did not change after injury at any time compared to shams. Cathepsin B binding partners Bak, Bcl-XL and AIF levels were also quantified and no differences were found after injury. However, the histological studies of Cathepsin B reveal significant Cathepsin B relocation from the lysosomes in membrane disrupted neurons. Additionally, Cathepsin B relocated and membrane disrupted neurons demonstrated cellular and nuclear atrophy. Therefore, with Cathepsin B relocation coinciding with late membrane disruption, it was proposed as a candidate involved in membrane disruption. Using Cathepsin B inhibitor, CA-074Me, we could evaluate Cathepsin B's role in membrane disruption and we also wanted to scrutinize the impact of Cathepsin B inhibition on ICP elevation. Through this pharmacological approach, we found that there were some changes in Cathepsin B and AIF proteins that were not significantly different. In addition, the vehicle, 10% DMSO, used to prepare the CA-074Me was found to have some ameliorative effects in membrane disruption, though the groups given the drug had more membrane disruption than the vehicle. Cathepsin B localization with CA-074Me is more localized in lysosomes in non- disrupted neurons, however, has the opposing effect in membrane disrupted neurons . This study also had somatosensory sensitivity increase among the injured and more so in injury/ ICP elevation animals. When given CA-074Me, injured/ICP elevated animals exhibit sensitivity lowered to injured levels. Taken all together, this work highlights the dynamic nature of membrane permeability following injury may have detrimental or ameliorative effects, as well as avenues for remediating secondary sequelae following TBI.

Introduction

Traumatic brain injury (TBI) affects 60 million people globally (Maas et al., 2022) and 2.8 million people in the United States, each year, and the annual number of TBIs may be higher, however often go unreported (Taylor et al., 2017). Globally, TBI has the highest rate of injury-related death. Among the age groups, geriatric and pediatric populations have the highest rates of injury. When filtered by sex, men more frequently sustain TBIs (Maas et al., 2022). The cost of TBI related hospital admissions as of 2016 was estimated to be \$21 billion per year and rising (Marin et al., 2017; Taylor et al., 2017). TBI-related disability occurs in approximately 2% of people in the United States (Dams-O'Connor et al., 2023; Ma et al., 2014).

What is a TBI?

TBI is damage to the brain as a result of a physical disturbance to the head from a number of sources, such as falls, motor vehicle accidents, assault, sports injuries, and blast injuries (Langlois et al., 2006). These varying modalities exert forces that strain and impose stress on the brain and can penetrate through the skull or harm the brain against the skull, leaving a contusion where there is visible damage such as bleeding. Commonly, rotational/acceleration trauma displaying no obvious wounding is termed concussive. Often the penetrating injuries are considered severe TBI, and the closed head injuries can range on the spectrum from mild, moderate, to severe TBI. The phrase concussion is used interchangeably with mild TBI (mTBI) and The American Congress of Rehabilitative medicine describes a mild traumatic brain injury as brain dysfunction as a result of trauma that leads to subsequent 1. loss of consciousness, 2. Memory loss/post-traumatic amnesia, 3. changes in mental state such as confusion (Kay et al., 1993). In a hospital setting, the internationally used Glasgow Coma Scale used by neurosurgeons and other clinicians to measure motor responses (1-6), verbal responses (1-5), and eye-opening

(1-4) is a standardized way to measure impairment in consciousness and has become a foundational part of triaging head trauma (Ahmadi et al., 2022; Andriessen et al., 2010; Teasdale & Jennett, 1974; Williams et al., 1984). GCS is reported as the sum of the rankings from each category as such: 3-7=severe TBI; 8-12=moderate TBI; and 13-15=mild TBI, with the ranking of 1 from any category representing the absence of response (Teasdale & Jennett, 1974). Even with mild TBI, many patients affected by cognitive problems are at risk for additional health consequences (Langlois et al., 2006).

Additionally, TBI can be categorized as focal or diffuse. Focal TBI has an epicenter, usually as a result of a contusion or head penetrating injury. Contusions are brain bruises that arise from the brain compressing against the skull due to an external blunt force. In addition, clinical presentations also include epidural hematomas and subarachnoid hemorrhages (Andriessen et al., 2010; Granacher, 2007). On the other hand, diffuse TBI results in some sort of rotational/acceleration force that applies abnormal levels of strain onto the brain. Consequences of diffuse injury present as vast vascular and axonal injury, which can be accompanied edema(Andriessen et al., 2010).

The main event is not isolated, symptoms that follow TBI include headache, dizziness, blurred vision, sensitivity to light and sound, nausea, irritability, difficulty concentrating, memory impairments, anxiety, and irritability(McLean et al., 1984). These repercussions of TBI endure years following the initial insult and involve long-term impairments/disabilities as TBI patients can experience symptoms chronically. Often, these lasting morbidities are due to secondary diffuse pathology throughout the brain (McMahon et al., 2014).

Much is known in regard to the pathology of focal injuries, such as ischemia, excitotoxicity, metabolic deficiency, elevated intracranial pressure (ICP), alterations in cerebral blood flow and the various pathways of necrosis and apoptosis that emerge from these processes(Granacher, 2007; Kochanek et al., 2013). Diffuse pathologies that have been noted clinically include diffuse axonal injury, edema/ brain swelling, blood-brain barrier (BBB) disruption and neuroinflammation.

(Andriessen et al., 2010; Marmarou et al., 2006; Werner & Engelhard, 2007) However, the division between focal and diffuse injury begins to blur as these two modalities share cellular sequelae in different intensities ((Andriessen et al., 2010). Both include altered metabolism and even delayed pathologies, such as elevated ICP.

Intracranial Hypertension

Intracranial pressure (ICP) is the force of the cerebrospinal fluid and brain within the cranial vault and can increase as a result of injury or infection (Hawthorne & Piper, 2014). Secondary intracranial pressure (ICP) elevation to levels at or above 20mmHg has been well demonstrated to significantly and consistently increase morbidity and mortality in TBI patients(Bratton et al., 2007; Farahvar et al., 2012; Miller et al., 1977; Shim et al., 2023; Stocchetti et al., 2017). There, however, aren't any treatments that work for all cases of TBI-related elevated ICP. Current treatments consist of a stepwise approach: initially ventilation and sedation are employed, then CSF drainage, followed by mannitol or hypertonic saline, hyperventilation, hypothermia, barbituates, or finally decompressive craniotomy if the following approaches do not level out ICP(Stocchetti & Maas, 2014). These aforementioned strategies come with significant risks, such as electrolyte, fluid imbalance, or even infection. Thus far, there have been no direct molecular mechanisms identified to combat the exacerbation in morbidity linked to secondary ICP elevation. Notably, the Lafrenaye lab's novel model of CFPI followed by secondary ICP elevation, without attendant ischemia due to hypoperfusion demonstrated significant exacerbation of diffuse neuronal membrane disruption hours following injury and enhanced cell death, weeks following TBI+ICP elevation (Lafrenaye et al., 2014). Using animal models, these powerful tools also have provided insight into potential occurring pathologies that cannot yet be identified clinically, such as membrane disruption. Membrane disruption is a pathology in which the cellular phospholipid bilayer is compromised.

Membranes

The plasma membrane, which is the cell's primary defense from the extracellular environment, consists of a phospholipid bilayer with other structures like bound proteins such as ion channels, water pores, adenosine triphosphate exchangers, glycoproteins/proteoglycans involved in cellular signaling and connections to the scaffolding of the cell, the cytoskeleton. These membrane-embedded proteins have secondary proteins that mobilize to different locations of the cell, like the nucleus, in order to change protein expression or communicate with other surrounding cells. In addition, this amphiphilic structure compartmentalizes various chemicals/macromolecules, such as catalytic proteins, containing reactions necessary for cell homeostasis and survival and creating ionic gradients that are essential for paracrine signaling in the brain. There are additional phospholipid membranes within the cell that are important for compartmentalization, such as the bilayered nuclear envelope, mitochondria, as well as the single layered, endoplasmic reticulum, the Golgi apparatus, endosomes, and lysosomes (Heald & Cohen-Fix, 2014).

Why study membrane disruption?

Membrane disruption is a pathology in which the cellular phospholipid bilayer, which is the cell's primary defense from the extracellular environment, is compromised. Throughout the years this pathology has been referred to as plasmalemmal/membrane permeability, membrane perturbation, loss of membrane integrity, membrane injury, membrane damage, mechanoporation, and membrane poration, however, in this dissertation the term "membrane disruption" will be used. Neuronal membrane disruption has been found in various TBI models both in vitro and in vivo in rodents and swine models (Harris et al., 2023; Keating et al., 2020, 2021; Lafrenaye et al., 2012, 2014; LaPlaca et al., 2019; Prado & LaPlaca, 2020; Ryu et al., 2021, 2022)). Membrane disruption has been shown to occur acutely following injury, primarily within

neurons, however, the progression of TBI-induced membrane disruption remains undefined. Some neurons that are impacted by membrane disruption experience cell death, and others demonstrate delayed disruption, providing an opportunity for therapeutic intervention.

This pathology is visualized using infusions of cell impermeable tracers, such as dextran, horseradish peroxidase, calcein, lucifer yellow, YO-YO-1, and propidium iodide in the living animal followed by fixation for microscopic analysis (Cullen et al., 2011; Farkas et al., 2006; Geddes, Cargill, et al., 2003; Halford et al., 2017; Lafrenaye et al., 2012, 2014; LaPlaca et al., 2019; LaPlaca & Prado, 2010; Levine et al., 2016; Singleton & Povlishock, 2004; Whalen et al., 2008; Wofford et al., 2017), and therefore little is known about membrane disruption clinically. However, membrane disruption has been well-documented to occur in various pre-clinical models of traumatic brain injury (TBI).

In vitro Membrane disruption in TBI

Membrane disruption was initially referred to as “mechanoporation,” which is a specific subset of cellular membrane disruption that occurs at the time of mechanical insult. In the mid-1990s, the LaPlaca group imaged neuronal mechanoporation in vitro immediately following fluid shear stress (FSS) injury of NT2-N human cells and found significant levels of lactate dehydrogenase, a ubiquitously expressed intracellular enzyme, in the extracellular fluid minutes following injury (LaPlaca et al., 1997). Further research found that cultured rat neurons subjected to biaxial stretch injury showed increased levels of cell impermeable tracer uptake based on the size of the tracer and the degree of strain used, suggesting that membrane disruption is non-uniform and directly linked to the severity of injury (Geddes, Cargill, et al., 2003). Disruption of the plasmalemma was also shown to result in increases of intracellular calcium within minutes, which can trigger the release of proteases that cleave proteins needed to transport vesicles and endosomes to the membrane surface for repair and cellular packaging (Geddes, LaPlaca, et al.,

2003; LaPlaca et al., 1997)). Other groups employed the fluid strain stress injury to look at another subset of membrane permeability, specifically in axons (Kilinc et al., 2008). Further developments were made using three-dimensional(3-D) co-cultures of neurons and astrocytes from Sprague-Dawley rats. In these 3-D neuron-astrocyte cultures, using a 3-D cell compression device, membrane disruptions were compared in shear and compression injuries at various intensities of injury (Cullen et al., 2011). The 3-D culture model was chosen in this study to better simulate in vivo mechanics. The former study, along with other laboratories, has demonstrated that glia can also be susceptible to membrane disruption in in vitro models of astrocyte stretch injuries (Halford et al., 2017). Even in more recent literature, in vitro models are still active in connecting the mechanics of culture membrane permeability to in vivo models of TBI (LaPlaca et al., 2019).

In vivo Membrane disruption TBI

During investigations into diffuse axonal injury, the Povlishock group also identified mechanoporated neuronal axons following a diffuse TBI using the central fluid percussion injury (CFPI) model in cats (Pettus et al., 1994). Following induction of CFPI in Sprague-Dawley rats, signs of soma mechanoporated neurons were observed as early as five minutes and as late as eight hours post-injury in various brain regions (Singleton & Povlishock, 2004). The anatomical regions that were affected included the lateral neocortex, the hippocampus, particularly in CA1 region. Other regions mentioned, not shown, included the cerebellum and the pontine region of the corticospinal tract (Singleton & Povlishock, 2004). Another study from that group employed the Marmarou weight drop diffuse injury model, and infused fluorescent 10 kDa green and red dextrans pre- and post-injury into the lateral ventricle in Sprague Dawley rats. Those animals were evaluated 4 and 8 hours post-injury for membrane disruption. Through this study, they were able to capture some of the dynamics of membrane disruption as some reseal immediately, and some neurons retain enduring membrane disruption. They also found an increase in intracranial pressure following injury that was not induced by dextran infusion (Farkas et al., 2006).

Membrane permeability is not limited to diffuse animal models as it has also been under scrutiny in a focal model of TBI, cortical controlled impact (CCI). Mice were injured using CCI laterally and given propidium iodide (PI) intraperitoneally or ICV prior to injury (Whalen et al., 2008). Neurons with membrane permeabilization were detected in the cortex beneath and adjacent to the region of injury. PI labeling was even detected contralateral to injury (Whalen et al., 2008). Some of the neurons found with membrane disruption (PI+) presented with abnormal nuclei, while other membrane disrupted neurons appeared normally. The duration of membrane permeabilization, PI+ cells were detected out to two days post-injury, but by day seven, those injured neurons were gone (Whalen et al., 2008). These investigators also utilized a secondary tracer, YOYO-1, infused 23 hours following injury. Many of the PI+ neurons also co-labeled with YOYO-1; however, there was no total overlap of these subpopulations. Their findings highlight that some of the membrane permeable neurons do seal, as a portion of YOYO-1 negative/PI-positive cells were found. More recently, the focal CCI model was employed in male Sprague-Dawley rats with either TRITC-dextran or lucifer yellow tracers. Membrane-disrupted neurons were found proximal to injury site in the cortex and hippocampus, as well as in those regions on the contralateral side, but in significantly less quantity (LaPlaca et al., 2019).

Neuronal mechanoporation and has been speculated to lead to dysregulated ionic flux, apoptosis, and radical oxidative damage often assessed in TBI and spinal cord injuries. In fact, some studies found correlations between mechanoporation and cell death following focal brain and spinal cord injury (LaPlaca et al., 2019; Whalen et al., 2008). However, in the central fluid percussion injury (CFPI) model of TBI, most of the mechanoporated and acutely membrane disrupted neurons did not demonstrate the traditional signs of death; rather, they appeared ultrastructurally normal (Singleton and Povlishock, 2004; Lafrenaye et al., 2012).

As mentioned above in the discussion about intercranial hypertension-associated pathology, membrane disrupted neurons were found to be correlated to secondary insults, such as elevations in intracranial pressure (ICP) and appeared to be the subpopulation of membrane

disrupted neurons that progressed to cell death following diffuse TBI exacerbated by secondary intracranial pressure elevations (Lafrenaye et al., 2014). Initially, membrane disruption and ICP elevation in Fischer 344 rats were assessed after CFPI (Lafrenaye et al., 2012). Elevated ICP without ischemia, is a complication of diffuse brain injury that has not previously associated with a particular molecular mechanism. In this study, membrane disrupted neurons in the lateral neocortex of injured animals were visualized by 10kDa 488 or 568 Alexa Fluor dextran, infused ICV pre- and post-injury. Neuronal identity was determined using Neuronal Nuclei (NeuN), discussed in the following section. The results of the study revealed that Fischer 344 rats with naturally elevated ICP following CFPI demonstrated 20% higher subpopulation of membrane disrupted neurons containing the post-injury dextran (40% membrane disrupted neurons total) compared to low ICP which had about 20% membrane disrupted neurons. Lafrenaye and colleagues switched to Sprague-Dawley rats, and manual ICP elevations were used, as this strain of rat does not have naturally elevated ICP after injury (Reid et al., 2010). The results seen in Sprague Dawley rats were similar, as manual ICP elevation with injury experienced 30% more membrane disruption compared to injury alone (Lafrenaye et al., 2014). Further findings in that study also present a loss of neurons at four weeks with injury+ ICP elevation (Lafrenaye et al., 2014). Another layer of the investigation by Lafrenaye et al 2014 proposed that perhaps there is additional pathology driven by membrane disruption between six hours and four weeks. As mentioned above, the WNT score was significantly higher than sham for injured animals, and the injured+ICP elevation score was significantly higher than sham and injury alone, suggesting that membrane disruption can manifest into behavioral morbidities.

Membrane disruption also occurs in higher order animals. The Cullen group has employed experimental TBI investigation in pigs using the closed head rotational inertial head injury pig model with lucifer yellow given ICV to measure membrane disruption. This study showed that membrane disruption occurs in higher-order animals, like pigs which are gyroencephalic compared to mice and rats which are lissencephalic, and that microglia are in closer proximity to

these membrane disrupted neurons(Wofford et al., 2017). The Wanner group also used a spinal cord injury crush model in swine to comprehend in vivo dynamics of astroglial membrane permeability which increased astrocytic reactivity and eventual cell death (Halford et al., 2017).

NeuN

NeuN was identified in 1992 and is commonly used as a pan-neuronal marker. It functions in alternative splicing of various proteins important for neuronal development and differentiation, leading to the notion that loss of NeuN following injury could be linked to an ameliorative developmental reversion (Darlot et al., 2017; Duan et al., 2016; Kim et al., 2013; McPhail et al., 2004). The monoclonal a60 antibody, Neuronal nuclei, NeuN has been used to identify neuronal nuclei throughout the central and peripheral nervous system. A60 anti-NeuN did not target glia, but also did not label neurons such as Purkinje cells, olfactory mitral bulb cells, and dorsal cochlear nuclear cells (Mullen et al., 1992; Wolf et al., 1996). NeuN was identified by mass spectrometry as the RNA-binding protein, Rbfox3, related to fox-1, feminizing on x protein found in drosophila(Kim et al., 2009). Rbfox3 has been implicated in neuronal development and its expression signifies a post mitotic state (Gusel'nikova et al., 2015; Kim et al., 2013). Rbfox3 is seen more frequently in neurons compared to Rbfox-1 found in neurons, skeletal muscle, and heart. Rbfox2 is expressed in embryonic stem cells and can later be found in various tissue types (Jin et al., 2003; Kim et al., 2009, 2011). The work described in further chapters interrogates membrane disruption in regard to a NeuN subpopulation. The pathological consequences of elevated ICP beyond the more catastrophic repercussions of hypoperfusion and herniation are not well understood. Neuronal membrane disruption is an understudied and captivating diffuse pathology defined by holes in the membrane that initially arise as a result of damage to the neuronal plasmalemma. Intriguing findings from our lab demonstrate that active membrane disruption occurs for weeks following diffuse TBI discussed in Chapter 1. Interestingly, we also found a novel subpopulation of membrane disrupted cortical neurons that did not express the

traditional marker of mature neurons, NeuN. Studies have shown that neuronal reversion to an immature phenotype, in which NeuN is not expressed, is a potential compensatory mechanism following injury, yet the role of the NeuN negative (NeuN-) membrane disrupted neurons remains unknown.

Therefore, I hypothesize that the NeuN- subpopulation is reverting to an immature state to compensate for injury. In addition, the Lafrenaye lab found that secondary ICP elevations doubled the population of membrane disrupted neurons hours following TBI, however, the chronic effects of elevated ICP on membrane disrupted neurons, and particularly the NeuN- subpopulation, remain nebulous. I posit that following diffuse TBI and secondary ICP elevation we will see increases in the membrane disrupted population chronically and a reduction in the NeuN- population, as the neurons will not be able to compensate for the secondary insult. The mechanism mediating neuronal membrane disruption is also unknown, however, work from our lab identified the lysosomal protease Cathepsin B (Cath B), as a potential mediator. Re-localization of Cath B from the lysosome to the cytosol has been demonstrated to initiate cell damage/death. Therefore, we hypothesize that Cath B re-localization from the lysosomes to the cytosol is driving neuronal membrane disruption.

Chapter 1

These results were previously published as:

Hernandez ML, Chatlos T, Gorse KM and Lafrenaye AD (2019) Neuronal Membrane Disruption Occurs Late Following Diffuse Brain Trauma in Rats and Involves a Subpopulation of NeuN Negative Cortical Neurons. *Front. Neurol.* 10:1238. doi: 10.3389/fneur.2019.01238

Abstract

The repercussions of traumatic brain injury (TBI) endure years following the initial insult and involve chronic impairments/disabilities. Studies indicate that these morbidities stem from diffuse pathologies, however, knowledge regarding TBI-mediated diffuse pathologies, and in particular, diffuse neuronal membrane disruption, is limited. Membrane disruption has been shown to occur acutely following injury, primarily within neurons, however, the progression of TBI-induced membrane disruption remains undefined. Therefore, the current study investigated this pathology over a longer temporal profile from 6h to 4w following diffuse TBI induced using the central fluid percussion injury (CFPI) model in rats. To visualize membrane disruption, animals received an intracerebroventricular infusion of tagged cell-impermeable dextran 2h prior to experimental endpoints at 6h, 1d, 3d, 1w, 2w or 4w post-CFPI. The percentage of total neurons demonstrating dextran uptake, indicative of membrane disruption, was quantified within the lateral neocortex layers V and VI from 6h-4w post-injury. We found that membrane disruption displayed a biphasic pattern, where nearly half of the neurons were membrane disrupted sub-acutely, from 6h-3d post-TBI. At 1w the membrane disrupted population was dramatically reduced to levels indistinguishable from sham controls. However, by 2w and 4w following CFPI, approximately half of the neurons analyzed displayed membrane disruption. Moreover, our data revealed that a subset of these late membrane disrupted neurons were NeuN negative (NeuN-). Correlative western blot analyses, however, revealed no difference in NeuN protein expression in the lateral

neocortex at any time following injury. Furthermore, the NeuN- membrane disrupted neurons did not co-label with traditional markers of astrocytes, microglia, oligodendrocytes, or NG2 cells. Immunohistochemistry against NeuN, paired with a hematoxylin and eosin counter-stain, was performed to quantify the possibility of overall NeuN+ neuronal loss following CFPI. A NeuN- population was observed consistently in both sham and injured animals regardless of time post-injury. These data suggest that there is a consistent subpopulation of NeuN- neurons within the lateral neocortex regardless of injury and that these NeuN- neurons are potentially more vulnerable to late membrane disruption. Better understanding of membrane disruption could provide insight into the mechanisms of diffuse pathology and lead to the discovery of novel treatments for TBI.

Introduction

Traumatic brain injury (TBI) is a continuing healthcare problem, resulting in mortality and long-lasting morbidities that coalesce into various impairments and/or disabilities (Wilson et al., 2017). In the United States, approximately 2.8 million people report suffering a TBI annually and this number is likely an underestimate since TBI often goes unreported (Langlois et al., 2006; Taylor et al., 2017). Various studies have demonstrated links between disabilities/impairments and diffuse pathologies (Andriessen et al., 2010). However, diffuse pathologies are highly heterogeneous (Farkas et al., 2006; Singleton & Povlishock, 2004; Thomas et al., 2018). Additionally, while substantial progress has been made in understanding the pathophysiology of TBI-induced focal injuries, knowledge about diffuse pathologies following TBI remain limited.

One such pathology is diffuse membrane disruption, which is characterized by leaky somatic plasmalemma (Farkas et al., 2006; McNeil & Steinhardt, 2003; Pettus et al., 1994). Membrane disruption has been well established to occur in various models of TBI, both *in vitro* using cell stretch and *in vivo* following focal brain and spinal cord injury as well as after diffuse TBI (Choo et al., 2007; Cullen et al., 2011; Farkas et al., 2006; Geddes et al., 2003; Halford et al.,

2017; Lafrenaye et al., 2012, 2014; LaPlaca et al., 2019; Levine et al., 2016; Singleton & Povlishock, 2004; Whalen et al., 2008). These studies found that membrane disruption occurred upon physical impact (mechanoporation), as well as sub-acute membrane disruption, in which mechanical transduction is less likely to be directly instigating damage (Cullen et al., 2011; Farkas et al., 2006; Geddes et al., 2003; Lafrenaye et al., 2012, 2014; LaPlaca et al., 1997, 2019; Singleton & Povlishock, 2004; Whalen et al., 2008). Membrane disruption has primarily been evaluated in models of focal TBI, wherein the pathological progression is linked to cell death in the pericontusional lesion, however, less is known regarding the pathological progression of membrane disruption in a diffuse model of TBI, in which cell death is not observed (Farkas et al., 2006; Lafrenaye et al., 2012, 2014; Mbye et al., 2012; Whalen et al., 2008; Zhu et al., 2012). We previously demonstrated that neuronal membrane disruption is induced in layers V and VI of the lateral neocortex hours following diffuse central fluid percussion injury (CFPI). This diffuse membrane disruption did not progress to cell death, but could be exacerbated by secondary insults, such as increased intracranial pressure, which did precipitate neuronal loss (Lafrenaye et al., 2012, 2014). However, the natural progression of this pathology to later time points following experimental diffuse TBI has not been explored previously.

Neuronal Nuclei (NeuN) is an RNA-binding protein potentially involved in neuronal maturation and is exclusively expressed by post-mitotic neurons throughout the brain and spinal cord (Kim et al., 2009; Mullen et al., 1992; Wolf et al., 1996). Due to this neuron-specific expression, NeuN has been widely adopted as a ubiquitous marker for mature neurons throughout the central nervous system (Giannaris & Rosene, 2012; Sedmak & Judaš, 2019). However, there are subsets of neurons that never express NeuN, including cerebellar Purkinje cells, olfactory mitral cells, retinal photoreceptors, subsets of interneurons, and inner granule cells (Mullen et al., 1992; Wolf et al., 1996). Studies have also indicated that damaged neurons could reduce NeuN expression upon reversion to a less mature growth-permissive state (Darlot et al.,

2017; McPhail et al., 2004). The expression of NeuN within the diffusely membrane disrupted population of cortical neurons, however, has not previously been assessed.

It has been theorized that membrane disruption would inevitably progress to cell death as mechanoporation has been demonstrated to precipitate uncontrolled calcium influx, ATP dysregulation, and eventual cell death *in vitro* (Geddes et al., 2003; Lusardi et al., 2004). However, neurons sustaining membrane disruption minutes to hours post-diffuse TBI have also been demonstrated to be capable of membrane resealing and cell survival, making membrane disruption a targetable pathology for therapeutic intervention (Cullen et al., 2011; Farkas et al., 2006; Geddes et al., 2003; Lafrenaye et al., 2012, 2014; Whalen et al., 2008). Therefore, in this study we sought to establish a temporal profile for cortical membrane disruption following diffuse brain injury.

Throughout this study we found cortical neurons sustaining membrane disruption, weeks following TBI, that appear temporally distinct from the disrupted populations sustaining membrane disruption hours to days post-CFPI. Furthermore, we also discovered a subpopulation of NeuN negative (NeuN-) membrane disrupted neurons that were most apparent 2w post-injury. Interestingly, we found that there was a consistently present NeuN- subpopulation diffusely distributed throughout layers V and VI of the lateral neocortex regardless of injury. Together, the findings presented below highlight the complexity of diffuse neuronal membrane disruption. Better understanding of membrane disruption could provide insight into the mechanisms of diffuse pathology and lead to the discovery of novel treatments following TBI.

Methods

Animals

Experiments were conducted using protocols in accordance with the Virginia Commonwealth University institutional ethical guidelines concerning the care and use of

laboratory animals (Institutional Animal Care and Use Committee, Virginia Commonwealth University), which adhere to regulations including, but not limited to, those set forth in the Guide for the Care and Use of Laboratory Animals, 8th Edition (National Research Council). Animals were housed in individual cages on a 12h light-dark cycle with free access to food and water. Adult male Sprague-Dawley rats, n=66 weighing 350–450g were used for this study. Any animal that lost more than 20% of their pre-injury body weight or precipitated gross brain pathology (contusion, subdural hematoma, or gross tissue loss) was excluded from analysis. No animals met exclusion criteria in this study. Animal injury state and survival time point were randomly determined using a random number generator on the day of surgery. All surgeries were conducted by the same surgeon during the same times of day to reduce variability.

Surgical preparation and injury induction

Animals were anesthetized with 4% isoflurane in 30% O₂ and 70% N₂O then intubated and ventilated with 2% isoflurane in 30% O₂ and 70% N₂O throughout the duration of the surgery, injury, and post-injury physiological monitoring. Heart rate, respiratory rate, and blood oxygenation were monitored via a hind-paw pulse oximetry sensor (STARR Life Sciences, Oakmont, PA) for the duration of anesthesia, except during the induction of injury. Body temperature was maintained at 37°C with a rectal thermometer connected to a feedback-controlled heating pad (Harvard Apparatus, Holliston, MA). All animals were placed in a stereotaxic frame (David Kopf Instruments, Tujunga, CA). A midline incision was made, and a 4.8 mm circular craniectomy was made along the sagittal suture midway between bregma and lambda for injury induction. A 2mm burr hole was also drilled in the left parietal bone overlying the left lateral ventricle (0.8 mm posterior, 1.3 mm lateral, and 2.5- 3 mm ventral to bregma) through which a 25-gauge needle, connected to a pressure transducer and micro infusion pump (11 Elite syringe pump; Harvard Apparatus) via sterile saline filled PE50 tubing, was placed into the left

lateral ventricle. Appropriate placement was verified via a 1.3 μ l/min infusion of sterile saline within the closed fluid-pressure system during needle placement (Sullivan et al., 1976). The needle was held in the ventricle for at least 5min to record pre-injury intracranial pressure (ICP). After the 5-min reading, the needle was slowly removed and the burr hole was covered with bone wax before preparation for sham or CFPI (Dixon et al., 1987; Lafrenaye et al., 2014). Briefly, a Leur-Loc syringe hub was affixed to the craniectomy site and dental acrylic (methyl-methacrylate; Hygenic Corp., Akron, OH) was applied around the hub and allowed to harden. Anesthetized animals were removed from the stereotaxic frame and injured at a magnitude of 2.05 ± 0.15 atmospheres ($F_{5,24} = 0.565$, $p = 0.726$; 6h= 2.03 ± 0.08 ; 1d= 2.06 ± 0.1 ; 3d= 2.07 ± 0.05 ; 1w= 2.02 ± 0.8 ; 2w= 2.1 ± 0.04 ; 4w= 2.05 ± 0.1) and duration of ~ 22 msec. The pressure pulse was measured by a transducer affixed to the injury device and displayed on an oscilloscope (Tektronix, Beaverton, OR). Immediately after the injury, the animal was reconnected to the ventilator and physiologic monitoring device and the hub and dental acrylic were removed en bloc. Gelfoam was placed over the craniectomy/injury site and the scalp was sutured. The animal was then replaced in the stereotaxic device and the ICP probe was reinserted into the lateral ventricle, as described above, for post-injury ICP monitoring. The animals were then allowed to recover and were returned to clean home cages. Identical surgical procedures were followed for sham-injured animals, without release of the pendulum to induce injury.

Tracer infusion

Two hours prior to sacrifice, tagged dextran (40mg/ml in sterile 0.9% saline; ~ 1.6 mg/kg) was infused into the lateral ventricle as described previously (Lafrenaye et al., 2012). Briefly, 15 μ l of 10kDa dextran conjugated to either 488-Alexa Fluor (Cat#: D22910, Invitrogen, Carlsbad, CA), 568-Alexa-Fluor (Cat#: D22912; Invitrogen, Carlsbad, CA), or biotin (Cat#: D1956; Invitrogen, Carlsbad, CA) was infused into the left lateral ventricle at 0.5-1.3 μ l/min, with continuous ICP monitoring. To avoid bias caused by differences in fluorescent signal detectability animals were

randomly assigned a tag (Alexa 488, Alexa 568 or biotin). The tracer was allowed to diffuse throughout the parenchyma for 2h prior to transcardial perfusion at 6h, 1d, 3d, 1w, 2w, or 4w post-sham or CFPI.

Tissue processing

At appropriate time-points between 6h and 4w post-injury, the animals were injected with 150mg/kg euthanasia-III solution (Henry Schein, Dublin, OH), then underwent transcardial perfusion with cold 0.9% saline. Lateral neocortices were dissected from the right hemisphere of the brain for molecular assessments of protein expression followed by a switch in transcardial perfusate to 4% paraformaldehyde/ 0.2% glutaraldehyde in Millonig's buffer (136mM sodium phosphate monobasic/109mM sodium hydroxide) to fix the left side of the brain for subsequent immunohistochemical or electron microscopic (EM) processing and analysis. After transcardial perfusion, the brains were removed, post-fixed for 24-48h, then sectioned coronally in 0.1M phosphate buffer with a vibratome (Leica, Banockburn, IL) at a thickness of 40µm from bregma to 4.0mm posterior to bregma. Sections were collected serially in 12 well-plates and stored in Millonig's buffer at 4°C. A random starting well (wells 1–12) was selected using a random number generator and four serial sections, each 480µm apart, were used for histological analyses. All histological analyses were restricted to layers V and VI of the lateral somatosensory neocortex extending from the area lateral to CA1 to the area lateral to CA3 of the hippocampus.

Western blotting

Lateral neocortices of sham n=6 (n=1/time point) and TBI rats n=4/time point were homogenized in NP40 Buffer (150 mM NaCl, 50 mM Tris pH 8.0, 1% Triton) and protease inhibitor cocktail (AEBSF 10.4mM, Aprotinin 8µM, Bestatin 400µM, E-64 140µM, Leupeptin 8µM, Pepstatin A 150µM, Cat#: P8340, Sigma, Saint Louis, MO). Protein concentrations were

measured using a NanoDrop Lite (Thermo Fisher Scientific, Wilmington, DE). Protein (20 µg) was boiled for 10min in 50mM dithiothreitol (Cat#: 1610610; Bio-Rad; Hercules, CA), 2x Laemmli loading buffer (Cat#: 1610737; Bio-Rad; Hercules, CA) and run at 200 Volts for 30min on Mini-PROTEAN TGX Stain-Free 4-20% precast polyacrylamide gels (Cat#: 4568096; Bio-Rad, Hercules, CA). Protein was transferred onto 0.45µm PVDF membranes using Bio-Rad Transblot Turbo transfer system using mixed molecular weight manufacturer setting (1.3-2.5 Amps, 25 Volts for 7min). Western blotting was done on an iBind flex apparatus (Invitrogen, Carlsbad, CA) using primary antibody rabbit anti-NeuN (1:2000; Cat#: ab104225; Abcam; Cambridge, MA) and anti-rabbit-HRP secondary antibody (1:5000; Cat#: 111-030-003; Jackson Laboratories, West Grove, PA)(Hahn et al., 2015). Total protein (Stain Free) and chemiluminescent images were taken on a ChemiDoc imaging system (BioRad). Densitometric analysis was done in ImageJ (National Institutes of Health; Bethesda, MD) and all NeuN protein bands were normalized to total protein and sham controls.

Membrane Disruption Analysis

Consistent with previous studies, we assessed the potential for neuronal membrane disruption via the utilization of 10kDa dextrans, which are impermeable to cells with intact membranes (Cullen et al., 2011; Farkas et al., 2006; Geddes et al., 2003; Lafrenaye et al., 2012; LaPlaca et al., 2009; Singleton & Povlishock, 2004). Fluorescently tagged dextran-containing cells, indicative of membrane perturbation, could be visualized via confocal microscopy without further processing, however, biotin-conjugated dextran required immunolabeling for visualization. Tissue sections from sham n=7 and TBI animals n=5 per time point were blocked with 5% normal goat serum (NGS) or 5% normal horse serum (NHS), 2% bovine serum albumin (BSA), and permeabilized with 1.5% triton-X for 2h. This was followed by immunolabeling using primary antibodies mouse anti-NeuN (1:500-700; Cat#: MAB377; MilliporeSigma; Temecula, CA) and Goat anti-biotin (1:2000; Cat#: 31852; Thermo Scientific, Rockford, IL). Secondary antibodies

Alexa-568 conjugated goat anti-mouse (1:700; Cat#: A11004; Life Technologies, Carlsbad, CA) and Alexa-488 conjugated donkey anti-goat (1:700; Cat#: A11055; Life Technologies, Carlsbad, CA) and the tissue was mounted onto slides using Vectashield hardset mounting medium with 4',6-diamidino-2-phenylindole (DAPI) (Cat#: H-1500; Vector Laboratories, Burlingame, CA). Sections were analyzed by confocal microscopy using a Zeiss LSM 710 System (Carl Zeiss). Quantitative analysis was performed as described previously (Lafrenaye et al., 2014b). Briefly, confocal images of the left neocortical region of interest were taken at 40X magnification in a systematically random fashion by a blinded investigator using DAPI labeling to verify focus. Image acquisition settings were held constant for comparable regions (layer V or VI) for all groups analyzed. Analyses of neurons exhibiting dextran uptake were performed using the ImageJ colocalization finder plugin (overlap coefficient ≥ 0.9) and traditional cell counting. Dextran containing neurons were quantified for each image and averaged for each animal.

Glial Analysis

Tissue slices from 2w post-TBI animals n=5, including sham n=1, containing tagged dextrans were blocked with 5% NGS, 2% BSA, and 1.5% triton-X for 2h, then incubated with mouse anti glial fibrillary acidic protein (GFAP) (1:1000; Cat#: MAB3402; MilliporeSigma, Temecula, CA) in 5% NGS/2% BSA/ 0.5% triton-X overnight at 4°C. The following day, the tissue was rinsed in 1% NGS/1%BSA/0.2% triton-X, then incubated in goat anti-mouse 568 (1:700; Cat. #: A11004; Life Technologies, Carlsbad, CA). Additional tissue slices were labeled for microglia using ionized calcium binding adaptor molecule 1 (Iba-1) and for oligodendrocytes via Adenomatous Polyposis Coli (APC/CC-1). Triple-labeled samples were prepared by blocking tissue in 5% NGS/2% BSA/1.5% triton-X for 2h, then incubating with mouse anti-APC/CC-1(1:200; Cat#: OP80 MilliporeSigma, Temecula, CA) and rabbit anti-Iba-1 (1:1000; Cat#: 19-19741; Wako Chemicals, Richmond, VA) overnight at 4°C. Tissue was then incubated with goat

anti-mouse Alexa Fluor 568 and Alexa Fluor 633 conjugated goat anti-rabbit (1:700; Cat#: A21071; Invitrogen, Carlsbad, CA) for 2h. Tissue probed for NG2 cells was blocked in 5% NGS/2% BSA/1.5% triton-X for 2h, then incubated with rabbit anti-NG2 Chondroitin Sulfate Proteoglycan (1:200, Cat#: AB5320; MilliporeSigma, Temecula, CA) in 5% NGS/2% BSA/ 0.5% triton-X overnight at 4°C. The next day the tissue was rinsed then incubated with Alexa Fluor 633 conjugated goat anti-rabbit secondary antibody for 2h. All labeled tissue was mounted using Vectashield hardset mounting medium with DAPI (Cat#: H-1500; Vector Laboratories, Burlingame, CA). Tissue with 488-conjugated dextrans, labeled for GFAP or CC-1 and Iba-1 or NG2 was visualized on a Zeiss LSM 710 system (Carl Zeiss, Oberkochen, Germany). To determine if dextran-containing cells also labeled for glia, co-labeling with either GFAP, Iba-1, CC-1, or NG2 was assessed using a Zeiss 710 confocal microscope by an investigator blinded to animal group during image acquisition and through the analysis. Three micrographs/regions of interest (ROIs) for each section were taken using a 40x objective; two random sections were assessed for each animal. The total number of dextran-containing cells co-labeling with either GFAP, Iba-1, CC-1, or NG2 were counted by eye for each image in Zen (Carl Zeiss, Oberkochen, Germany). The number of dextran-containing glia per 0.44 mm² was averaged for each animal and compared to sham.

TUNEL Analysis

One section of tissue from each animal sham n=6, 6h n=5, 1d n=6, 3d n=6, 1w n=5, 2w n=6, 4w n=5 were mounted on slides for TUNEL. All samples were incubated in proteinase K (1:25). The positive control was subjected to DNase I (2U/μL; Cat#: M0303S; New England BioLabs; Ipswich, MA) prior to TUNEL. Slides were incubated in terminal deoxynucleotidyl transferase (TdT) reaction according to the Click-iT Plus TUNEL assay (Cat#: C10619; Invitrogen; Carlsbad, CA), except for the negative control, which received water instead. The Click-iT Plus TUNEL reaction cocktail containing Alexa Fluor 647 picolyl azide was used to label fragmented

DNA as an indicator of cell death. All slides were blinded against animal group and images were taken on a Zeiss 710 confocal microscope holding the imaging settings consistent. For all images, the number of TUNEL+ cells were quantified by eye per 0.43 mm².

Preparation of tissue for light microscopy for neuronal quantification

In preparation for light microscopy, tissue was labeled with mouse anti-NeuN (1:700; Cat#: MAB377; MilliporeSigma; Temecula, CA). Tissue slices were blocked with 5% NGS, followed by incubation with biotinylated goat anti-mouse (1:1000; Cat#: BA-9200; Vector Laboratories) secondary antibody. Sections were then incubated in avidin biotinylated enzyme complex using the Vectastain ABC kit (Vector Laboratories) followed by visualization with 0.05% diaminobenzidine/0.01% hydrogen peroxide/ 0.3% imidazole (DAB) in 0.1M phosphate buffer. For light microscopy, tissue was mounted on gelatin-coated slides before dehydration and rehydration. Rehydrated tissue was incubated in Gills hematoxylin (Leica Biosystems) followed by bluing agent (Leica Biosystems) and three dips in 0.25% eosin Y/0.005% acetic acid/95% ethanol before sections were cleared through increasing concentrations of ethanol and cover-slipped with Permount (Thermo Fisher Scientific, Waltham, MA). Light micrographs were acquired with a Nikon Eclipse 800 microscope (Nikon, Tokyo, Japan) equipped with an Olympus DP71 camera (Olympus, Center Valley, PA). To evaluate numbers of total neuronal population following injury, four sections per animal (sham n=6; 6h n=7; 1d n=4; 3d n=5; 1w n=5; 2w n=5; 4w n=4 animals) were stained with NeuN and H&E as described above. An investigator, blinded to animal group, imaged and analyzed all slides. Approximately 8-10 images spanning the lateral neocortex were taken per section in a systematically random fashion. Neurons were denoted by hematoxylin and eosin stained cell bodies that were at least 2x larger than the surrounding glial cells (Lafrenaye et al., 2014). All cell numbers were counted by eye and any cells that were morphologically determined to be neurons but didn't contain labeling for NeuN were denoted as NeuN-.

Ultrastructural assessment of membrane disrupted neurons

In preparation for electron microscopic (EM) analysis, tissue was labeled with rabbit antibodies targeted to Alexa Fluor 488 (1:5000; Cat#: A11094; Invitrogen; Carlsbad, CA). Tissue slices were then blocked with 5% NGS, followed by incubation with biotinylated goat anti-rabbit (1:1000; Cat#: BA-5000; Vector Laboratories) secondary antibody. Sections were then incubated in avidin biotinylated enzyme complex using the Vectastain ABC kit (Vector Laboratories) followed by visualization with DAB in 0.1M phosphate buffer. Tissue sections were osmicated, dehydrated, and embedded in epoxy resin on plastic slides. After resin curing, areas of interest were identified using light microscopy. These areas were removed, mounted on plastic studs, and 70nm sections were cut and mounted on Formvar-coated slotted grids. The grids were stained in 5% uranyl acetate in 50% methanol and 0.5% lead citrate. Electron micrographs were imaged using a JEOL JEM 1230 transmission electron microscope equipped with an Orius SC1000 CCD cameras (Gatan, Pleasanton, CA).

Statistical analysis

Data were tested for normality prior to utilizing parametric or non-parametric assessments, which were conducted in SPSS (IBM Corporation, Armonk, NY). Animal numbers for each group were determined by an a priori power analysis using effect size and variability previously observed in the lab when assessing pathology between sham and injured groups using the CFPI model, an $\alpha = 0.05$, and a power of 80%. One-way analysis of variance (ANOVA) and Bonferroni post hoc test were performed for all between group histological analyses. Non-normal data underwent non-parametric analysis Kruskal-Wallis mean rank sum testing to compare groups. Statistical significance was set to $p < 0.05$. Data are presented as mean \pm standard error of the mean.

Results

Neuronal membrane disruption is biphasic and extends out to 4 weeks following CFPI.

Based on our previous findings of substantial neuronal membrane disruption hours following CFPI without subsequent cell death, unless compounded by secondary insult, we evaluated the temporal progression of diffuse membrane disruption from hours to weeks post-injury (Figure 1; (Lafrenaye et al., 2014)). As has been well established, tagged 10kDa dextrans that are normally excluded from cells with intact membranes can be reliably used to identify membrane disrupted neurons after injury both *in vitro* and *in vivo* (Cullen et al., 2011; Geddes et al., 2003; Lafrenaye et al., 2012, 2014; LaPlaca et al., 1997; Singleton & Povlishock, 2004). Therefore, we infused tagged dextran intracerebroventricularly (ICV) prior to sacrifice at various time points ranging from 6h-4w post-CFPI. Cells containing dextran were considered membrane disrupted and were quantified throughout layers V and VI of the lateral neocortex. Within sham animals (Figure 1A), membrane disruption was rarely detected ($13.88\% \pm 3.25$ total neurons), however, rats sustaining TBI demonstrated significant membrane disruption (Figure 1; one way-ANOVA $F_{6,29}=8.20$ $p=3.1 \times 10^{-5}$). At 6h following injury (Figure 1B), over half of the total neurons assessed demonstrated membrane disruption ($52.29\% \pm 3.73$ total neurons; $p=2.34 \times 10^{-4}$ vs. sham). At 1d and 3d post-injury (Figure 1C & D), membrane disruption remained significantly elevated (1d: $37.94\% \pm 5.66$, $p=0.013$ vs. sham and 3d: $39.23\% \pm 6.39$ total neurons, $p=0.012$ vs. sham, respectively). At 1w post-CFPI (Figure 1E), though, the number of neurons that were disrupted declined to levels indistinguishable from sham, ($32.32\% \pm 4.99$, $p=0.233$ vs. sham). However, late (Figure 1F & G) membrane disruption resurged to levels similar to that observed hours-days post-CFPI, (2w: $51.19\% \pm 6.08$, $p=1.37 \times 10^{-4}$ vs. sham and 4w: $52.02\% \pm 5.39$, $p=9.80 \times 10^{-5}$ vs. sham). It was also noted that the intensity of tagged dextran within the parenchyma was drastically increased in injured animals as compared to sham (Figure 1).

Chronic membrane disruption is associated with a transient shift toward a NeuN negative phenotype

Membrane disrupted cells that didn't label with NeuN were also quantified in sham controls and at 6h-4w post-TBI (Figure 1). Very few NeuN- membrane disrupted cells were present in sham injured rats ($1.10 \pm 0.27\%$ of total neurons; Figure 1A). However, a NeuN- membrane disrupted subpopulation was present within the lateral neocortex of animals following CFPI (one way-ANOVA $F_{6,29}=0.604$, $p=0.020$). While the percent of total membrane disrupted cells that displayed this NeuN- phenotype were not significantly different from sham sub-acutely (6h= $12.94 \pm 3.07\%$; 1d= $7.70 \pm 1.861\%$; 3d= $7.56 \pm 2.09\%$; 1w= $12.53 \pm 3.30\%$), or at the 4w time point ($13.11 \pm 4.19\%$), at 2w post-injury there was a significant shift in the late membrane disrupted population towards a NeuN- phenotype ($19.99 \pm 6.25\%$, $p=0.007$ vs. sham).

NeuN negative membrane disrupted cells are not glia

The presence of a transient shift towards this NeuN- subpopulation of late membrane disrupted cells indicated the possibility of passing glial membrane disruption. Therefore, 2w post-injury tissue was probed with various glial markers including GFAP for astrocytes, CC-1 for oligodendrocytes, Iba-1 for microglia, and NG2 for NG2 cells, to assess possible overlap with the NeuN- late membrane disrupted subpopulation. There were no indications of substantial membrane disruption within astrocytes (0.37 membrane disrupted somas/ 0.44 mm^2 , Figure 2A), oligodendrocytes, (0.10 membrane disrupted somas/ 0.44 mm^2 , Figure 2B), microglia (0.57 membrane disrupted somas/ 0.44 mm^2 , Figure 2C), or NG2 cells (1.23 membrane disrupted somas/ 0.44 mm^2 , Figure 2D), indicating that the NeuN- late membrane disrupted subpopulation are likely neurons.

Cortical NeuN protein expression does not change following TBI

The overall expression of NeuN within the lateral neocortex was also evaluated for changes following CFPI. Investigation of NeuN protein expression was conducted in sham and TBI rats throughout the 6h to 4w post-injury time course. Western blot analysis revealed

consistent NeuN protein levels in sham animals ($100.00 \pm 2.29\%$) and TBI animals at 6h ($110.28 \pm 2.22\%$ of sham), 1d ($108.11 \pm 5.53\%$ of sham), 3d ($116.58 \pm 7.12\%$ of sham), 1w ($112.22 \pm 5.53\%$ of sham), 2w ($100.26 \pm 8.71\%$ of sham), and 4w ($102.07 \pm 11.09\%$ of sham) post-CFPI (Figure 3; one-way ANOVA $F_{6,23}=1.036$, $p=0.428$).

Late membrane disruption is not associated with cell death/loss post-CFPI

As previous studies have shown that membrane disruption could lead to cell death, TUNEL was done to assess DNA damage indicative of late-stage cell death out to 4w post-CFPI. In agreement with the literature and our previous study using the CFPI model in rats (Gorse & Lafrenaye, 2018; Greer et al., 2011; Lafrenaye et al., 2012; Lifshitz et al., 2007; Witcher et al., 2018) there was no difference in the number of TUNEL positive cells among sham animals compared to timepoints post-CFPI (Figure 4A-G; Kruskal Wallis mean rank comparison $\chi^2=5.713$, $p=0.456$). Further assessment for potential cell loss was performed with H&E staining of sham and injured rats. Again, in agreement with the literature and our previous studies (Gorse & Lafrenaye, 2018; Greer et al., 2011; Lafrenaye et al., 2012, 2014; Witcher et al., 2018), there was no significant difference in overall neuronal numbers within layers V and VI of the lateral neocortex (Figure 4H; Kruskal Wallis mean rank comparison, $\chi^2=11.580$, $p=0.072$).

Additionally, ultrastructural analysis of membrane disrupted neurons, as identified by immunoelectron microscopy against the dextran was used to further scrutinize potential subcellular alterations indicative of cell damage/death in both the sub-acutely and late membrane disrupted populations ((Farkas et al., 2006; Lafrenaye et al., 2012); Figure 5). In agreement with our previous assessments, a subset of membrane disrupted neurons, particularly those with both plasmalemmal and nuclear membrane disruption at 6h following CFPI, demonstrated some ultrastructural changes, such as organelle vacuolization, which indicated organelle pathology, and nucleolar holes, which potentially indicates altered nucleolar activity ((Macovei et al., 2018) Figure 5B). However, the majority of membrane disrupted neurons, did not demonstrate the

ultrastructural characteristics of actively dying cells, including mitochondrial change, pyknosis, or extreme vacuolization, indicating that membrane disrupted neurons were not progressing to cell death (Figure 5C-F). The ultrastructural features of the membrane disrupted cells were also characteristic of neurons but not of glial cells (Figure 5).

The lateral neocortex contains a subpopulation of NeuN negative neurons regardless of injury

To assess the possibility that there was a general shift toward the NeuN- phenotype in the lateral neocortex at 2w post-injury, regardless of membrane disruption, the total NeuN+ and NeuN- neuronal populations were quantified following CFPI using immunohistochemistry against NeuN paired with H&E staining (Figure 6). As expected, a sub-population of NeuN- neurons was apparent in layers V and VI of the lateral neocortex at 2w post-injury ($19.76 \pm 2.75\%$ total neurons/ROI). However, there was also a NeuN- subpopulation at 6h ($24.47 \pm 1.91\%$), 1d ($26.51 \pm 2.74\%$), 3d ($28.59 \pm 2.25\%$), 1w ($25.06 \pm 1.10\%$), and 4w ($21.59 \pm 0.85\%$) following CFPI (Figure 6). Surprisingly, the proportion of neurons with a NeuN- phenotype was comparable with that seen within the lateral neocortex of sham controls ($22.64 \pm 1.83\%$; one-way ANOVA, $F_{6,35}=1.930$, $p=0.10$), demonstrating that this NeuN- subpopulation of neurons is a consistent phenomenon in rats.

Discussion

The current study demonstrates active neuronal membrane disruption weeks following diffuse TBI that appears to involve a shift in neuronal sub-population phenotype not seen in the membrane disrupted neurons at earlier time points. Specifically, membrane disruption following CFPI potentially occurs in a biphasic fashion, producing significant membrane disruption sub-acutely hours to days post-injury and weeks post-injury that are temporally segregated by a reduction at 1w post-injury. We also observed a difference in the intensity of dextran within the parenchyma, potentially indicating additional issues with clearance mechanisms following CFPI.

Based on *in vitro* studies demonstrating the lack of cellular dextran uptake in non-injured cultures despite the presence of dextran in the media, it is likely that while potential changes in dextran clearance and neuronal membrane disruption may be occurring concurrently, they do not appear to be interdependent (Cullen et al., 2011; Geddes et al., 2003). The possible change in parenchymal clearance of dextran is an intriguing finding and will be further probed in future studies. Membrane disruption, however, has been demonstrated in various models of TBI, both *in vitro* using cell stretch models and *in vivo* following focal brain and spinal cord injury as well as after diffuse TBI (Choo et al., 2007; Cullen et al., 2011; Farkas et al., 2006; Geddes et al., 2003; Halford et al., 2017; Lafrenaye et al., 2012, 2014; LaPlaca et al., 2019; Levine et al., 2016; Singleton & Povlishock, 2004; Whalen et al., 2008).

Membrane disruption following trauma is primarily attributed to the mechanical force of injury directly altering membrane integrity, known as “mechanoporation” (Farkas et al., 2006; Geddes et al., 2003; Halford et al., 2017; Kilinc et al., 2008; LaPlaca et al., 1997; Laplaca & Prado, 2010; LaPlaca & Thibault, 1998; Levine et al., 2016; Singleton & Povlishock, 2004)). Studies from the LaPlaca and Wanner labs found that mechanoporation, in both neurons and glia, is highly dynamic, occurring within seconds of injury and fluctuating for minutes post-insult (Cullen et al., 2011; Halford et al., 2017; Laplaca & Prado, 2010; Levine et al., 2016). Additional studies, both *in vitro* and in various animal models of injury, have demonstrated sub-acute neuronal membrane disruption occurring hours to days following the initial mechanical insult (Cullen et al., 2011; Farkas et al., 2006; Geddes et al., 2003; Lafrenaye et al., 2012, 2014; LaPlaca et al., 1997; Singleton & Povlishock, 2004; Whalen et al., 2008)). This study, however, is the first to demonstrate a late phase of diffuse neuronal membrane disruption weeks following the initial mechanical injury. Based on the reduction in active membrane disruption at 1w post-injury, it appears that late diffuse membrane disruption is not directly attendant to either mechanoporation or membrane disruption occurring hours to days following trauma.

It has been widely theorized that membrane disruption would inevitably progress to cell death. Uncontrolled calcium influx and dysregulation of ATP capable of acute cellular damage and progression to cell death has been demonstrated to occur immediately following mechanoporation *in vitro* (Geddes et al., 2003; LaPlaca et al., 1997; LaPlaca & Thibault, 1998; Levine et al., 2016). Following focal injury in a mouse model of TBI all mechanoporated and sub-acutely membrane disrupted neurons labeled with the membrane impermeable irreversible DNA binder, propidium iodide, were lost within the first week of injury, supporting the idea that membrane disruption is a terminal cellular pathology (Mbye et al., 2012). However, as focal and diffuse pathological progressions are distinct, and based on our previous and current findings, it appears that a different progression is occurring in the sub-acutely membrane disrupted populations following diffuse TBI as compared to the progression of these same cells in focal TBI models (Figure 1, (Abu Hamdeh et al., 2018; Lafrenaye et al., 2012)). In this study, the unchanged total neuronal count throughout the temporal profile post-injury (Figure 4) and lack of ultrastructural characteristics indicative of late-stage apoptosis or necrosis (Figure 5), demonstrate that neurons are not dying in the lateral neocortex up to 4w following CFPI. The lack of cell death is in alignment with other studies utilizing the CFPI model of diffuse TBI (Greer et al., 2011; Lifshitz et al., 2007; Witcher et al., 2018). Although these membrane disrupted neurons do not appear to progress to cell death following diffuse TBI alone, our previous data suggests that these cells are potentially more susceptible to secondary insults, which, paired with diffuse TBI, can result in significant cell loss (Lafrenaye et al., 2014). A possible mechanism for this increased susceptibility of diffusely membrane disrupted neurons is Cathepsin B mislocalization, as indicated by our previous studies, however, further investigation into this possibility is needed (Lafrenaye et al., 2012)

The occurrence of membrane disruption both hours to days and weeks to a month post-CFPI with a significant reduction in active membrane disruption visualized at 1w post-injury, indicates that diffuse neuronal membrane disruption occurs biphasically. As the survival time points were randomly assigned we cannot ignore the possibility that the reduction in membrane

disruption at 1w post-CFPI may be an artifact of slightly reduced injury intensity in animals survived to that end point. An alternative possibility is that at least sub-acutely membrane disrupted neurons undergo membrane resealing following diffuse TBI (Figure 1). Membrane resealing of mechanoporated and sub-acutely membrane disrupted neurons has been identified in various models using multiple membrane-impermeable tracers administered at pre and various post-injury time-points (Cullen et al., 2011; Farkas et al., 2006; Geddes et al., 2003; Lafrenaye et al., 2012, 2014; Whalen et al., 2008). Heterogeneity within the mechanoporated population, in which neighboring neurons demonstrated variable levels of susceptibility to membrane disruption and capacity for subsequent membrane resealing was also seen *in vitro* (Laplaca & Prado, 2010). Therefore, it is highly likely that the sub-acutely membrane disrupted neurons in the current study retain the capability to reseal their membranes, which may explain the reduction in membrane disruption seen at 1w following CFPI.

Moreover, we also observed a significant increase in the proportion of late membrane disrupted neurons that lacked expression of the traditional mature neuronal marker, NeuN (Figure 1). Previous studies have demonstrated that glia, and specifically astrocytes, are susceptible to membrane disruption within neural-astrocyte co-cultures and enriched astrocyte cultures following stretch injury (Cullen et al., 2011; Halford et al., 2017; Levine et al., 2016). However, *in vivo* this has only been recapitulated in a model of spinal cord injury in swine (Halford et al., 2017) but was not observed following focal brain injury in rodents (Laplaca & Prado, 2010). In agreement with the previous rodent brain injury study, we did not observe any significant glial membrane disruption at any time point following CFPI (Figure 2). This may be due to species differences, as we have previously reported species-dependent TBI-induced glial alterations (Gorse & Lafrenaye, 2018). It could also be due to the ability of astrocytes to rapidly reseal their membranes, as demonstrated *in vitro* (Laplaca & Prado, 2010). However, ultimately our findings demonstrate that the NeuN- subpopulation of membrane disrupted cells are most likely neuronal.

In various studies NeuN was shown to be expressed exclusively by post-mitotic neurons throughout the brain and spinal cord (Mullen et al., 1992; Wolf et al., 1996). Due to this neuron-specific expression, NeuN has been widely used as a marker of mature neurons within the central nervous system and has been utilized to assess the number of neurons in various brain regions during development and following injury/pathologies (Giannaris & Rosene, 2012; Hahn et al., 2015; Morin et al., 2011; Sedmak & Judaš, 2019; Sugawara et al., 2002; Weyer & Schilling, 2003; Wolf et al., 1996; Zimatkin & Karnyushko, 2017). There are, however, subsets of neurons that don't express NeuN, including cerebellar Purkinje cells, olfactory mitral cells, retinal photoreceptor, and inner granule cells as well as some neurons in the superchiasmatic nucleus and substantia nigra (Cannon & Greenamyre, 2009; Morin et al., 2011; Mullen et al., 1992; Wolf et al., 1996). There is a possibility that the NeuN- neuronal subpopulation belongs to a certain NeuN- neuronal subtype; a possibility that will be thoroughly investigated in future studies. To our knowledge, however, this is the first study to quantify NeuN- cells morphologically identified as neurons within the adult rat cortex following diffuse brain injury. Surprisingly, we found a consistent neuronal subpopulation exhibiting a NeuN- phenotype that were diffusely dispersed throughout layers V and VI of the lateral neocortex. This NeuN- subpopulation comprised approximately 30% of the total lateral cortical neurons identified in both sham and injured animals and was consistent from hours to weeks post-CFPI (Figure 6). Taken together with the significant increase in the membrane disrupted NeuN- subpopulation 2w post-CFPI, this could indicate that NeuN- neurons within the cortex are more susceptible to late, but not sub-acute membrane disruption. It is also possible that NeuN- neurons are particularly sensitive to injury intensity, as the 2w survival group had a slightly higher level of injury. The reduction in the NeuN- subpopulation to levels consistent with sham and sub-acutely membrane disrupted neurons by 4w post-injury further suggests that at least some of these susceptible NeuN- neurons undergo membrane resealing.

Reduction of NeuN expression without correlative cell death could also indicate neuronal compromise and/or issues with proper neuronal maturation, as was proposed following sudden

infant death syndrome and/or sudden intrauterine unexplained death syndrome (Lavezzi et al., 2013). NeuN, which was identified as RNA-binding Fox-3 (Rbfox3), has been theorized to play a role in neuronal development by regulating neuron-specific alternative gene splicing (Jacko et al., 2018; Kim et al., 2013). Following ischemic injury, Ünal-Çevik and colleagues observed reduced NeuN labeling without correlative changes in NeuN protein expression, however, they did not quantify the NeuN- population (Ünal-Çevik et al., 2004). Another study found a population of medullary respiratory neurons displaying a NeuN- phenotype following a cervical spinal cord hemisection that co-expressed with markers of axonal regeneration, suggesting that these NeuN- neurons could play an ameliorative role following injury (Darlot et al., 2017). Therefore, it is possible that the NeuN- population could represent reversion to a growth-permissive immature state following diffuse TBI, however, that is currently speculative and would require additional follow-up studies to rigorously evaluate this possibility.

Taken together, the findings presented here highlight the complexity of TBI-induced neuronal membrane disruption. Neuronal membrane disruption can occur much later than previously thought and involves subpopulations of cortical neurons demonstrating both NeuN+ and NeuN- phenotypes. Due to its biphasic nature, late membrane disruption appears to be distinct from mechanoporation and sub-acute membrane disruption. Additionally, this study indicates that membrane disruption, either acute or late, maintains the capacity for membrane repair and therefore potential therapeutic amelioration over a broad post-injury timeframe. Gaining a better understanding of TBI-induced membrane disruption could lead to the discovery of novel treatments to reduce morbidity associated with diffuse pathology in the human population.

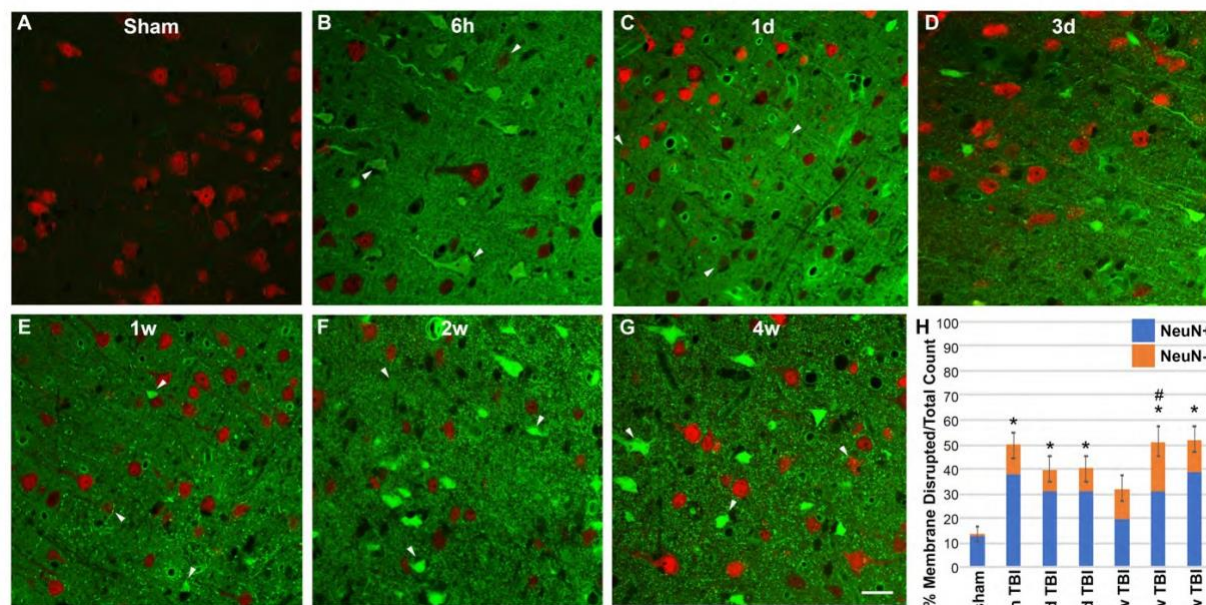


Figure 1.1. TBI-induced membrane disruption occurs biphasically and involves a NeuN negative subpopulation. **(A-G)** Representative photomicrographs of lateral neocortex from animals sustaining either **(A)** sham injury or **(B-G)** CFPI at **(B)** 6h, **(C)** 1d, **(D)** 3d, **(E)** 1w, **(F)** 2w, and **(G)** 4w post-injury. Neurons expressing NeuN are in red. Cells containing the cell-impermeable fluorescent-conjugated dextran (green) were considered membrane disrupted (arrow heads). **(H)** Bar graph depicting the mean percentage of membrane disrupted neurons per total number of neurons analyzed. Note that while hardly any membrane disruption was seen in shams, robust membrane disruption occurred both 6h-3d and 2-4w post-CFPI. While the majority of membrane disrupted neurons expressed NeuN (NeuN+; blue bars), a population of membrane disrupted cells that were not labeled with NeuN (NeuN-, orange bars) emerged following CFPI. This NeuN-membrane disrupted subpopulation was significantly pronounced at 2w post-CFPI. Data presented as mean±S.E.M. * $p < 0.05$ percent of total membrane disrupted cells compared to sham, # $p < 0.05$ percent NeuN- membrane disrupted cells compared to sham. Scale bar=20μm

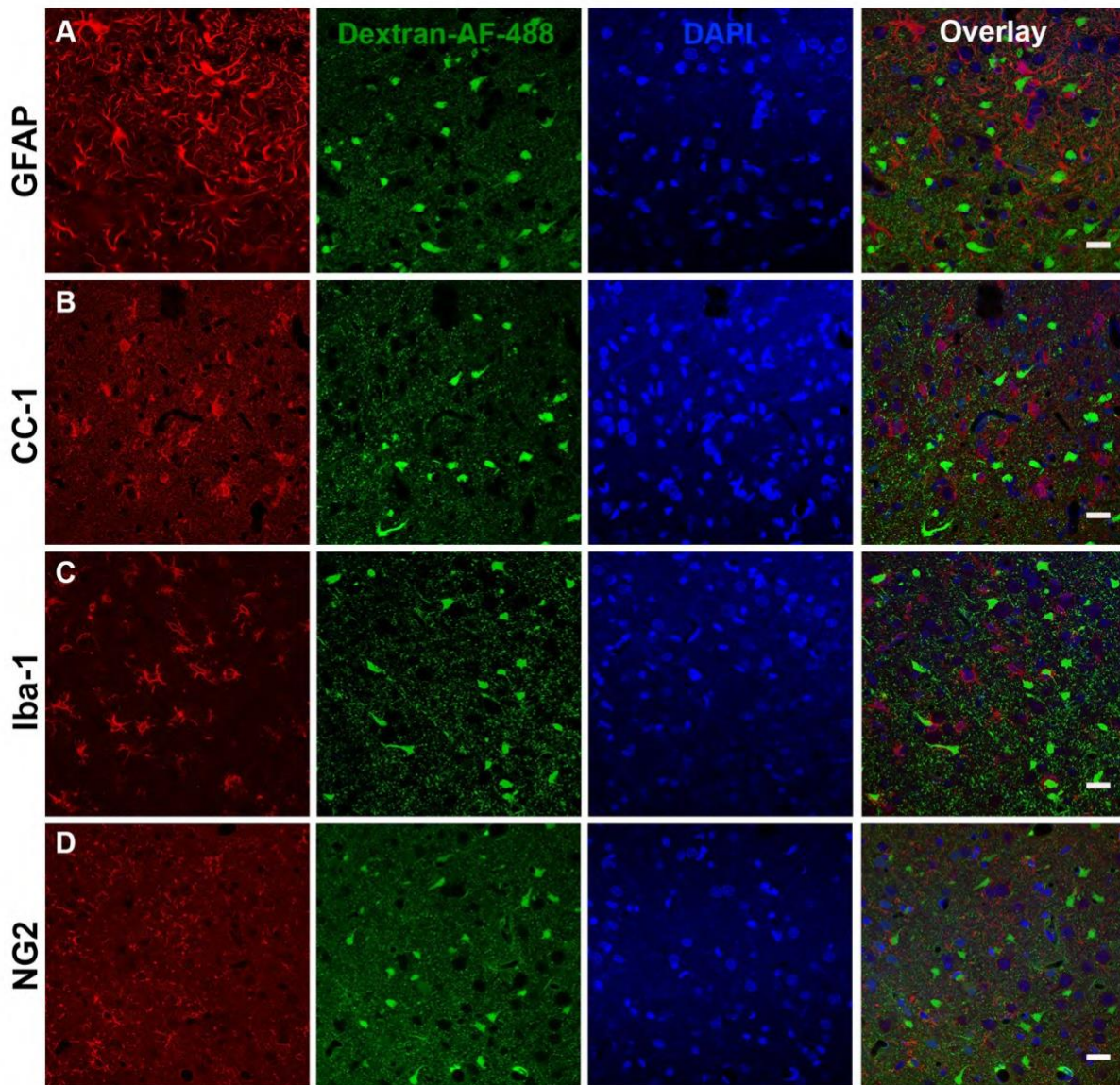


Figure 1.2. Glia do not appear to be membrane disrupted following CFPI. Representative photomicrographs of the lateral neocortex 2w following CFPI labeled with **(A)** GFAP (astrocytes), **(B)** CC-1/APC (oligodendroglia), **(C)** Iba-1 (microglia), and **(D)** NG2 (NG2 cells) (far left panel; red). Membrane disrupted cells containing Alexa-488 conjugated dextran (green) are represented in the second panel. The third panel in blue are DAPI labeled nuclei. The last panel is the overlay images. Arrows depicted cells labeled with each representative marker in relation to the

membrane disrupted cells (arrowheads). Note that there were no indications of glial cells sustaining membrane disruption at 2w post-injury. Scale bar= 20 μ m.

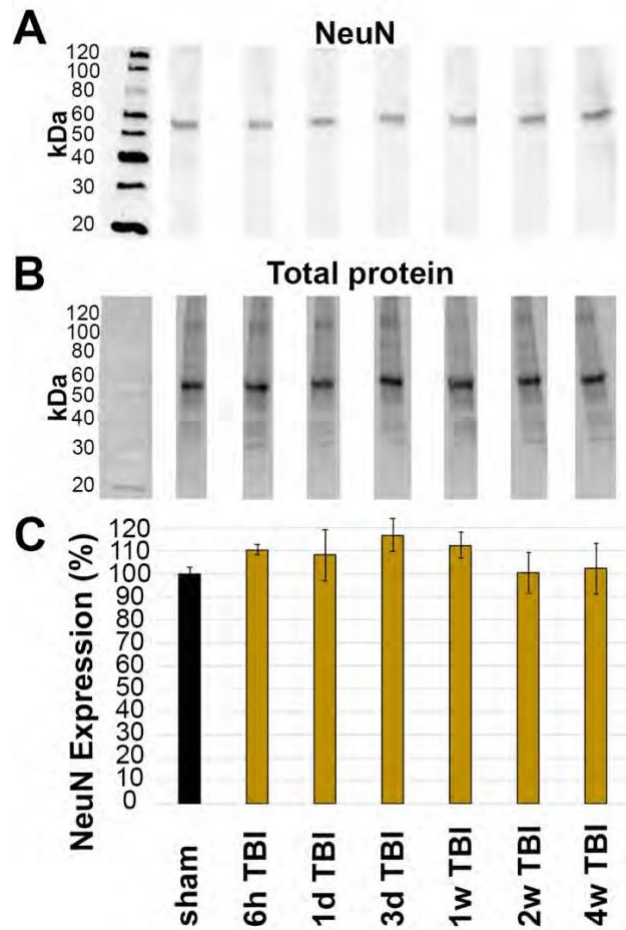


Figure 1.3. Expression of NeuN did not change in the lateral neocortex after TBI. Western blot analysis of **(A)** amount of NeuN protein (band at ~50kDa) in lateral neocortical homogenates normalized to **(B)** total loaded protein. **(C)** Bar graph depicting the average percent change in NeuN expression in TBI rats at 6h-4w post-CFPI as compared to sham. Notice that there was no difference between sham and CFPI at any timepoint, denoted as mean \pm S.E.M.

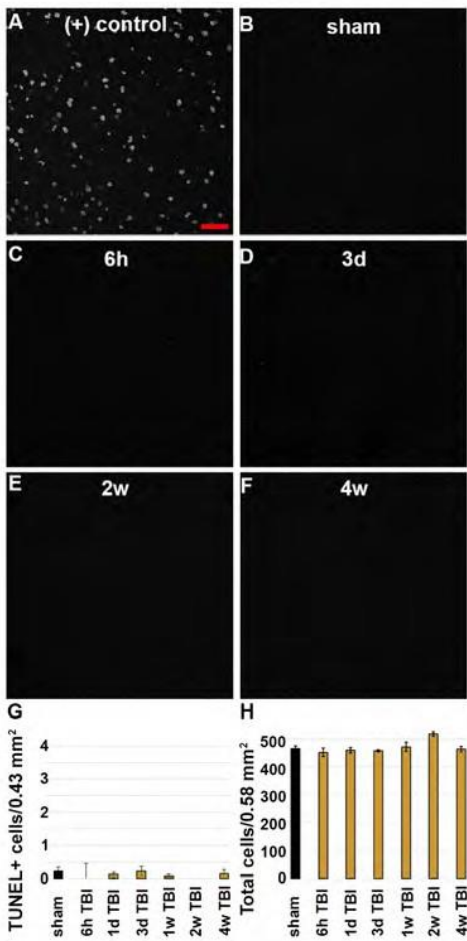


Figure 1.4. There is no indication of cell death in the lateral neocortex following CFPI. Representative micrographs depicting **(A)** sham and **(B)** 6h, **(C)** 3d, **(D)** 2w, or **(E)** 4w post-CFPI labeled for DNA damage using TUNEL. **(F)** TUNEL was verified using a DNase-treated positive control. Bar graphs depicting the average number of **(G)** TUNEL+ cells or **(H)** cells in general in layers V and VI of the lateral neocortex following sham (black bar) or CFPI (yellow bars) at 6h-4w post-injury. Note that there were very few TUNEL+ cells and no cell loss found in the lateral neocortex at any timepoint following injury. Scale bar= 50 μ m.

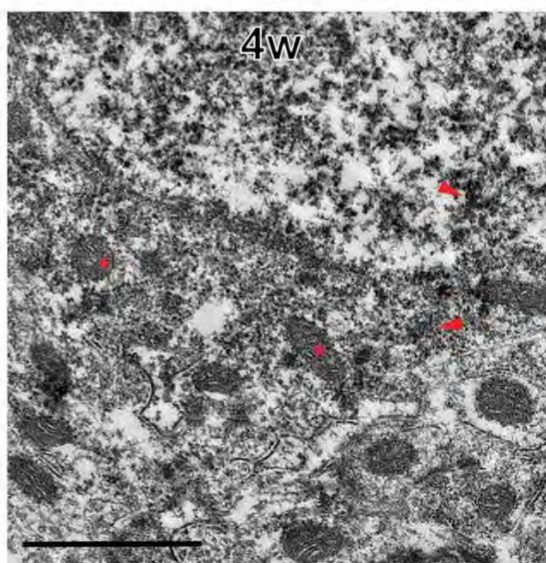
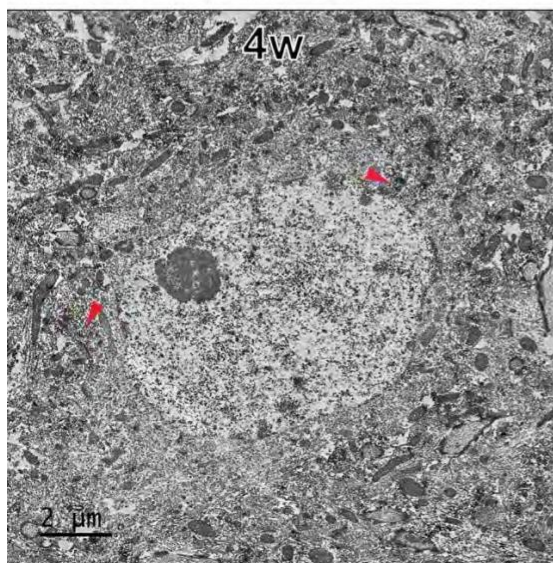
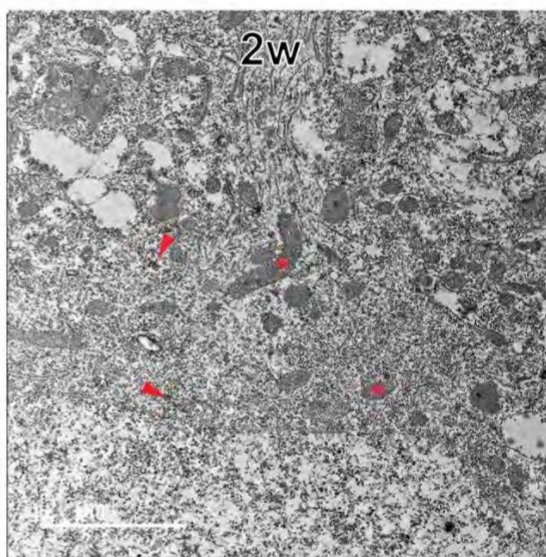
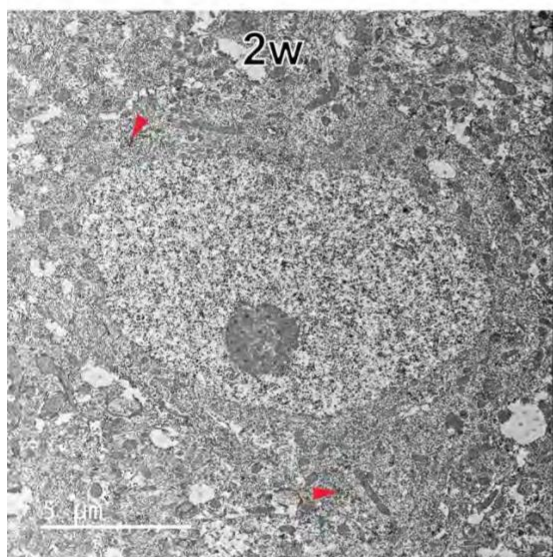
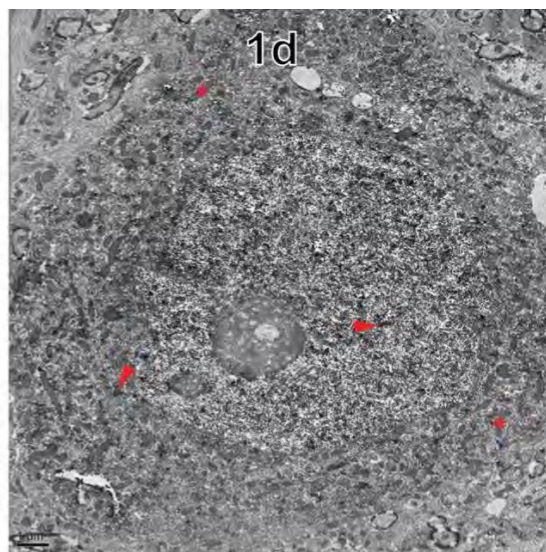
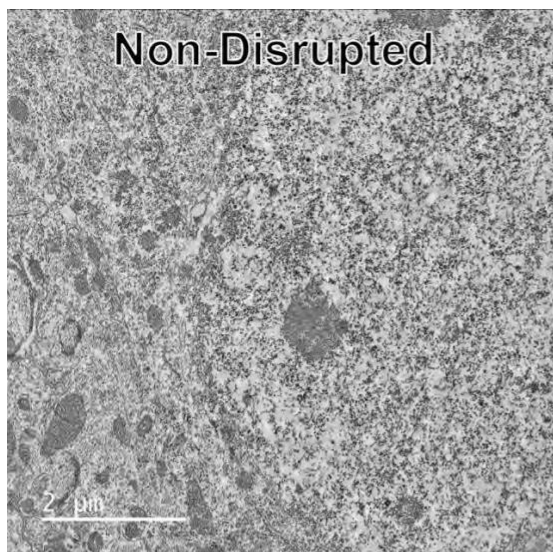


Figure 1.5. Neurons sustaining membrane disruption weeks post-injury display few signs of ultrastructural damage indicative of cell death. Representative electron micrographs of **(A)** non-membrane disrupted neurons and neurons sustaining membrane disruption sub-acute at **(B)** 1d and chronically at **(C-D)** 2w and **(E&F)** 4w post-injury. Some membrane disrupted neurons, particularly those that contained dextran (arrow heads) within both the cytoplasm and nucleus (N) at sub-acute time points, demonstrated ultrastructural changes, such as organelle vacuolization (v) and occasional holes (h) within the nucleolus (nl), indicative of enhanced nucleolar activity. However, the majority of late membrane disrupted neurons were largely unremarkable with no overt mitochondrial damage (*) and, in cases, intact nuclear envelope (NE). These features are better observed in the enlarged panels **(D and F)**.

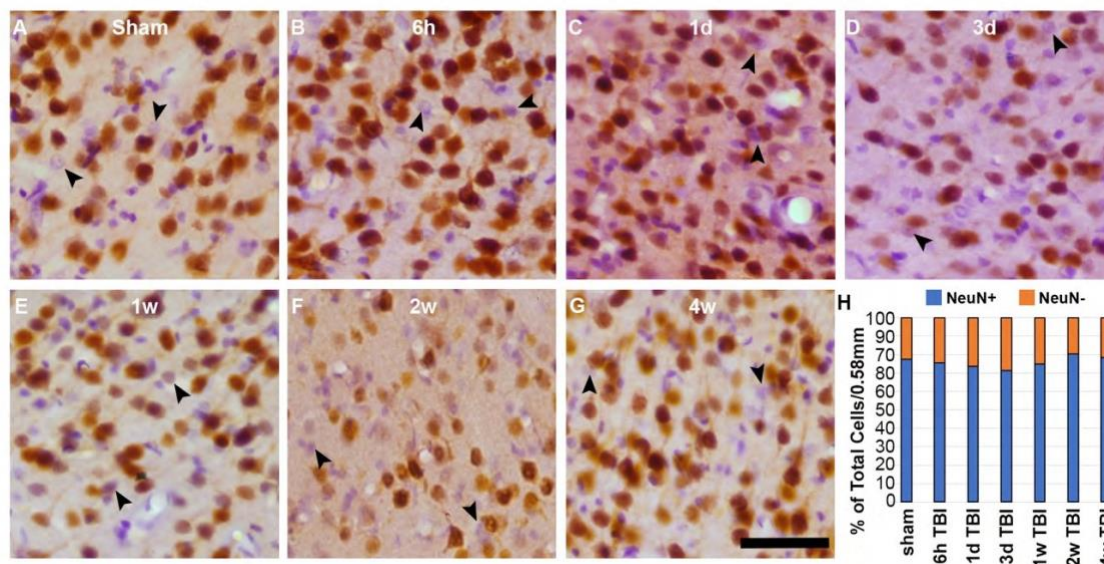


Figure 1.6. There is a consistent NeuN- subpopulation in layers V and VI of the lateral neocortex. Representative photomicrographs of cortices labeled with NeuN (brown) and counterstained with H&E (purple and pink respectively) from **(A)** sham-injured rats and rats at **(B)** 6h, **(C)** 1d, **(D)** 3d, **(E)** 1w, **(F)** 2w, or **(G)** 4w after sustaining a CFPI. Glial cells with smaller cell bodies and nuclei, were not counted. Neurons that do not label for NeuN (NeuN- neurons) are indicated by the arrow heads. **(H)** Stack graph depicting the percent of NeuN+ (blue bars) and NeuN- (orange bars) neurons in layers V and VI of the lateral neocortex in sham and CFPI rats. Interestingly, there was a consistent NeuN- subpopulation in all animals regardless of injury. Scale bar= 50 μ m.

Chapter 2: Investigating the Immaturity Phenotype of the NeuN- Membrane Disrupted Subpopulation

Introduction

Neuronal membrane disruption is an understudied and captivating diffuse pathology defined by holes in the membrane that initially arise as a result of damage to the neuronal plasmalemma. Intriguing findings from our lab demonstrate that active membrane disruption occurs for weeks following diffuse TBI. Interestingly, we also found a novel subpopulation of membrane disrupted cortical neurons that did not express the traditional marker of mature neurons, NeuN, particularly at 2w post-injury(Hernandez et al., 2019). Subsequent cell death, however, has not been observed in the membrane disrupted neurons in our model of diffuse TBI out to 4w post-injury, revealing a rather long potential therapeutic window.

Previous studies have shown that neuronal reversion to an immature phenotype, in which NeuN is not expressed, is a potential compensatory mechanism following injury. A previous study found that a medullary respiratory neuronal subpopulation lost NeuN expression following axonal transection (Darlot et al., 2017). This loss of NeuN was associated with subsequent axonal regeneration, which suggests that the NeuN- population could be reverting to a growth-permissive immature state. Resection of facial motoneurons also demonstrated a loss of NeuN presentation at 3d that returned 28d post-injury(McPhail et al., 2004). Yet the role of the NeuN negative (NeuN-) membrane disrupted neurons remains unknown.

Therefore, we interrogated if the NeuN- subpopulation is reverting to an immature state to compensate for injury. One of those immature markers doublecortin (DCX). DCX is often associated with immature neurons and upregulated prior to the expression of NeuN and then begins to downregulate with NeuN increased expression(Brown et al., 2003; Francis et al., 1999; Gleeson et al., 1999; Zimatkin & Karnyushko, 2017). Additionally, an immediate early gene, cFos,

that which is usually used in the field for measuring neural activity it's also and is found to be upregulated following injury was also used to interrogate the NeuN- population.

Multiplexed immunohistochemistry for the 40 μ m sections against the mature neuronal marker, NeuN, and various immature neuronal markers, doublecortin (DCX), and cFos, was done as well as western blotting of the lateral neocortex of DCX and cFos.

Methods

Animals

Experiments were conducted using protocols in accordance with the Virginia Commonwealth University institutional ethical guidelines concerning the care and use of laboratory animals (Institutional Animal Care and Use Committee, Virginia Commonwealth University), which adhere to regulations including, but not limited to, those set forth in the Guide for the Care and Use of Laboratory Animals, 8th Edition (National Research Council). Animals were housed in individual cages on a 12h light-dark cycle with free access to food and water. Archived tissue and homogenates from our previous studies (Hernandez et al., 2019), adult male Sprague-Dawley rats, n=28 weighing 350– 450g were used for this study. Any animal that lost more than 20% of their pre-injury body weight or precipitated gross brain pathology (contusion, subdural hematoma, or gross tissue loss) was excluded from analysis. No animals met exclusion criteria in this study.

Surgical preparation and injury induction

Animals were anesthetized with 4% isoflurane in 30% O₂ and 70% N₂O then intubated and ventilated with 2% isoflurane in 30% O₂ and 70% N₂O throughout the duration of the surgery, injury, and post-injury physiological monitoring. Heart rate, respiratory rate, and blood oxygenation were monitored via a hind-paw pulse oximetry sensor (STARR Life Sciences, Oakmont, PA) for the duration of anesthesia, except during the induction of injury. Body

temperature was maintained at 37°C with a rectal thermometer connected to a feedback-controlled heating pad (Harvard Apparatus, Holliston, MA). All animals were placed in a stereotaxic frame (David Kopf Instruments, Tujunga, CA). A midline incision was made, and a 4.8 mm circular craniectomy was made along the sagittal suture midway between bregma and lambda for injury induction. A 2mm burr hole was also drilled in the left parietal bone overlying the left lateral ventricle (0.8 mm posterior, 1.3 mm lateral, and 2.5- 3 mm ventral to bregma) through which a 25-gauge needle, connected to a pressure transducer and micro infusion pump (11 Elite syringe pump; Harvard Apparatus) via sterile saline filled PE50 tubing, was placed into the left lateral ventricle. Appropriate placement was verified via a 1.3 μ l/min infusion of sterile saline within the closed fluid-pressure system during needle placement (Sullivan et al., 1976). The needle was held in the ventricle for at least 5min to record pre-injury intracranial pressure (ICP). After the 5-min reading, the needle was slowly removed and the burr hole was covered with bone wax before preparation for sham or CFPI (Dixon et al., 1987a; Lafrenaye et al., 2014b). Briefly, a Leur-Loc syringe hub was affixed to the craniectomy site and dental acrylic (methyl-methacrylate; Hygenic Corp., Akron, OH) was applied around the hub and allowed to harden. Anesthetized animals were removed from the stereotaxic frame and injured at a magnitude of 2.05 ± 0.15 atmospheres and duration of ~22msec. The pressure pulse was measured by a transducer affixed to the injury device and displayed on an oscilloscope (Tektronix, Beaverton, OR). Immediately after the injury, the animal was reconnected to the ventilator and physiologic monitoring device and the hub and dental acrylic were removed en bloc. Gelfoam was placed over the craniectomy/injury site and the scalp was sutured. The animal was then replaced in the stereotaxic device and the ICP probe was reinserted into the lateral ventricle, as described above, for post-injury ICP monitoring. The animals were then allowed to recover and were returned to clean home cages. Identical surgical procedures were followed for sham-injured animals, without release of the pendulum to induce injury.

Tracer infusion

Two hours prior to sacrifice, tagged dextran (40mg/ml in sterile 0.9% saline; ~1.6mg/kg) was infused into the lateral ventricle as described previously (Lafrenaye et al., 2012b). Briefly, 15µl of 10kDa dextran conjugated to either 488-Alexa Fluor (Cat#: D22910, Invitrogen, Carlsbad, CA) or biotin (Cat#: D1956; Invitrogen, Carlsbad, CA) was infused into the left lateral ventricle at 0.5-1.3µl/min, with continuous ICP monitoring. To avoid bias caused by differences in fluorescent signal detectability animals were randomly assigned a tag (Alexa 488 or biotin). The tracer was allowed to diffuse throughout the parenchyma for 2h prior to transcardial perfusion at 1d, 1w, or 2w, post-sham or CFPI.

Tissue processing

At appropriate time-points between 1d and 2w post-injury, the animals were injected with 150mg/kg euthanasia-III solution (Henry Schein, Dublin, OH), then underwent transcardial perfusion with cold 0.9% saline. Lateral neocortices were dissected from the right hemisphere of the brain for molecular assessments of protein expression followed by a switch in transcardial perfusate to 4% paraformaldehyde/ 0.2% glutaraldehyde in Millonig's buffer (136mM sodium phosphate monobasic/109mM sodium hydroxide) to fix the left side of the brain for subsequent immunohistochemical or electron microscopic (EM) processing and analysis. After transcardial perfusion, the brains were removed, post-fixed for 24-48h, then sectioned coronally in 0.1M phosphate buffer with a vibratome (Leica, Banockburn, IL) at a thickness of 40µm from bregma to 4.0mm posterior to bregma. Sections were collected serially in 12 well-plates and stored in Millonig's buffer at 4°C. A random starting well (wells 1–12) was selected using a random number generator and four serial sections, were used for histological analyses. All histological analyses were restricted to layers V and VI of the lateral somatosensory neocortex extending from the area lateral to CA1 to the area lateral to CA3 of the hippocampus.

Western blotting

Lateral neocortices of sham n=6 and TBI rats n=6/time point were homogenized in NP40 Buffer (150 mM NaCl, 50 mM Tris pH 8.0, 1% Triton) and protease inhibitor cocktail (AEBSF 10.4mM, Aprotinin 8µM, Bestatin 400µM, E-64 140µM, Leupeptin 8µM, Pepstatin A 150µM, Cat#: P8340, Sigma, Saint Louis, MO). Protein concentrations were measured using a BCA Protein Assay Kit (Pierce Biotechnology, Thermo Fisher Scientific, Rockford, IL, Cat#: 23227). Protein (7.5 µg Doublecortin and 20 µg cFos) was boiled for 10min in 50mM dithiothreitol (Cat#: 1610610; Bio-Rad; Hercules, CA), 2x Laemelli loading buffer (Cat#: 1610737; Bio-Rad; Hercules, CA) and run at 200 Volts for 30min on Mini-PROTEAN TGX Stain-Free 4-20% precast polyacrylamide gels (Cat#: 4568096; Bio-Rad, Hercules, CA). Protein was transferred onto 0.45µm PVDF membranes using Bio-Rad Transblot Turbo transfer system using mixed molecular weight manufacturer setting (1.3-2.5 Amps, 25 Volts for 7min). Western blotting was done on an iBind flex apparatus (Invitrogen, Carlsbad, CA) using primary antibodies rabbit anti-Doublecortin(1:1000; Cat#: 4604S; RRID:AB_561007) and rabbit anti-cFos (1:1000; Cat#:4384S; RRID:AB_2106617) (Cell Signaling Technologies; Danvers, MA) and anti-rabbit-HRP secondary antibody (1:5000; Cat#: 111-030-003; Jackson ImmunoResearch Laboratories, West Grove, PA; RRID:AB_2313567) (Hahn et al., 2015). Total protein (Stain Free) and chemiluminescent images were taken on a ChemiDoc imaging system (BioRad). Densitometric analysis was done in ImageJ (National Institutes of Health; Bethesda, MD), and Doublecortin and cFos protein bands were normalized to total protein and a naïve control. All western blots were run in triplicates on three separate gels to reduce run-to-run variability, biasing the results.

Immature Histological Analyses

Doublecortin

Tissue slices from 1d, 1w, and 2w post-TBI animals n=6/timepoint, including sham n=3 (1/timepoint), containing tagged dextrans were blocked with 5% normal horse serum (NHS), 2% bovine serum albumin (BSA), and 1.5% triton-X for 2h, then incubated with rabbit anti-Doublecortin (DCX) (1:800; Cat#: 4604S; Cell Signaling Technologies; Danvers, MA; RRID:AB_561007) and mouse anti- NeuN (1:500; Cat#: MAB377; MilliporeSigma; Temecula, CA, RRID:AB_2298772) in 5% NHS/2% BSA/ 0.5% triton-X and Goat anti-biotin (1:2000; Cat#: 31852; Thermo Scientific, Rockford, IL, RRID:AB_228243) as needed for animals infused with biotin-conjugated dextrans, overnight at 4°C. The following day, the tissue was rinsed in 1% NHS/1%BSA/0.2% triton-X. Tissue was then incubated with Alexa-568 conjugated goat anti-rabbit (1:800; Cat#:A11036; Life Technologies, Eugene, OR; RRID:AB_2534102), Alexa-647 conjugated goat anti-mouse(1:700; Cat#:A32728; Life Technologies, Rockford, IL; RRID:AB_10563566) and Alexa-488 conjugated donkey anti-goat (1:700; Cat#:A11055; Life Technologies, Carlsbad, CA, RRID:AB_2534102) for 2h. These sections were stained with 1:500 dilution of NeuroTrace 435/455 blue fluorescent Nissl Stain (Life Technologies, Eugene, OR, Cat# N21479). The tissue was mounted onto slides using Vectashield Vibrance mounting medium with (Cat#: H-1700; Vector Laboratories, Burlingame, CA). Sections were analyzed by fluorescent optical sectioning microscopy using a Keyence BZ-X800 microscope (Keyence Corporation of America, Itasca, IL, USA). An investigator blinded to animal group during image acquisition and through the analysis. Three micrographs/regions of interest (ROIs) for each section were taken using a 40x objective; two random sections were assessed for each animal. The total number of DCX positive cells was counted and assessed for NeuN positivity in ImageJ using the cell counter plugin. The number of DCX+/NeuN+ per 0.098 mm² was averaged for each animal and compared to sham.

cFos

Tissue slices from 2w post-TBI animals n=6 and sham n=6, containing 488 dextrans were blocked with 5% NGS, 2% BSA, and 1.5% triton-X for 2h, then incubated with rabbit anti-cFos (1:500; Cat#:RPCA-cFos, EnCor Biotechnology Inc., Gainesville, FL; AB_2572236) and mouse anti- NeuN (1:500; Cat#: MAB377; MilliporeSigma; Temecula, CA, RRID:AB_2298772) in 5% NGS/2% BSA/ 0.5% triton-X overnight at 4°C. Tissue was then incubated with Alexa-568 conjugated goat anti-rabbit (1:800; Cat#:A11036; Life Technologies, Eugene, OR; RRID:AB_2534102), Alexa-647 conjugated goat anti-mouse(1:700; Cat#:A32728; Life Technologies, Rockford, IL; RRID:AB_10563566) for 2h. All labeled tissue was mounted using Vectashield hardset mounting medium with DAPI (Cat#: H-1500; Vector Laboratories, Burlingame, CA). Sections were analyzed by fluorescent optical sectioning microscopy using a Keyence BZ-X800 microscope (Keyence Corporation of America, Itasca, IL, USA). An investigator blinded to animal group during image acquisition and through the analysis. Three micrographs/regions of interest (ROIs) for each section were taken using a 40x objective; two random sections were assessed for each animal. The total number of cFos-positive cells was counted and assessed for NeuN positivity and membrane disruption in ImageJ using the cell counter plugin. The number of cFos+/NeuN+ and cFos/membrane disrupted cells per 0.098 mm² were averaged for each animal and compared to sham.

Statistical analysis

Data were tested for normality prior to utilizing parametric or non-parametric assessments, which were conducted in SPSS (IBM Corporation, Armonk, NY). Animal numbers for each group were determined by an a priori power analysis using effect size and variability previously observed in the lab when assessing pathology between sham and injured groups using the CFPI model, an alpha = 0.05, and a power of 80%. One-way analysis of variance (ANOVA) and Bonferroni post hoc test were performed for all between-group analyses, and non-normal data underwent Kruskal-Wallis multiple comparisons for between-group analyses. For the analyses that only had two

groups, a T-test was used. Non-normal data for two-group non-parametric analysis used a Mann-Whitney U testing to compare groups. Statistical significance was set to $p < 0.05$. Data are presented as mean \pm standard error of the mean.

Results

There are no changes in protein quantity for Doublecortin and cFos following TBI

The overall expression of DCX and cFos were interrogated within the lateral neocortex following CFPI. DCX and cFos protein expression was examined in sham (n=6) and TBI rats (n=6/timepoint) throughout the 1d to 2w post-injury time course. Western blot analysis revealed no statistically different DCX protein levels in sham animals ($168.15 \pm 52.50\%$) compared TBI animals at 1d ($94.11 \pm 26.45\%$), 1w ($107.96 \pm 35.93\%$), and 2w ($105.17 \pm 32.40\%$). (Figure 2.1.; Kruskal-Wallis $\chi^2 = 3.377$ $p = 0.337$). Similarly, cFos protein expression was not significantly different in between sham ($176 \pm 27.14\%$), and 1d ($163.07 \pm 11.65\%$), 1w ($166.08 \pm 8.10\%$), and 2w ($153.43 \pm 6.03\%$) post-CFPI. (Figure 2.3.; one-way ANOVA $F_{3,21} = 0.312$, $p = 0.817$).

NeuN cells are half immunopositive for Doublecortin and all cFos cells contain NeuN

Therefore, 1d, 1w, and 2w post-injury tissue was probed with immature neuronal marker DCX and immediate-early gene cFos, to assess whether the NeuN- *late* membrane disrupted subpopulation seen in (Hernandez et al. 2019) is reverting to an immature phenotype. Neuronal quantification of DCX positive (+) and NeuN positive (+) cells were sham ($56.73 \pm 5.91\%$), 1d (52.42 ± 4.68), 1w (50.24 ± 7.27), 2w ($53.10 \pm 3.28\%$); no difference was found between sham and the other injured timepoints related to the number of DCX+/NeuN+ cells, (Figure 2.2.) (one-way ANOVA $F_{3,12} = 0.198$, $p = 0.90$). DCX+ cells that also are NeuN negative(-) percentages were sham ($44.73 \pm 5.03\%$), 1d (52.46 ± 2.64), 1w (49.76 ± 7.27), 2w ($46.90 \pm 3.28\%$) per 0.098mm^2 within the lateral neocortex. No differences were found in the amount of DCX+/NeuN- percentages in sham

compared to the other injured timepoints (Figure 2.4.) (one-way ANOVA $F_{3,12}=0.307, p=0.82$). Neuronal quantification of cFos positive (+) and NeuN positive (+) cells were as reported: sham ($98.94\pm0.23\%$) and 2w ($99.44\pm0.53\%$); no differences were found between sham and 2w-injured animals (Mann-Whitney U, $U=22.00, p=0.589$). and cFos + cells that also are membrane disrupted: sham ($46.69\pm4.11\%$) and 2w ($41.97\pm10.24\%$) per 0.098mm^2 within the lateral neocortex. (T-test $t(10)=0.57, p=0.58$)

Discussion

Overall, no changes were found and doublecortin (DCX) or cFos protein levels in sham compared to injured animals at 1d, 1w, and 2w. These same animals from chapter 1 and 2 demonstrated no changes in the NeuN, Cath B, Bak/Bcl-XL or AIF westerns. The lack of protein changes globally in the lateral neocortex may result from the nature of diffuse injuries, presenting a technical challenge to detect cellular subpopulation discrepancies (Hernandez et al., 2019, 2022; Ryu et al., 2021, 2022). Reflecting on the immunohistological studies of DCX: the percentage of DCX and NeuN positive cells (NeuN+) and DCX and NeuN negative are not actually significantly different between sham, 1d, 1w, and 2w in layers V and VI of the lateral neocortex. About half of all DCX-positive cells also have NeuN. Qualitatively, we rarely see membrane disrupted DCX + cells. Therefore, it cannot be said that these NeuN- membrane disrupted cells are reverting to an immature phenotype containing DCX. Astrocytes can also label with DCX (Coomans et al., 2021; Verwer et al., 2007). Originally, I excluded astrocytes from the membrane disrupted population, after I looked for colocalization between GFAP and membrane disruption. I found no colocalization. However, more recent studies have found that astrocytes are heterogenous and do not always label for GFAP (Escartin et al., 2021; Shandra et al., 2019). Membrane-disrupted astrocytes have been found in other studies using rats and pigs (Cullen et al., 2011; Levine et al., 2016).

I also evaluated cFos by immunolabelling sham and 2w injured tissue, as cFos is not just a marker for neuronal activity, but also an immediate-early gene (Gonzales et al., 2020; S. Kim et al., 2018). We saw no differences between sham and injury when it came to NeuN+/ cFos colocalization, the NeuN+ and cFos+ populations virtually overlapped. My other finding from that experiment was that only half of membrane disrupted neurons labeled with cFos. Therefore, I could conclude that cFos was not an ideal marker for the NeuN- membrane disrupted population. A limitation of this cFos histological analysis is that the injured and sham 2w animals were given DMSO. The membrane disrupted cFos positive percentages may be overestimated in the sham animals, considering DMSO alters membrane permeability.

Upon investigation, a NeuN- membrane disrupted population of neurons was observed to be present at all post-injury time points and were found to be significantly increased at 2w post-CFPI (Hernandez et al., 2019). However, protein assessments did not reveal differences in NeuN expression in the lateral neocortex at any time following injury. This result indicates that the changes in NeuN could be occurring within a small subpopulation that would not be discernable with an evaluation of overall NeuN expression within the cortex.

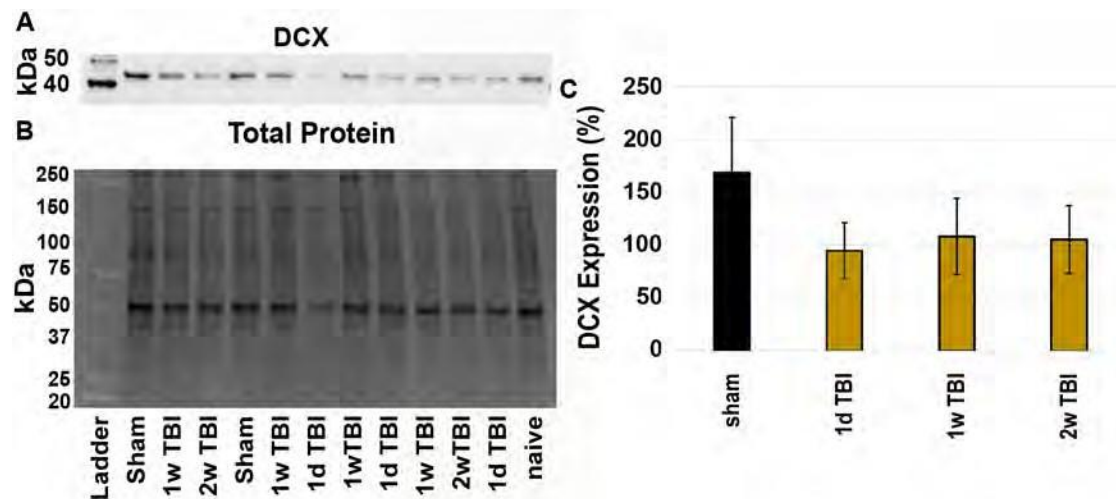
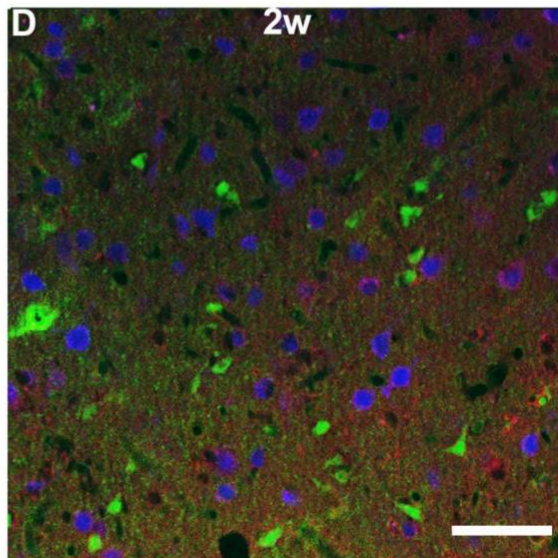
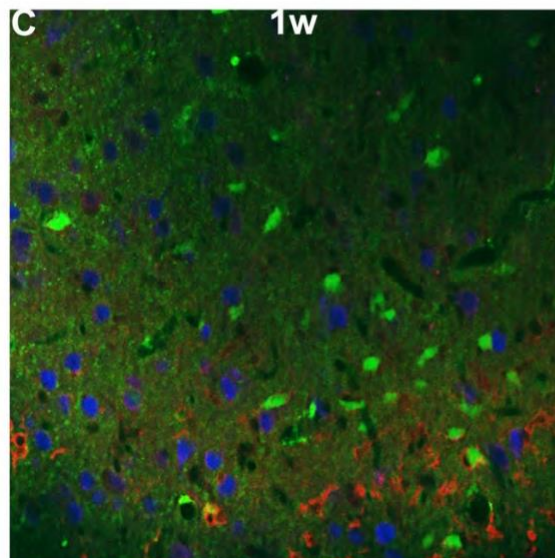
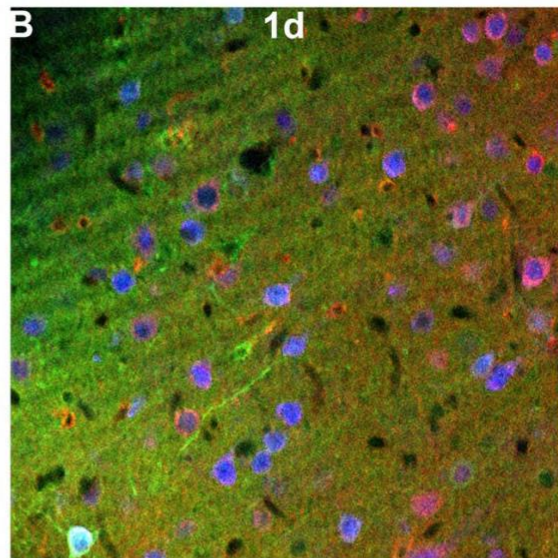
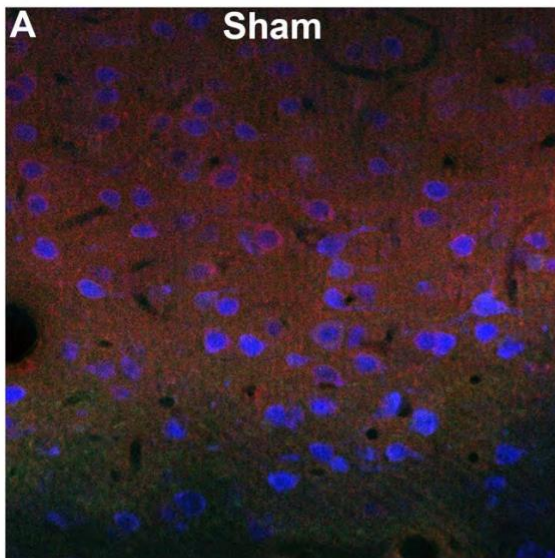


Figure 2.1. Doublecortin (DCX) Protein Quantities after TBI were unchanged from sham. Depicted above is the chemiluminescent blot assessment of DCX bands (around 45kDa) (**A**) of lateral neocortical homogenates normalized to total protein loaded on gel (**B**). Bar graph (**C**) shows sham injury (n=6), [black bar]; 1d post-TBI (n=6), 1w post-TBI (n=6), and 2w post-TBI (n=6) [gold bars]. No significant differences were found in the quantity of doublecortin in between sham and injured. Data are shown as Mean \pm SEM.



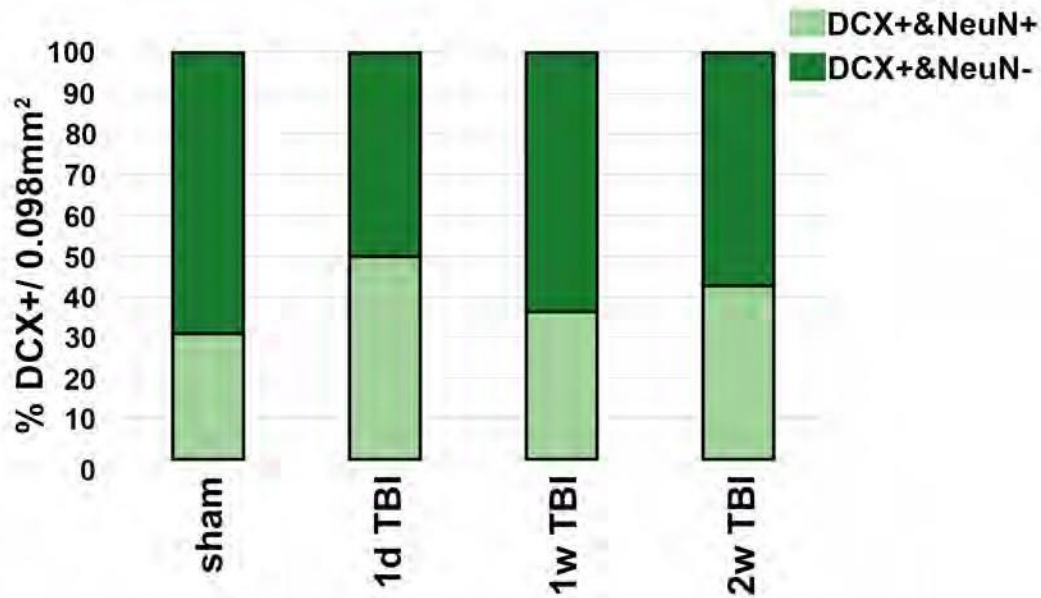


Figure 2.2. About 40% of DCX positive cells are NeuN positive. Representative fluorescent images **(A)** sham (n=3), **(B)** 1d post-TBI (n=5), **(C)** 1w post-TBI (n=3), **(D)** 2w post-TBI (n=6) of membrane disruption [green], DCX [red], and NeuN [blue]. The total percent of DCX cells per image (100%, sham n=46 cells, 1d post-TBI n=45, 1w post-TBI n=44, 2w post-TBI n=48) were counted in layer V and VI and designated as NeuN positive or negative in bar graph **(E)**. No significant differences were found in the quantity of NeuN negative/DCX positive [dark green bars] and NeuN positive/DCX positive [light green] in between sham and injured. Reported as Mean \pm SEM. Scale bar 50 μ m.

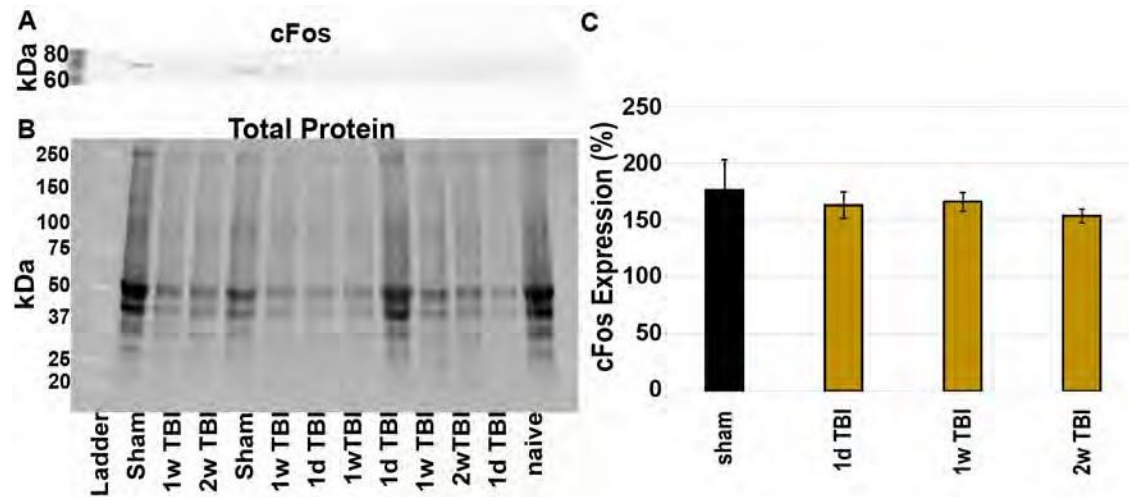


Figure 2.3. cFos expression after TBI were unchanged from sham. Depicted above is the chemiluminescent blot assessment of DCX bands (around 60-75 kDa) **(A)** of lateral neocortical homogenates normalized to total protein loaded on gel **(B)**. Bar graph **(C)** shows sham injury (n=6), [black bar]; 1d post-TBI (n=6), 1w post-TBI (n=6), and 2w post-TBI (n=6) [gold bars]. No significant differences were found in the cFos quantity between sham and injured. Data are shown as Mean \pm SEM.

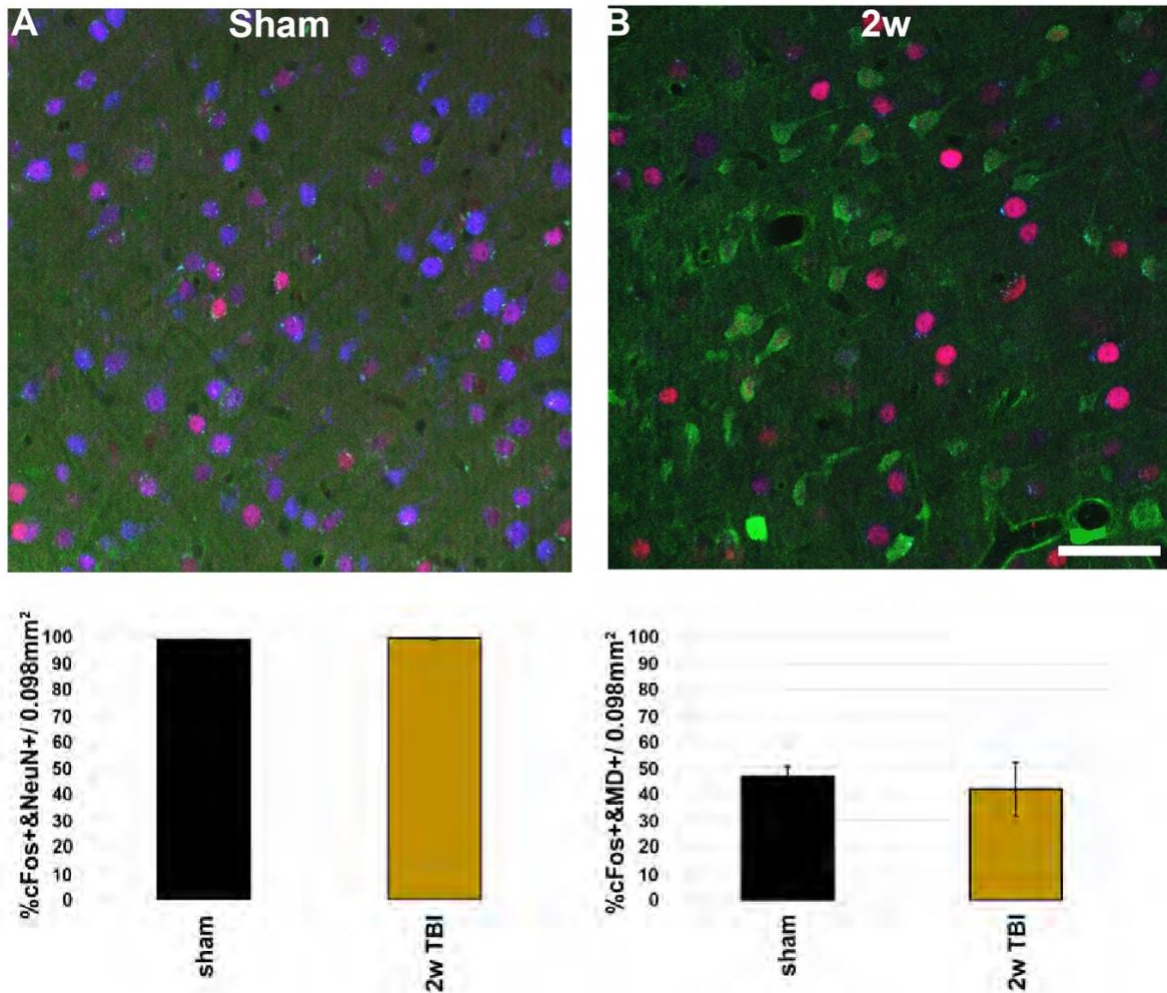


Figure 2.4. cFos positive cells are NeuN-positive, and only half of cFos positive cells are membrane disrupted. Representative fluorescent images **(A)** sham (n=6), [black bars] **(B)** 2w post-TBI (n=6) of membrane disruption [green], cFos [red], and NeuN [blue]. The cFos cells were counted in layer V and VI and designated as NeuN positive in **(C)** and cFos cells were also quantified for membrane disruption**(D)** Both graphs show no differences between sham and 2w post-TBI were found in the quantity of cFos positive and NeuN positive and cFos positive membrane disruption between sham and injured. Reported as Mean \pm SEM. Scale bar 50 μ m.

Chapter 3

These results were previously published as:

Hernandez ML, Marone M, Gorse KM, Lafrenaye AD. Cathepsin B Relocalization in Late Membrane Disrupted Neurons Following Diffuse Brain Injury in Rats. *ASN Neuro*. 2022;14. doi:[10.1177/17590914221099112](https://doi.org/10.1177/17590914221099112)

Abstract

Traumatic brain injury (TBI) has consequences that last for years following injury. While TBI can precipitate a variety of diffuse pathologies, the mechanisms involved in injury-induced neuronal membrane disruption remain elusive. The lysosomal cysteine protease, Cathepsin B (Cath B), and specifically its redistribution into the cytosol has been implicated in cell death. Little is known about Cath B or neuronal membrane disruption chronically following diffuse TBI. Therefore, the current study evaluated Cath B and diffuse neuronal membrane disruption over a more chronic post-injury window (6h-4w). We evaluated Cath B in adult male Sprague-Dawley rats following central fluid percussion injury (CFPI). Expression of Cath B, as well as Cath B-associated pro (Bak and AIF) and anti-apoptotic (Bcl-xl) proteins, were assessed using western blot analysis. Cath B activity was also assessed. Localization of Cath B was evaluated in the membrane disrupted and non-disrupted population following CFPI using immunohistochemistry paired with quantitative image analysis and ultrastructural verification. There was no difference in expression or activity of Cath B or any of the associated proteins between sham and CFPI at any time post-injury. Immunohistological studies, however, showed a sub-cellular re-localization of Cath B at 2w and 4w post-injury in the membrane disrupted neuronal population as compared to the time-point matched non-disrupted neurons. Both membrane disruption and Cath B relocalization appear linked to neuronal atrophy. These observations are indicative of a late secondary pathology that represents an opportunity for therapeutic treatment of these neurons following diffuse TBI.

Introduction

Traumatic brain injury (TBI) affects at least 2.8 million people in the US every year as of 2017, and the cost of TBI related- hospital admissions as of 2016 was estimated to be \$21 billion per year and rising ((Marin et al., 2017; Taylor et al., 2017)). The main event is not isolated, as TBI patients experience chronic symptoms due to secondary diffuse pathology throughout the brain (McMahon et al., 2014). This diffuse pathology is often hard to find on radiological and medical imaging and is relatively understudied compared to focal pathology, which has been highly characterized pre-clinically and clinically.

Neuronal membrane disruption has been found in various TBI models both in vitro and in vivo and in rodents and swine models (Hernandez et al., 2019; Keating et al., 2020; LaPlaca et al., 2019; Prado & LaPlaca, 2020; Ryu et al., 2021). A study found that neuronal membrane disruption presents 6h to 4w in a biphasic manner (Hernandez et al., 2019). They documented acute membrane disruption following injury at 6h, 1d, 3d, then decreasing at 1w. However, at 2w and 4w, we see a resurgence of the membrane disrupted population indicative of a secondary pathology occurring late that extends beyond the mechanical damage immediately seen post-injury. The reemergence of membrane disruption at late time points has an unknown etiology. Earlier studies honed onto a molecular mechanism for sub-acute membrane disruption driven by Cathepsin B (Cath B), however it is not known if this continues at later time points (Lafrenaye et al., 2012).

Cath B is a ubiquitously expressed lysosomal cysteine protease that performs regulatory functions such as recycling and breakdown of intramembrane proteins and cleavage of precursor proteins (Cavallo-Medved et al., 2011). However, Cath B has also been implicated in cell death, autophagy and various other cell-damage pathways (Boya et al., 2003; Chaitanya & Babu, 2008; Chowdhury et al., 2019; de Castro et al., 2016; Foghsgaard et al., 2001; Mollan et al., 2016; Nagakannan et al., 2021; Oberle et al., 2010). Cath B has been previously shown to mediate cell

death via lysosomal membrane permeabilization. This pathway appears to evolve in multiple ways; either via cleavage of B-cell lymphoma 2 (Bcl-2)/Bcl-XL, pro-survival proteins, which in turn releases the pro-apoptotic proteins Bak/Bax, that then enter the mitochondria to release cytochrome C leading to cell damage/death or via direct interaction of Cath B with apoptosis initiating factor (AIF) which goes to the mitochondria to induce the apoptotic cascade (Boya et al., 2003; Chaitanya & Babu, 2008; Chowdhury et al., 2019; Oberle et al., 2010). While Cath B usually functions within the acidic environment of the lysosome, it also has endopeptidase activity at the more neutral pH of the cytosol, unlike other lysosomal proteases. Within the context of TBI, Cath B has been found to be upregulated in rodent TBI models of focal lesions, such as the controlled cortical impact (CCI) and penetrating ballistic-like brain injury (PBBi) (Boutté et al., 2020; Hook et al., 2013; Luo et al., 2010). Additional findings within patient cerebrospinal fluid also indicated an upregulation of Cath B within hours or days post-penetrating TBI compared to non-TBI controls, providing further evidence that Cath B could play a role in TBI pathology (Boutté et al., 2020). Another study presented that Cath B was re-localized from the lysosome and into the cytosol at 6h post-central fluid percussion injury (CFPI) and secondary elevations of intracranial pressure (Lafrenaye et al., 2012). However, potential changes in Cath B throughout the progression of diffuse injury remain elusive, specifically at later time points where it could be a driving molecular mechanism for sub-acute/chronic diffuse membrane disruption.

We, therefore, explored Cath B in the context of protein expression and activity in rats from 6h to 4w post-CFPI. We also evaluated proteins involved in both of the Cath B-mediated cell damage pathways, Bak, Bcl-XL, and AIF via western blot. Protein analyses were followed by a microscopic exploration of subcellular localization of Cath B throughout the post-injury time course. Finally, we assessed indications of cellular and nuclear atrophy in relation to membrane disruption and Cath B re-localization. The findings reported below underline that the role of Cath B following TBI may be more variable with pathological presentations of diffuse TBI compared to focal TBI.

Materials and Methods

Animals

Experiments were conducted using protocols in accordance with the Virginia Commonwealth University institutional ethical guidelines concerning the care and use of laboratory animals (Institutional Animal Care and Use Committee, Virginia Commonwealth University), which adhere to regulations including, but not limited to, those set forth in the Guide for the Care and Use of Laboratory Animals, 8th Edition (National Research Council). Animals were housed in individual cages on a 12h light-dark cycle with free access to food and water. Archived tissue and homogenates from our previous study using adult male Sprague-Dawley rats, $n=57$ weighing 350–450g, were used for this study (Hernandez et al., 2019). Our a priori exclusion criteria included weight loss of more than 20% of their pre-injury body weight or gross brain pathology (contusion, subdural hematoma, or gross tissue loss). No animals met exclusion criteria in this study. Animal injury state and survival timepoint were randomly determined using a random number generator on the day of surgery. All surgeries were conducted by the same surgeon during the same times of day to reduce variability.

Surgical preparation and injury induction

Corresponding to (Hernandez et al., 2019), Animals were anesthetized with 4% isoflurane in 30% O₂ and 70% N₂O then intubated and ventilated with 2% isoflurane in 30% O₂ and 70% N₂O throughout the duration of the surgery, injury, and post-injury physiological monitoring. Heart rate, respiratory rate, and blood oxygenation were monitored via a hind-paw pulse oximetry sensor (STARR Life Sciences, Oakmont, PA) for the duration of anesthesia, except during the induction of injury. Body temperature was maintained at 37°C with a rectal thermometer connected to a feedback-controlled heating pad (Harvard Apparatus, Holliston, MA). All animals

were placed in a stereotaxic frame (David Kopf Instruments, Tujunga, CA). A midline incision was made, and a 4.8 mm circular craniectomy was made along the sagittal suture midway between bregma and lambda for injury induction. A 2mm burr hole was also drilled in the left parietal bone overlying the left lateral ventricle (0.8 mm posterior, 1.3 mm lateral, and 2.5- 3 mm ventral to bregma) through which a 25-gauge needle, connected to a pressure transducer and microinfusion pump (11 Elite syringe pump; Harvard Apparatus) via sterile saline-filled PE50 tubing, was placed into the left lateral ventricle. Appropriate placement was verified via a 1.3µl/min infusion of sterile saline within the closed fluid-pressure system during needle placement. The needle was held in the ventricle for at least 5min to record pre-injury intracranial pressure (ICP). After the 5-min reading, the needle was slowly removed, and the burr hole was covered with bone wax before preparation for sham or CFPI (Dixon et al., 1987; Lafrenaye et al., 2014). Briefly, a Leur-Loc syringe hub was affixed to the craniectomy site, and dental acrylic (methyl-methacrylate; Hygenic Corp., Akron, OH) was applied around the hub and allowed to harden. Anesthetized animals were removed from the stereotaxic frame and injured at a magnitude of 2.05 ± 0.15 atmospheres and duration of ~22msec. The pressure pulse was measured by a transducer affixed to the injury device and displayed on an oscilloscope (Tektronix, Beaverton, OR). Immediately after the injury, the animal was reconnected to the ventilator and physiologic monitoring device and the hub and dental acrylic were removed en bloc. Gelfoam was placed over the craniectomy/injury site, and the scalp was sutured. The animal was then replaced in the stereotaxic device, and the ICP probe was reinserted into the lateral ventricle, as described above, for post-injury ICP monitoring. The animals were then allowed to recover and were returned to clean home cages. Identical surgical procedures were followed for sham-injured animals, without release of the pendulum to induce injury (Hernandez et al., 2019).

Tracer infusion

Two hours prior to sacrifice, tagged dextran (40mg/ml in sterile 0.9% saline; ~1.6mg/kg) was infused into the lateral ventricle as described (Hernandez et al., 2019; Lafrenaye et al., 2012). Briefly, 15µl of 10kDa dextran conjugated to either 488-Alexa Fluor (Cat#: D22910, Invitrogen, Carlsbad, CA), 568-Alexa-Fluor (Cat#: D22912; Invitrogen, Carlsbad, CA), or biotin (Cat#: D1956; Invitrogen, Carlsbad, CA) was infused into the left lateral ventricle at 0.5-1.3µl/min, with continuous ICP monitoring. To avoid bias caused by differences in fluorescent signal detectability, animals were randomly assigned a tag (Alexa 488, Alexa 568 or biotin). The tracer was allowed to diffuse throughout the parenchyma for 2h prior to transcardial perfusion at 6h, 1d, 3d, 1w, 2w, or 4w post-sham or CFPI.

Tissue processing

At appropriate time-points between 6h and 4w post-injury, the animals were injected with 150mg/kg euthanasia-III solution (Henry Schein, Dublin, OH), then underwent transcardial perfusion with cold 0.9% saline. Lateral neocortices were dissected from the right hemisphere of the brain and frozen for assessments of protein expression and activity followed by a switch in transcardial perfusate to 4% paraformaldehyde/ 0.2% glutaraldehyde in Millonig's buffer (136mM sodium phosphate monobasic/109mM sodium hydroxide) to fix the left side of the brain for subsequent immunohistochemical or electron microscopic (EM) processing and analysis. After transcardial perfusion, the brains were removed, post-fixed for 24-48h, then sectioned coronally in 0.1M phosphate buffer with a vibratome (Leica, Banockburn, IL) at a thickness of 40µm from bregma to 4.0mm posterior to bregma. Sections were collected serially in 12 well-plates and stored in Millonig's buffer at 4°C. A random starting well (wells 1–12) was selected using a random number generator and four serial sections (each 480µm apart) were used for histological analyses. All histological analyses were restricted to layers V and VI of the lateral somatosensory neocortex extending from the area lateral to CA1 to the area lateral to CA3 of the hippocampus (Hernandez et al., 2019).

Western blotting

As performed in (Hernandez et al., 2019), lateral neocortices of sham n=6 (n=1/time point) and TBI rats n=6/time point were homogenized in NP40 Buffer (150 mM NaCl, 50 mM Tris pH 8.0, 1% Triton) and protease inhibitor cocktail (AEBSF 10.4mM, Aprotinin 8μM, Bestatin 400μM, E-64 140μM, Leupeptin 8μM, Pepstatin A 150μM, Cat#: P8340, Sigma, Saint Louis, MO). Protein concentrations were measured using a NanoDrop Lite (Thermo Fisher Scientific, Wilmington, DE). Protein (20 μg for Cathepsin B, 10 μg Bak, Bcl-XL, and AIF) was boiled for 10min in 50mM dithiothreitol (Cat#: 1610610; Bio-Rad; Hercules, CA), 2x Laemmli loading buffer (Cat#: 1610737; Bio-Rad; Hercules, CA) and run at 200 Volts for 30min on Mini-PROTEAN TGX Stain-Free 4-20% precast polyacrylamide gels (Cat#: 4568096; Bio-Rad, Hercules, CA). Protein was transferred onto 0.45μm PVDF membranes using a Bio-Rad Transblot Turbo transfer system set to the mixed molecular weight manufacturer setting (1.3-2.5 Amps, 25 Volts for 7min). Western blotting was done on an iBind flex apparatus (Invitrogen, Carlsbad, CA) using primary antibodies rabbit anti-Cathepsin B (1:1000; Cat#: 31718, RRID:AB_2687580), rabbit anti-Bak (1:1000; Cat#: 12105, RRID:AB_2716685), rabbit anti-Bcl-xl (1:1000; Cat#: 2764, RRID:AB_2228008) or rabbit anti-AIF (1:1000; Cat#: 5318, RRID:AB_10634755) (Cell Signaling Technology, Danvers, MA) and anti-rabbit-HRP secondary antibody (1:5000; Cat#: 111-035-003; Jackson ImmunoResearch Laboratories, West Grove, PA, RRID:AB_2313567). Total protein (Stain Free) and chemiluminescent images were taken on a ChemiDoc imaging system (BioRad). Densitometric analyses of Cathepsin B, AIF, Bak, and Bcl-XL were performed in ImageJ (National Institutes of Health; Bethesda, MD). Cathepsin B, AIF, Bak and Bcl-XL protein bands were normalized to total protein and sham controls. Additionally, the ratio of normalized Bak and Bcl-XL was calculated. All western blots were run in triplicates on three separate gels to reduce run-to-run variability biasing the results.

Cellular Cathepsin B Localization Analysis

Fluorescently tagged dextran-containing cells, indicative of membrane disruption, could be visualized via confocal microscopy without further processing, however, biotin-conjugated dextran required immunolabeling for visualization. Two tissue sections/animal from 6h (n=5), 1d (n=5), 3d (n=4) 1w (n=5), 2w (n=5), 4w (n=5) were blocked with 5% normal goat serum (NGS) or 5% normal horse serum (NHS), 2% bovine serum albumin (BSA), and permeabilized with 1.5% triton-X for 2h. This was followed by immunolabeling using primary antibodies rabbit anti-Cathepsin B (1:700; Cat#: 31718 Cell Signaling Technology, Danvers, MA, RRID:AB_2687580) and Goat anti-biotin (1:2000; Cat#: 31852; Thermo Scientific, Rockford, IL, RRID:AB_228243) as needed for animals infused with biotin-conjugated dextrans. Tissue was incubated in secondary antibodies Alexa-633 conjugated goat anti-rabbit(1:700; Cat#: A21070; Life Technologies, Carlsbad, CA, RRID:AB_2535731) and Alexa-488 conjugated donkey anti-goat (1:700; Cat#: A11055; Life Technologies, Carlsbad, CA, RRID:AB_2534102) and the tissue was mounted onto slides using Vectashield hardset mounting medium with 4',6-diamidino-2-phenylindole (DAPI) (Cat#: H-1500; Vector Laboratories, Burlingame, CA). Quantitative analysis was performed as described previously (Hernandez et al., 2019; Lafrenaye et al., 2012). Briefly, 4 confocal images each section; 2 sections/animal of the left neocortical region of interest were taken at 40X magnification using a Zeiss LSM 710 System (Carl Zeiss) in a systematically random fashion by an investigator blinded to animal group using the dextran tag to verify images included neurons with and without membrane disruption. Image acquisition settings were held constant for comparable regions (layer V or VI) and dextran (488-tagged, 568-tagged or biotin-tagged) for all groups analyzed. Equal numbers of membrane disrupted, and non-disrupted neurons were randomly selected in each image. The cell body and nucleus of all neurons assessed were traced and the area of the soma and nucleus were quantified via the measure tool in FIJI (ImageJ). Localization (either punctate or diffuse) of Cathepsin B was assessed for each neuron by eye using the traces and without seeing the dextran labeling. Membrane disrupted and non-disrupted neurons were randomized for each image to reduce investigator bias during assessment of

Cathepsin B localization. The localization of Cathepsin B was expressed as a percentage of neurons demonstrating punctate (lysosomal) Cathepsin B localization of the total membrane disrupted or non-disruption neuronal population assessed at each time point (6h-4w). In addition, somal and nuclear size were assessed for both membrane disruption (membrane disrupted vs. non-disrupted) and Cathepsin B localization (punctate vs. diffuse localization) subpopulations at each time point (6h-4w).

Quantification of Cathepsin B Activity

Portions of the dissected right lateral neocortices of 6h-4w sham and injured animals were homogenized in 50 μ M citric acid at a pH 6.0, spun at 12,000 xg at 4° C for 10 minutes and the supernatant of the whole homogenate was collected. Protein concentrations were measured using a NanoDrop Lite (Thermo Fisher Scientific, Wilmington, DE) and Cathepsin B activity was measured in a 96-well plate, each well containing 2x Assay Buffer (100mM sodium acetate pH 5.5, 2mM EDTA, 200mM sodium chloride, 8mM DTT), 2 μ g of neocortex whole homogenate, and Z-Phe-Arg-7-amino-4-(trifluoromethyl) coumarin (ZFR-AMC), a substrate for cysteine proteases that fluoresces upon cleavage by Cathepsin B (Boutté et al., 2020; Hook et al., 2013; Yoon et al., 2021). The plate was read 30- and 60-minutes post-substrate addition at 365/450 nm excitation/emission. Each sample was loaded in triplicate per plate for three independent runs to reduced pipetting and run-to-run variability biasing the results. A positive control well with purified human liver Cathepsin B 5 ng and a negative control well with only assay buffer and substrate were included in every run.

Ultrastructural assessment of Cathepsin B localization

In preparation for electron microscopic (EM) analysis, tissue was labeled with rabbit antibodies targeted to Cathepsin B (1:500; Cat#: 31718 Cell Signaling Technology, Danvers, MA).

Tissue slices were then blocked with 5% NGS, followed by incubation with biotinylated goat anti-rabbit (1:1000; Cat#: BA-5000; Vector Laboratories) secondary antibody. Sections were incubated in avidin biotinylated enzyme complex using the Vectastain ABC kit (Vector Laboratories) followed by visualization with diaminobenzidine (DAB) in 0.1M phosphate buffer. Tissue sections were osmicated, dehydrated, and embedded in epoxy resin on plastic slides as published (Hernandez et al., 2019). After resin curing, areas in the lateral neocortex within layers V and VI that contained adequate Cathepsin B labeling and in regions approximate to locations of membrane disruption were identified using light microscopy. These areas were removed, mounted on plastic studs, and 70nm sections were cut and mounted on Formvar-coated slotted grids. The grids were stained in 5% uranyl acetate in 50% methanol and 0.5% lead citrate. Electron micrographs were imaged using a JEOL JEM 1230 transmission electron microscope equipped with an Orius SC1000 CCD camera (Gatan, Pleasanton, CA). Every neuron within each grid, 3 grids total, n=2 animals, 1 grid for 1 animal and 2 grids for the other, were imaged and all images were qualitatively assessed for distribution of Cathepsin B within or in approximation to the lysosomal compartment.

Statistical analysis

Data were tested for normality prior to utilizing parametric or non-parametric assessments, which were conducted using SPSS (IBM Corporation, Armonk, NY) software. Animal numbers for each group were determined by an a priori power analysis using effect size and variability previously observed in the lab when assessing pathology between sham and injured groups using the CFPI model, an alpha = 0.05, and a power of 80%. Two-way or one-way analysis of variance (ANOVA) and Bonferroni post hoc tests were performed for all between-group analyses. Statistical significance was set to $p < 0.05$. Data are presented as mean \pm standard error of the mean (SEM).

Results

Protein expression of Cathepsin B or its proteolytic activity was unchanged following CFPI

The overall expression of Cath B within the lateral neocortex was evaluated for changes following CFPI throughout the 6h to 4w post-injury time course. Western blot analysis revealed that Cath B protein levels were not significantly different for sham animals ($100.91 \pm 4.85\%$) and TBI animals at 6h ($87.27 \pm 4.53\%$ of sham), 1d ($85.93 \pm 4.84\%$ of sham), 3d ($110.24 \pm 14.49\%$ of sham), 1w ($83.48 \pm 5.03\%$ of sham), 2w ($100.86 \pm 8.79\%$ of sham), and 4w ($105.25 \pm 10.88\%$ of sham) post-CFPI (Figure 1A&B; one-way ANOVA $F_{6,35} = 1.527$, $p = 0.198$).

Cath B has been implicated in various cell damage pathways. One of these pathways involved AIF, which is cleaved by cathepsins from the mitochondria to set forth cell death (Chaitanya & Babu, 2008; Chowdhury et al., 2019). Additionally, Cath B can cleave Bcl-XL, a pro-survival protein that interacts with Bak, a pro-apoptotic protein which advances cell death by release of cytochrome C (Boya et al., 2003; Oberle et al., 2010). Therefore, the protein expression of AIF as well as the expression ratio of the antagonizing proteins Bcl-XL and Bak were also assessed over the 4w time course following injury. The quantity of AIF following CFPI at 6h ($96.16 \pm 9.47\%$ of sham), 1d ($87.61 \pm 8.08\%$ of sham), 3d ($87.88 \pm 6.63\%$ of sham), 1w ($85.24 \pm 11.57\%$ of sham), 2w ($98.93 \pm 10.37\%$ sham), 4w ($102.18 \pm 10.65\%$ of sham) was comparable to AIF levels in the lateral neocortex of sham controls ($100 \pm 0.36\%$; Figure 1C&D; one-way ANOVA $F_{6,35}=0.604$, $p=0.725$). There was also no difference in the Bak/Bcl-XL expression ratio between sham (101.66 ± 3.85) and TBI animals at 6h (101.06 ± 22.66), 1d (97.70 ± 9.36), 3d (98.76 ± 12.73), 1w (101.05 ± 13.02), 2w (107.77 ± 7.62), and 4w (101.35 ± 7.62 ; Figure 1E&F; one-way ANOVA $F_{6,35}= 0.069$, $p=0.999$).

Whereas most Cathepsins are active at the lower pH of the lysosomes, Cath B is also active at more neutral pHs, such as that of the cytosol (Khoury et al., 1991; Nägler et al., 1997; Ruzza et al., 2006). Therefore, the question arose regarding Cath B's localization and proteolytic

activity over time following CFPI. Proteolytic activity of Cath B was not significantly different between sham animals ($99.81 \pm 9.99\%$) and TBI animals at 6h ($100.25 \pm 9.08\%$ of sham), 1d ($92.57 \pm 12.16\%$ of sham), 3d ($119.24 \pm 14.86\%$ of sham), 1w ($90.50 \pm 5.03\%$ of sham), 2w ($103.59 \pm 17.08\%$ of sham), and 4w ($125.01 \pm 25.60\%$ of sham) post-CFPI (one-way ANOVA $F_{6,23} = 0.753$, $p = 0.614$; Figure 2).

Cathepsin B re-localizes from lysosomes to cytosol in disrupted neurons at 2 and 4 weeks following central fluid percussion injury

The re-localization/redistribution of Cath B from the lysosome to the cytosol has been associated with pathological progression (Lafrenaye et al., 2012a). However, to our knowledge, Cath B localization has not been rigorously assessed in later stages of neuronal membrane disrupted populations following diffuse TBI alone. Therefore, Cath B localization was determined as punctate (intra-lysosomal) or diffuse (extra-lysosomal) for both membrane disrupted and non-disrupted neurons throughout the time course from 6hr-4w post-CFPI (Figure 3A). Sham animals were not assessed as they have no membrane disruption (Hernandez et al., 2019), thus provides no further information about the membrane disrupted population in relation to Cath B. (Hernandez et al., 2019) Cath B was found to be localized within puncta in non-disrupted neurons at 6h ($72.88 \pm 3.72\%$), 1d ($63.91 \pm 4.18\%$), 3d ($77.88 \pm 4.09\%$), 1w ($80.73 \pm 3.79\%$), 2w ($80.52 \pm 3.20\%$), 4w ($87.22 \pm 2.91\%$), post-CFPI. The majority of Cath B was also localized within lysosomal puncta in disrupted neurons at 6h ($86.99 \pm 2.79\%$) $p=0.425$, 1d ($50.34 \pm 4.11\%$) $p=0.636$, 3d ($66.99 \pm 4.66\%$) $p=1.00$, 1w ($65.63 \pm 4.21\%$) $p=0.552$, however, there was a significant reduction in the percentage of membrane disrupted neurons demonstrating punctate localization of Cath B at 2w ($43.84 \pm 4.66\%$) $p=4.88 \times 10^{-11}$, and 4w ($32.35 \pm 4.66\%$) $p=5.34 \times 10^{-19}$ post-CFPI (Figure 3B, one-way ANOVA; $F_{11,1539}=19.88$, $p=6.6 \times 10^{-38}$).

The percentages of neurons demonstrating punctate Cath B indicated an effect of membrane disruption (two-way ANOVA; $F_{1,1539}=74.83$, $p=1.27 \times 10^{-17}$) and time (two-way ANOVA; $F_{5,1539}=11.42$, $p=7.73 \times 10^{-11}$) on Cath B re-localization. There were also significant interactions between neuronal membrane disruption and time on Cath B localization (two-way ANOVA; $F_{5,1539}=19.02$, 2.12×10^{-18}).

Ultrastructural qualitative analysis of neurons with immunoelectron microscopy was used to further scrutinize subcellular localization of Cath B, in particular, that the diffuse distribution of Cath B that we saw in the confocal micrographs was indeed indicative of Cath B redistributing out of the lysosomal compartment. While we did observe immunolabeled Cath B completely contained within the lysosomal domain in neurons 6h-4w following CFPI (Figure 4A), a majority of the neurons analyzed demonstrated some degree of Cath B redistribution outside of the lysosome (Figure 5B-C). This redistribution of Cath B was observed in many of the neurons assessed within the lateral neocortex at 2w and 4w. These data support our confocal findings of Cath B re-localization from the lysosome into the cytosol at 2 and 4w post-CFPI.

Cathepsin B re-localization and neuronal membrane disruption are associated with reductions in cellular and nuclear area.

As diffuse neuronal injuries following TBI have been shown to precipitate cellular changes, such as atrophy, without leading to cell death (Greer et al., 2011b; Lifshitz et al., 2007b), we measured the somal and nuclear area of membrane disrupted and non-disrupted neurons and neurons demonstrating punctate or diffuse Cath B localization. This analysis also did not include sham animals as stated, as these were from the same images as Figure 3. The mean somal areas of non-disrupted neurons at 6h-4w post-CFPI were approximately $126 \mu\text{m}^2$; 6h ($131.11 \pm 3.28 \mu\text{m}^2$), 1d ($118.31 \pm 3.02 \mu\text{m}^2$), 3d ($133.00 \pm 2.76 \mu\text{m}^2$), 1w ($128.61 \pm 3.15 \mu\text{m}^2$), 2w ($110.60 \pm 3.15 \mu\text{m}^2$), and 4w ($134.31 \pm 3.49 \mu\text{m}^2$). The mean somal areas of membrane disrupted neurons

from 6h-4w post-CFPI were approximately $108\mu\text{m}^2$: 6h ($108.90 \pm 4.29\mu\text{m}^2$) $p=3.16 \times 10^{-4}$, 1d ($109.25 \pm 3.24\mu\text{m}^2$) $p=1.00$, 3d ($128.63 \pm 4.25\mu\text{m}^2$) $p=1.00$, 1w ($125.49 \pm 5.54\mu\text{m}^2$) $p=1.00$, 2w ($80.35 \pm 2.73\mu\text{m}^2$) $p=1.80 \times 10^{-8}$, and 4w ($92.65 \pm 3.37\mu\text{m}^2$) $p=1.85 \times 10^{-12}$ (Figure 5A, one-way ANOVA; $F_{11,1539}=22.13$, $p=2.12 \times 10^{-42}$). There was a significant decrease in somal area of membrane disrupted neurons at 6h, 2w and 4w post-injury.

Somal area had main effects on time (two-way ANOVA; $F_{5,1539}=75.923$, $p=8.79 \times 10^{-24}$) and membrane disruption (two-way ANOVA; $F_{1,1539}=24.479$, $p=7.48 \times 10^{-18}$). There was a significant interaction between membrane disruption and time on somal area (two-way ANOVA; $F_{5,1539}=8.568$, $p=5.12 \times 10^{-8}$).

The mean nucleus area of non-disrupted neurons 6h-4w post-CFPI were approximately $79\mu\text{m}^2$; 6h ($85.40 \pm 1.98\mu\text{m}^2$), 1d ($78.20 \pm 1.75\mu\text{m}^2$), 3d ($83.75 \pm 2.10\mu\text{m}^2$), 1w ($76.11 \pm 2.17\mu\text{m}^2$), 2w ($67.55 \pm 1.74\mu\text{m}^2$), and 4w ($82.21 \pm 2.04\mu\text{m}^2$). The mean nucleus area of disrupted neurons 6h-4w post-CFPI were approximately $60\mu\text{m}^2$; 6h ($53.62 \pm 2.42\mu\text{m}^2$) $p=1.64 \times 10^{-27}$, 1d ($67.86 \pm 1.82\mu\text{m}^2$) $p=0.027$, 3d ($75.56 \pm 2.51\mu\text{m}^2$) $p=1.00$, 1w ($73.46 \pm 3.33\mu\text{m}^2$) $p=1.00$, 2w ($43.70 \pm 2.00\mu\text{m}^2$) $p=2.22 \times 10^{-11}$, 4w ($44.79 \pm 2.38\mu\text{m}^2$) $p=7.47 \times 10^{-25}$, (Figure 5B, one-way ANOVA; $F_{11,1303}=37.92$, $p=4.12 \times 10^{-71}$). It was noted that membrane disrupted neurons 6h, 1d, 2w and 4w demonstrated significant reduction in nucleus area compared to non-disrupted neurons at the same timepoints.

Nucleus area had main effects from membrane disruption (two-way ANOVA; $F_{1,1303}=213.312$, $p=7.43 \times 10^{-45}$) and time (two-way ANOVA; $F_{5,1303}=27.379$, $p=2.03 \times 10^{-26}$). This data set was probed with a two-way ANOVA that highlights an interaction of membrane disruption and time on nucleus area (two-way ANOVA; $F_{5,1303}=19.064$, $p=2.43 \times 10^{-18}$).

When assessing somal area of neurons based on Cath B localization, we found that at 6h-4w cortical neurons demonstrating punctate localization were approximately $127\mu\text{m}^2$; 6h ($121.61 \pm 3.17\mu\text{m}^2$), 1d ($124.12 \pm 3.11\mu\text{m}^2$), 3d ($136.64 \pm 2.80\mu\text{m}^2$), 1w ($136.80 \pm 3.72\mu\text{m}^2$), 2w

($110.68 \pm 2.77\mu\text{m}^2$) and 4w ($129.46 \pm 3.54\mu\text{m}^2$) (Figure 5C). This was in contrast to the somal area of diffuse Cath B localization neurons that was approximately $99\mu\text{m}^2$; 6h ($113.21 \pm 5.69\mu\text{m}^2$) $p=1.00$, 1d ($99.63 \pm 2.73\mu\text{m}^2$) $p=3.50 \times 10^{-5}$, 3d ($115.51 \pm 4.96\mu\text{m}^2$) $p=0.053$, 1w ($100.79 \pm 5.98\mu\text{m}^2$) $p=8.09 \times 10^{-8}$, 2w ($71.04 \pm 2.54\mu\text{m}^2$) $p=3.09 \times 10^{-14}$, and 4w ($93.29 \pm 3.35\mu\text{m}^2$) $p=3.68 \times 10^{-9}$. (Figure 5C, one-way ANOVA; $F_{11,1539}=28.189$, $p=2.86 \times 10^{-54}$).

Somal area had main effects from Cath B localization (two-way ANOVA; $F_{1,1539}=147.413$, $p=1.84 \times 10^{-32}$) and time (two-way ANOVA; $F_{5,1539}=20.87$, $p=3.16 \times 10^{-20}$). An interaction of time and cath b localization on somal area was found (two-way ANOVA; $F_{5,1539}=4.483$, $p=4.64 \times 10^{-4}$).

When assessing nucleus area of neurons based on Cath B localization, we found that at 6h-4w cortical neurons demonstrating punctate localization were approximately $77\mu\text{m}^2$; 6h ($69.39 \pm 2.14\mu\text{m}^2$), 1d ($77.84 \pm 1.76\mu\text{m}^2$), 3d ($84.13 \pm 1.58\mu\text{m}^2$), 1w ($81.80 \pm 1.94\mu\text{m}^2$), 2w ($69.76 \pm 1.67\mu\text{m}^2$), and 4w ($80.05 \pm 2.17\mu\text{m}^2$). This was in contrast to the nucleus area of diffuse cath B localization neurons that was approximately $58\mu\text{m}^2$; 6h ($71.71 \pm 3.20\mu\text{m}^2$) $p=1.00$, 1d ($66.84 \pm 1.74\mu\text{m}^2$) $p=0.02$, 3d ($68.03 \pm 4.03\mu\text{m}^2$) $p=4.00 \times 10^{-3}$, 1w ($53.64 \pm 3.42\mu\text{m}^2$) $p=1.48 \times 10^{-10}$, 2w ($41.00 \pm 1.66\mu\text{m}^2$) $p=3.26 \times 10^{-16}$, and 4w ($46.56 \pm 2.67\mu\text{m}^2$) $p=1.70 \times 10^{-17}$ (Figure 5D, one-way ANOVA; $F_{11,1303}=29.764$, $p=2.53 \times 10^{-56}$).

Nucleus area had main effects from Cath B localization (two-way ANOVA; $F_{1,1303}=169.495$, $p=1.62 \times 10^{-36}$) and time (two-way ANOVA; $F_{5,1303}=18.102$, $p=2.14 \times 10^{-17}$). Main effects from time and localization were that nucleus area was significantly decreased at most post-injury time points. A significant interaction of Cath B localization and time on nucleus area was also found ($F_{5,1303}=14.462$, $p=8.23 \times 10^{-14}$).

Three-way ANOVA demonstrated significant effects of time ($F_{5,1527}=22.543$, $p=7.15 \times 10^{-22}$), Cath B localization ($F_{1,1527}=104.216$, $p=1.03 \times 10^{-23}$), and membrane disruption ($F_{1,1527}=26.553$, $p=2.90 \times 10^{-7}$) on somal area. Interactions between time and Cath B localization ($F_{5,1527}=2.17$, $p=0.055$) or interactions between membrane disruption and Cath B localization alone

($F_{1,1527}=2.60$, $p=0.107$) were not significant when assessing soma area using three-way ANOVA. However, interactions between membrane disruption and time were significant ($F_{5,1527}=2.913$, $p=0.013$). Additionally, three-way ANOVA demonstrated that there was an interaction of membrane disruption, Cath B localization, and time post-injury on soma area ($F_{5,1527}=2.964$, $p=0.011$).

Main effects from time ($F_{5,1291}=24.416$, $p=1.51 \times 10^{-23}$), Cath B localization ($F_{1,1291}=113.404$, $p=1.93 \times 10^{-23}$), and membrane disruption ($F_{1,1291}=80.778$, $p=8.76 \times 10^{-19}$) on nucleus area were found via three-way ANOVA. There was a significant interaction between membrane disruption and Cath B localization on nucleus area ($F_{1,1291}=15.813$, $p=7.40 \times 10^{-5}$). Another significant interaction was found between time and membrane disruption ($F_{5,1291}=9.327$, $p=9.68 \times 10^{-9}$). An additional significant interaction also noted was between time and Cath B localization ($F_{5,1291}=6.572$, $p=5.00 \times 10^{-6}$) on nucleus area. Looking at time, Cath B localization, and membrane disruption as factors for nucleus area did not have a significant interaction as indicated by three-way ANOVA ($F_{5,1291}=2.187$, $p=0.053$).

Discussion

In the current study we found no change in the expression of Cath B or any downstream signaling proteins (Bak, Bcl-XL, or AIF) from 6hr to 4w following CFPI in male Sprague Dawley rats compared to shams. While Cath B activity was also unchanged over time following diffuse TBI, Cath B was found to be re-localized into the cytosol in membrane disrupted neurons at 2w and 4w post-injury, a phenomenon not observed in non-membrane disrupted neuron at any time point or membrane disrupted neurons at more acute time points in this study (6hr-1w). Finally, while (Hernandez et al., 2019) demonstrated no neuronal loss out to 4w post CFPI, we found indications of neuronal atrophy in relation to membrane disruption and Cath B re-localization throughout the time course, indicating the potential for therapeutic rescue of these pathological populations.

Unlike other Cathepsins, Cath B demonstrates catalytic activity in the cytosol (Pratt et al., 2009). While previous studies assessing a range of neurological damages/diseases report an increase in both expression and activity of Cath B, in the current study, we did not find a change in Cath B protein expression or activity at any time throughout the post-injury time course (6h-4w)(Amritraj et al., 2009; Benchoua et al., 2004; Ellis et al., 2005; Feldstein et al., 2004; Foghsgaard et al., 2001; Rodríguez-Muela et al., 2015). Our findings are in contrast to what has been observed in previous TBI studies, which indicate an increase in both Cath B protein levels and activity (Boutté et al., 2020; Hook et al., 2013; Luo et al., 2010). Specifically, (Luo et al., 2010) analyzed both Cath B activity and expression in the cortex 1h-48h and 7d following CCI and found that Cath B activity increased starting at 6h increased significantly through 7d compared to sham. This group also quantified Cath B expression which doubled after 6h, continued to increase until it was increased 4x compared to sham by 48h. Finally, at 7d, they saw Cath B expression decrease, but still doubled from sham. (Hook et al., 2013) evaluated activity and saw a 1.5x increase 2h post-CCI. Hook et al also measured protein expression at 24h post-injury and also found an 4x increase in Cath B expression compared to sham. Another study by (Boutté et al., 2020) found an increase in Cath B protein expression following PBBI and demonstrated an increase in Cath B activity at 3d post-injury that remained increased at 7d post-injury, compared to craniotomy alone. However, this increase was not seen at 1d (Boutté et al., 2020).

The differences between our findings and the findings of the other groups may lie in the circumstances under which these studies were conducted. All of the previous TBI studies utilized injury models that induced a focal homogenous lesion to the brain (Boutté et al., 2020; Hook et al., 2013; Luo et al., 2010; Sarkar et al., 2020). However, our CFPI model, is a diffuse injury so the nature of the pathologies within the brain in this model are heterogenous, including the Cath B relocalization (Lafrenaye et al., 2012; Lifshitz et al., 2007; Singleton et al., 2002; Singleton & Povlishock, 2004). Therefore, measurement of the entire lateral neocortex Cath B activity may not capture the cells that could exhibit increased Cath B expression. Also, in combination with

different modalities of injury and consideration of the variance in pathology, the timeframes in which Cath B was assessed in the previous studies were acute and sub-acute, juxtaposed to our sub-acute and late timepoints. The results from those works and ours suggest that Cath B activity and protein expression could be time and pathology dependent.

In the current study we also found relocalization of Cath B that appears to be associated with neuronal membrane disruption post-CFPI. This observation of Cath B outside of the lysosomes could indicate neurons undergoing lysosomal membrane permeabilization (LMP). Brain injury-induced organelle membrane disruption, such as LMP, involving the Cath B pathway has been previously observed (Kilinc et al., 2010; Luo et al., 2010; Meyer et al., 2021; Oberle et al., 2010; Rodríguez-Muela et al., 2015; Windelborn & Lipton, 2008). Pathological findings of LMP indicate progression to cell death; however, there is no previous observation cell death in the CFPI animals (Hernandez et al., 2019). A possibility for the release of Cath B through LMP includes cytosolic phospholipase A2 (cPLA2). Studies looking at the role of other Cathepsins (D and L) in neurotrauma autophagy found that cPLA2 is directly involved in LMP in mice and that these sequelae involve the release of lysosomal enzymes (Li et al., 2019; Sarkar et al., 2020). cPLA2 has also been proposed to alter the neuronal plasma membrane (Lee et al., 2011). Therefore, cPLA2 could be disrupting the lysosomal membrane inducing the release of Cath B into the cytosol and also targeting the plasma membrane. Additionally, disruption of the lysosomes or replacement of Cath B with Cath L impedes neurite outgrowth. Cath B has been shown to remodel neurites in vitro through lysosomal membrane trafficking (Jiang et al., 2020). Perhaps the release of Cath B dysregulates plasma membrane remodeling through disruption of lysosomal function thus could be why membrane disruption is evident at later time points.

Work looking at 6h post-CFPI with intracranial pressure elevation highlighted that Cath B relocalizes from the lysosomal compartments into the cytosol in membrane disrupted neurons (Lafrenaye et al., 2012). In this study, however, Cath B relocalization was significant in the 2w and 4w groups, particularly in the membrane disrupted neurons, but not at 6h, even in the

membrane disrupted neuronal population. Fisher rats were used in the (Lafrenaye et al., 2012) study while the current study used Sprague Dawley rats, indicating that there could be strain difference that may exacerbate Cath B release from the lysosomes, as observed in our prior study. Furthermore, the majority of the animals evaluated for Cath B relocalization in the 2012 study had both a CFPI and elevated ICP. That group had also found ICP elevation exacerbates membrane disruption and causes cell loss at 4w (Lafrenaye et al., 2014), the combination of TBI and secondary ICP elevations may induce more severe Cath B relocalization, however, further assessments of this possibility are needed.

Finally, we found that while somal and nuclear area were consistent for non-membrane disrupted neurons and neurons demonstrating lysosomal-Cath B, neurons sustaining later stage membrane disruption or Cath B redistribution, had significantly smaller soma and nuclei, indicating atrophy. This atrophy occurred simultaneously with the resurgence of membrane disruption and Cath B relocalization found at the later post-injury time points of 2w and 4w. Interestingly, no difference was observed 3d and 1w somal and nucleus compared to acute (6h-1d) and late time points (2w-4w). These observations emphasize the findings in (Hernandez et al., 2019), that pathologies such as membrane disruption, are biphasic in this modality of injury. Notably, Hernandez *et al.* 2019 found that 6h-4w post CFPI animals did not feature neuronal loss nor evidence of cell death, supporting that idea that these atrophying neurons may be rescuable. Atrophy without concomitant cell death has also been observed by other groups following CFPI (Greer et al., 2011; Lifshitz et al., 2007), further corroborating this idea. This week-long therapeutic window of atrophy without cell death, provides an opportunity to salvage these membrane disrupted and Cath B relocalized neurons. Particularly, future studies focused on pharmacologically targeting Cath B for the recovery of the membrane disrupted neuronal population are warranted.

Overall, our study found that Cath B is being re-distributed into the cytosol, notably within the membrane disrupted neuron subpopulation. Moreover, these membrane disrupted neurons

significantly present Cath B relocalization late (2w-4w) following injury and the Hernandez *et al.* 2019 study highlighted that these neurons are not dying. While these Cath B relocalized neurons are not dying, they demonstrate both membrane disruption and atrophy. Both observations are indicative of a late secondary pathology and there is opportunity for therapeutic treatment of these neurons in diffuse TBI.

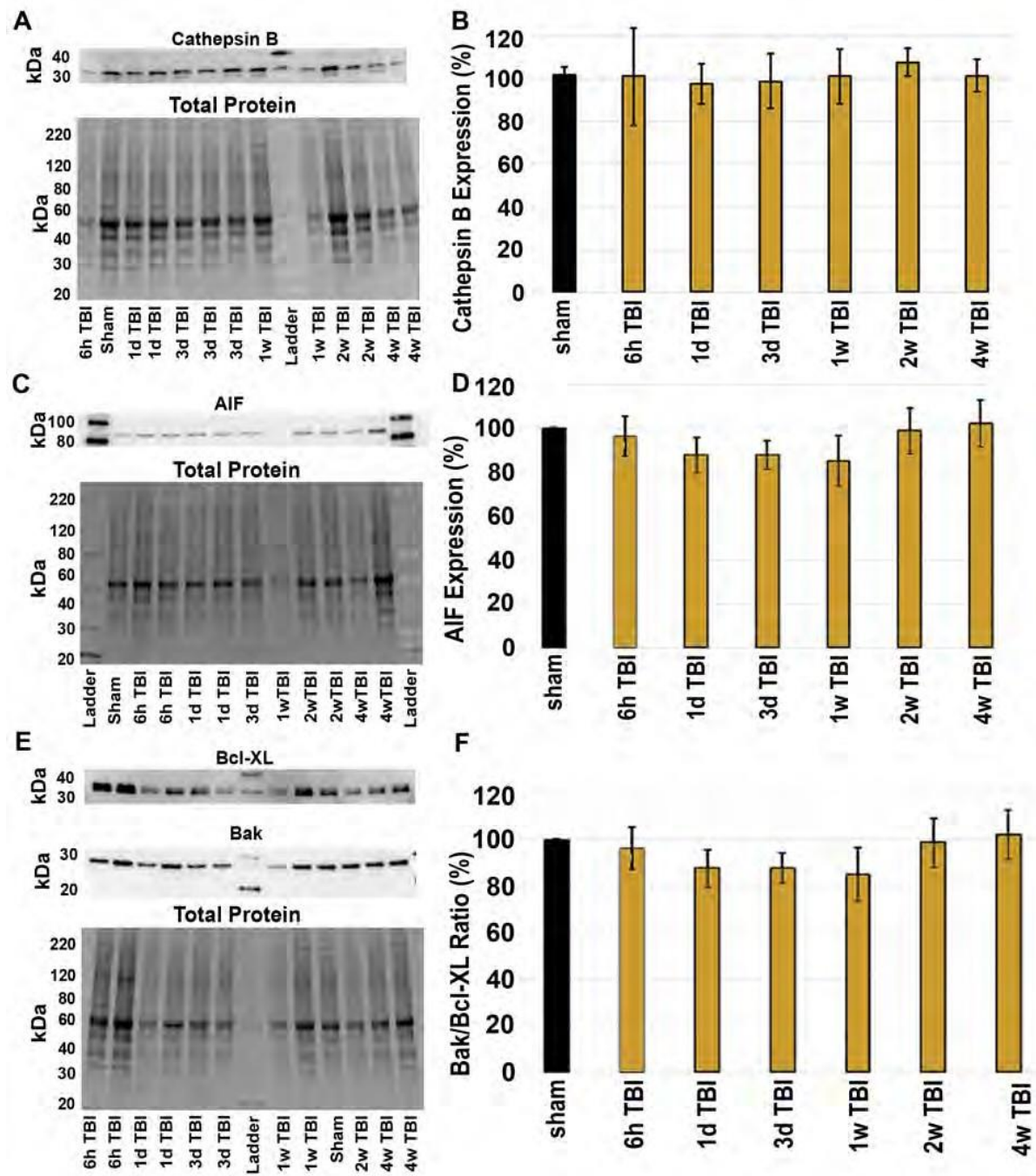


Figure 3.1. There were no differences in the expression of Cathepsin B (Cath-B) or Cath-B signaling proteins 6hr to 4w post-CFPI compared to sham. (A) representative chemiluminescent western blots depicting (A) Cath-B protein bands at 24/27 kDa, (C) AIF protein bands at ~67kDa, as well as (E) Bcl-XL and Bak protein bands at 30 and 25 kDa, respectively, from homogenized lateral cortices. All westerns were normalized to total protein as depicted below the corresponding western blot. Bar graphs depicting the averaged normalized protein expression of (B) Cath-B, (D) AIF, and (F) the expression ratio of Bcl-XL/Bak in sham animals (n=6) [black bars] and at 6hr-4w post-injury in TBI animals [yellow bars] (n=6/time point). There were no differences in the expression of any proteins assessed following CFPI compared to sham. Mean \pm S.E.M.

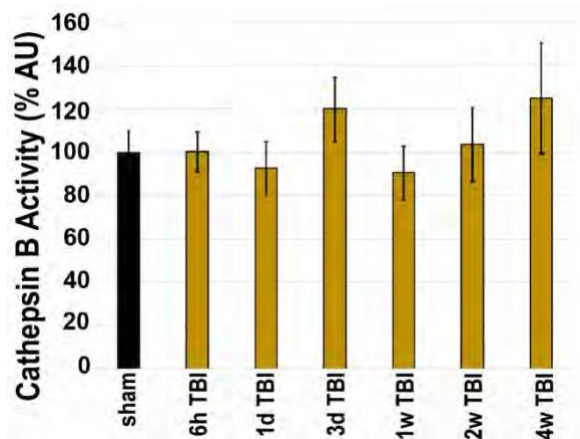


Figure 3.2. Cathepsin B activity does not significantly change following injury. Normalized average fluorescence intensity of Cathepsin B activity within whole homogenates of the lateral neocortex is reported in the bar graph. Sham animal (n=5) [black bars] (black bar) Cathepsin B activity was not found to be different from 6hr-4w post-CFPI (yellow bar; n=4/ time point) reported as mean \pm S.E.M.

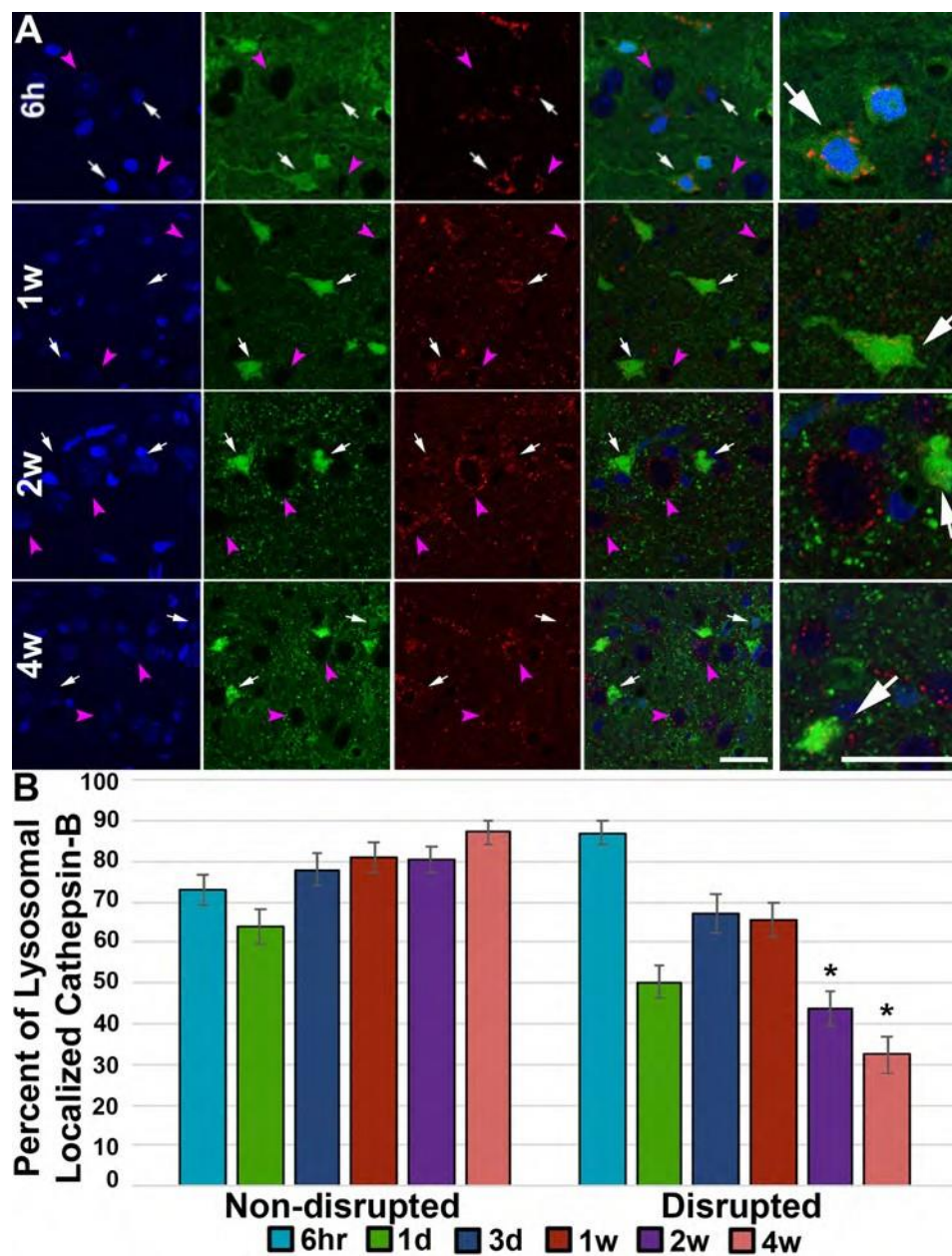


Figure 3.3. Representative confocal images at 6h, 1w, 2w, and 4w of immunolabeled Cathepsin B (red) in the lateral neocortex following CFPI (A). Membrane disrupted neurons were identified as containing the cell-impermeable Alexa-488 conjugated dextran (green). The nuclei were labeled with DAPI (blue) to identify the location of non-membrane disrupted neurons. The fourth panel is an overlay, and the last panel is a higher magnification image from the overlay panel. White arrows indicate membrane disrupted neurons and purple arrow heads indicate non membrane disrupted neurons. Scale bar=20 μ m. Cathepsin B localization shifts in membrane

disrupted neurons at 2 and 4w post-CFPI (B). Bar graph depicts the percentage of total analyzed neurons per timepoint with punctate lysosomal cathepsin B localization at 6h (n=290 neurons, 5 animals) [teal blue], 1d (n=282 neurons, 5 animals) [green], 3d (n=207 neurons, 4 animals) [dark blue], 1w (n=237 neurons, 5 animals) [red], 2w (n=300 neurons, 5 animals) [purple], and 4w (n=235 neurons, 5 animals) [pink] in non-disrupted and membrane disrupted neuronal populations reported as mean \pm S.E.M. * $p < 0.05$.

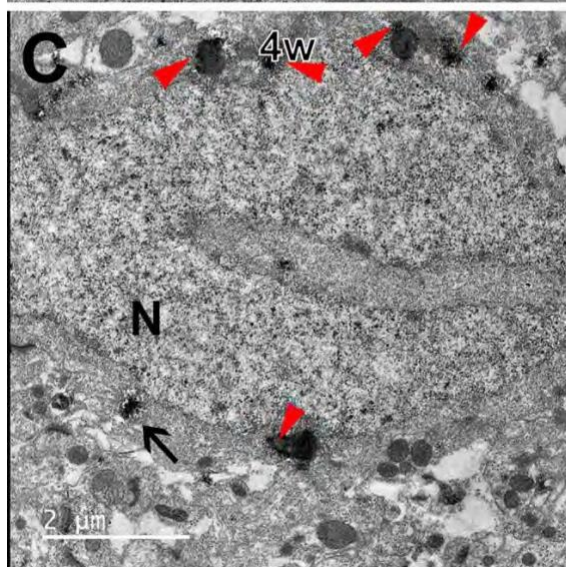
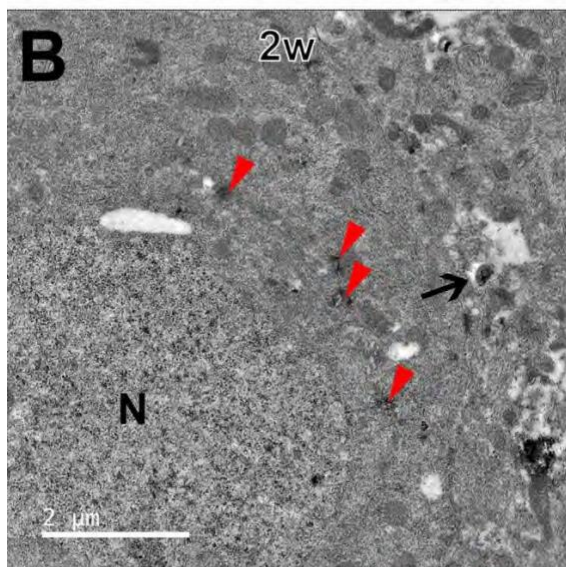
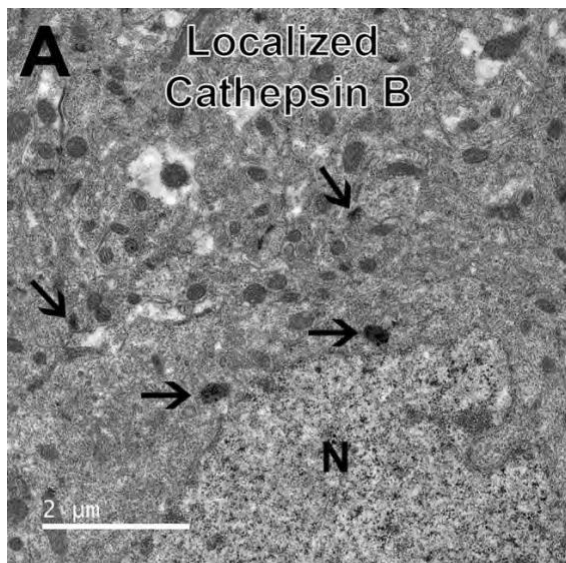


Figure 3.4. Qualitative ultrastructural confirmation of Cathepsin B redistribution outside of lysosomes following CFPI. Electron micrographs of neurons ("N" indicates the nucleus) immunolabeled for Cath-B (black granules) from a representative 2w and 4w TBI animal. (A) Some neurons in the injured brain displayed normally localized cathepsin B within lysosomes (black arrows). (B&C) Diffuse localization of Cathepsin B outside of the lysosomes (red arrow heads), however, was observed in many of the lateral neocortical neurons in these cases, substantiating the confocal quantitative assessments. Scale bar=2 μ m

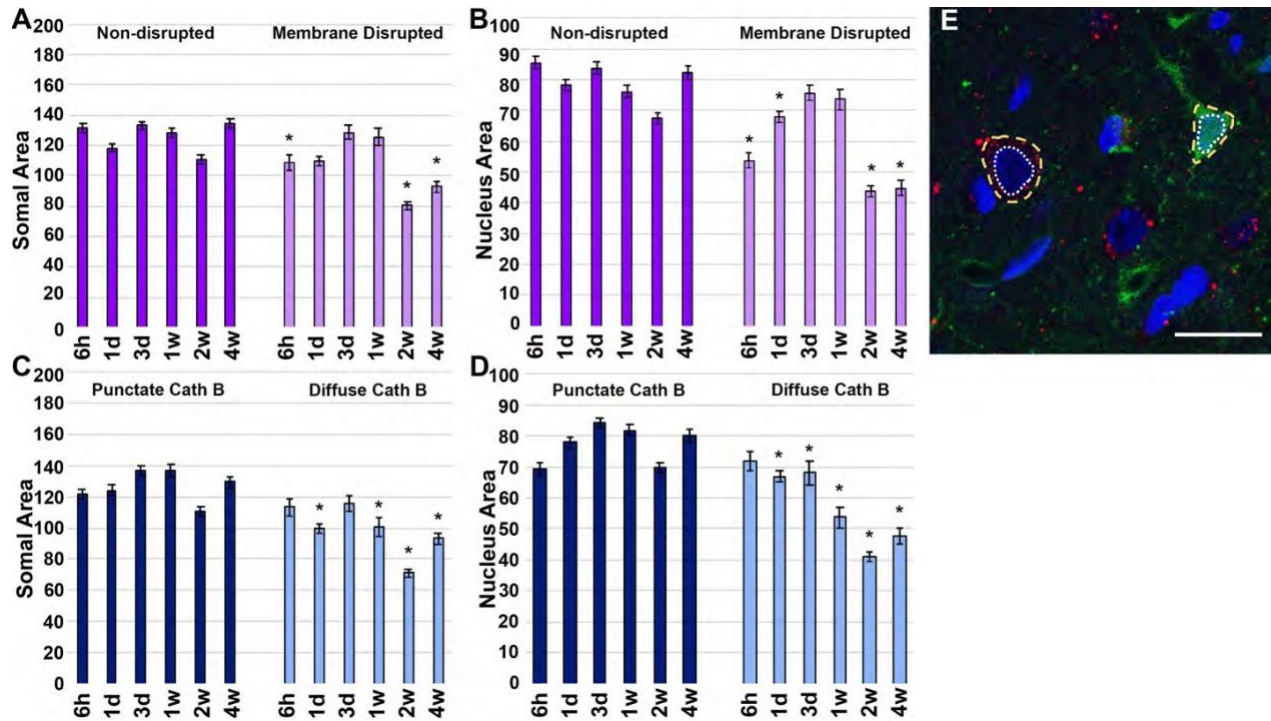


Figure 3.5. Membrane disruption and Cathepsin B mislocalization affect cell morphology. Bar graphs comparing the mean (A&C) somal area and (B&D) nucleus area 6h (n=738 neurons/5 animals), 1d (n=527 neurons/5 animals), 3d (n=388 neurons/4 animals), 1w (n=426 neurons/5 animals), 2w (n=577 neurons/ 5 animals), and 4w (n=434 neurons/5 animals) following CFPI. These neurons were designated as (A&B) membrane disrupted (light purple bars) and non-disrupted (dark purple bars) or (C&D) based on Cathepsin B localization into puncta (dark blue bars) or diffusely distributed throughout the cytoplasm (light blue bars) in each cell. (E) Representative image indicating somal area (dashed circle) and nucleus area (dotted circle) in a membrane disrupted and non-disrupted neuron at 1w post-injury. Scale bar=20 μm. The area of both the soma and nucleus was decreased in membrane disrupted neurons, and neurons with diffusely localized Cathepsin B. * $p < 0.05$ compared to timepoint-matched internal controls [(A&B) non-membrane disrupted or (C&D) punctate localized Cath B neurons].

Chapter 4: The effects of ICP and Cathepsin B inhibition on the Membrane Disrupted Population

Introduction

Traumatic brain injury (TBI) has devastating consequences for patients, their families, and communities. As of 2016, the prevalence rate globally was reported at 759 per 100,000 (James et al., 2019). This life-altering event can produce impairments in motor, cognitive, sensory, and affective function that can become chronic (Dams-O'Connor et al., 2023). Moreover, elevated intracranial pressure (ICP) following TBI can increase morbidity and mortality as well as induce secondary pathologies. The current treatments and strategies are invasive and elevated ICP is known to have high morbidities and mortalities (Farahvar et al., 2012; Miller et al., 1977). Currently, the molecular cascade prior to and following elevated ICP remains nebulous.

Early studies from our lab indicate that neuronal membrane disruption, a diffuse pathology following the central fluid percussion injury (CFPI) model, worsens with elevated intracranial pressure at the acutely 6h following injury (Lafrenaye et al., 2012, 2014). Neuronal membrane disruption has been surmised as the perturbation of neuronal plasma membrane. Using various molecular tracers, membrane disruption in neurons has been demonstrated acutely and subacutely in vitro and in vivo; from mice and rats to swine (Cullen et al., 2011; Farkas et al., 2006; Geddes, Cargill, et al., 2003; Geddes, LaPlaca, et al., 2003; Harris et al., 2023; Keating et al., 2020; Lafrenaye et al., 2012, 2014; LaPlaca et al., 2019; LaPlaca & Thibault, 1998; Prado & LaPlaca, 2020; Singleton & Povlishock, 2004; Wofford et al., 2017).

Earlier investigations from our group found Cathepsin B (Cath B), a lysosomal cysteine protease, relocalized from the lysosomes into the cytosol at 6h post-injury, and exhibited significantly higher relocalization in animals that sustained a TBI with an ICP elevation (Lafrenaye et al., 2012a). Cath B has been known to participate in various cell damage and death processes

(Chaitanya & Babu, 2008; Chowdhury et al., 2019; de Castro et al., 2016; Ellis et al., 2005; Foghsgaard et al., 2001; Guicciardi et al., 2000; Mizunoe et al., 2020; Moles et al., 2012; Oberle et al., 2010; Wang et al., 2021; Wen et al., 2008; Wu et al., 2015) so it was thought relocalized Cath B disrupted neurons are dying. Additionally, subacute neuronal membrane disruption with elevated ICP was associated with chronic effects, including neuronal cell loss as well as behavioral morbidities at 4w, that were not seen with injury alone(Lafrenaye et al., 2014). This prompted our probe into the duration of neuronal membrane disruption through the study 6h to 4w post-injury rats. highlighted membrane disruption having a biphasic timing, present at sub-acute times (6h-3d) and reemerging late (2w-4w), without ultrastructural signs of cell death (Hernandez et al., 2019).

Moreover, Cath B has been implicated in the pathologies seen in other models of TBI (Boutté et al., 2020; Hook et al., 2013; Luo et al., 2010), such as protein upregulation, lysosomal permeability, cell death, and behavioral deficits. Thus we also assessed Cath B in the 6h-4w animals; that data revealed there's a relocalization of Cath B, specifically in the membrane disrupted neurons at 2 and 4w post-injury (Hernandez et al., 2022). However, those injured animals did not have elevated ICP.

The focus of this study is to evaluate the effects of inhibition of Cath B on neuronal membrane disruption 2w following injury to see if elevated ICP is inducing death through Cath B. Therefore, this was accomplished using animals that survived out to 2w with either sham injury, CFPI only, or CFPI with subsequent ICP elevation. Following these surgical procedures, these animals were given a treatment of CA-074Me, a Cathepsin B selective inhibitor or 10% DMSO in sterile saline, the vehicle for CA-074Me for that 2w duration. We then assessed the activity of the lateral neocortices, evaluated Cathepsin B and other binding partners AIF, Bcl-XL, and Bak's protein levels. We also conducted histological analyses of membrane disruption and Cath B relocalization, total cell count to assess for cell loss, and whisker nuisance task to evaluate any behavioral changes. In doing such, our work demonstrated that Cath B is not a direct driver of

membrane disruption, however, in the group with TBI and elevated ICP, administration of CA-074Me reduces hypersensitivity, emphasizing Cath B being an important component in late secondary pathologies.

Materials and Methods

Animals

Experiments were conducted using protocols in accordance with the Virginia Commonwealth University institutional ethical guidelines concerning the care and use of laboratory animals (Institutional Animal Care and Use Committee, Virginia Commonwealth University), which adhere to regulations including, but not limited to, those set forth in the Guide for the Care and Use of Laboratory Animals, 8th Edition (National Research Council). Animals were housed in individual cages on a 12h light-dark cycle with free access to food and water. Archived tissue and homogenates from our previous study using adult male Sprague-Dawley rats, n=72, n=36 for westerns and protein analyses, n=36 for histological assessments; (n = 6/group) (1) Sham injury with 10% DMSO treatment, (2) Sham injury with CA-074Me treatment, (3) TBI with 10% DMSO treatment, (4) TBI with CA-074 treatment, (5) TBI+ ICP elevation with 10% DMSO, or (6) TBI+ ICP elevation with CA074Me, weighing 320–420g, were used for this study. Our a priori exclusion criteria included weight loss of more than 20% of their pre-injury body weight or gross brain pathology (contusion, subdural hematoma, or gross tissue loss). No animals met exclusion criteria in this study. Animal injury state and drug administration were randomly determined using a random number generator by a separate investigator from the surgeon. All surgeries were conducted by the same surgeon during the same times of day to reduce variability.

Surgical preparation and injury induction

Animals were anesthetized with 4% isoflurane in 30% O₂ and 70% room air and ventilated with 2% isoflurane in 30% O₂ and 70% room air throughout the duration of the surgery, injury, and post-injury physiological monitoring. Heart rate, respiratory rate, and blood oxygenation were monitored via a hind-paw pulse oximetry sensor (STARR Life Sciences, Oakmont, PA) for the duration of anesthesia, except during the induction of injury. Body temperature was maintained at 37°C with a rectal thermometer connected to a feedback-controlled heating pad (Harvard Apparatus, Holliston, MA). All animals were placed in a stereotaxic frame (David Kopf Instruments, Tujunga, CA). A midline incision was made, and a 4.8 mm circular craniectomy was made along the sagittal suture midway between bregma and lambda for injury induction. A 2mm burr hole was also drilled in the left parietal bone overlying the left lateral ventricle (0.8 mm posterior, 1.3 mm lateral, and 2.5- 3 mm ventral to bregma) through which a 25-gauge needle, connected to a pressure transducer and microinfusion pump (11 Elite syringe pump; Harvard Apparatus) via sterile saline-filled PE50 tubing, was placed into the left lateral ventricle. Appropriate placement was verified via a 1.3µl/min infusion of sterile saline within the closed fluid-pressure system during needle placement. The needle was held in the ventricle for at least 5min to record pre-injury intracranial pressure (ICP). After the 5-min reading, the needle was slowly removed, and the burr hole was covered with bone wax before preparation for sham or CFPI (Dixon et al., 1987; Lafrenaye et al., 2014). Briefly, a Leur-Loc syringe hub was affixed to the craniectomy site, and dental acrylic (methyl-methacrylate; Hygenic Corp., Akron, OH) was applied around the hub and allowed to harden. Anesthetized animals were removed from the stereotaxic frame and injured at a magnitude of 2.05 ± 0.16 atmospheres and duration of ~22msec. The pressure pulse was measured by a transducer affixed to the injury device and displayed on an oscilloscope (Tektronix, Beaverton, OR). Immediately after the injury, the animal was reconnected to the ventilator and physiologic monitoring device and the hub and dental acrylic were removed en bloc. Gelfoam/Surgifoam was placed over the craniectomy/injury. The animal was then

replaced in the stereotaxic device and the ICP probe was reinserted into the lateral ventricle, as described above, for post-injury ICP monitoring. At 15 minutes following injury, animals were given 0.9mg/kg buprenorphine-HCl slow release (Bup-HCl-SR) subcutaneous (SQ) as an analgesic and then monitored until 1 hour following injury. If the animals were selected for TBI and 20mmHg ICP elevation, that began immediately following Bup-HCl SR administration. ICP was manually elevated to 20 mmHg via infusion of sterile normal saline at 1.3 to 13 μ L /minute using the micro infusion Pump 11 Elite syringe pump controlled by the experimenter. Once 20 mm Hg was achieved, ICP was maintained until 1 hour after injury. Animals underwent drug or vehicle bolus infusion, followed by subcutaneous implantation of mini-osmotic pump; the animals were sutured and treated with lidocaine and triple-antibiotic ointment on the scalp, then recovered and returned to clean home cages. Identical surgical procedures were followed for sham-injured animals, without release of the pendulum to induce injury (Hernandez et al., 2019; Lafrenaye et al., 2014a).

Drug Preparation and Treatment Administration

CA-074 methyl ester (CA-074Me), the Cathepsin B selective inhibitor (MedChemExpress, Cat#: HY-100350, Monmouth Junction, NJ) was stored at -20 as a solid until added to 100% dimethylsulfoxide (DMSO), at a concentration of 100 μ g/ μ L in 31 μ L aliquots at -80. The day prior to surgery, the aliquot was brought to a concentration of 10 μ g/ μ L with sterile 0.9% saline by an investigator who was not the surgeon. The blinded treatment (CA-074Me in 10% DMSO-sterile saline or 10% DMSO-sterile saline) was pipetted into a separate tube for the bolus, and a tube to fill the osmotic pump and stored at 37 C. Sterile preparation of the sterile 250 μ L mini-osmotic pump (Alzet; Model 2002), with catheter tube and brain cannula was also performed by the surgeon blinded to treatment. The prepared pump was placed in a sterile tube with saline to initiate osmotic pressure and then stored at 37C alongside bolus. One hour following injury, 12.5 μ L of treatment was infusion into the left ventricle. Next, the caudal end of the midline incision was

probed with blunt scissors to lift the skin over the shoulder blades. The warmed osmotic pump with bolus-matching treatment was implanted, and using the stereotaxic cannula holder, the cannula was placed into the burr hole for lateral ventricle with spacers if needed. The cannula was held in place with cyanoacrylate. The pump was in the animal the entire 2w post-injury and infused at 0.5 μ L/h.

Tracer infusion

One hour prior to sacrifice, tagged dextran (0.6 mg/25 μ g in sterile 0.9% saline; ~1.6mg/kg) was infused into the lateral ventricle as described (Hernandez et al., 2019; Lafrenaye et al., 2012a). Briefly, 12.5 μ l of 10kDa dextran conjugated to 488-Alexa Fluor (Cat#: D22910, Invitrogen, Carlsbad, CA), was infused into the left and right lateral ventricle at 1.3 μ l/min, with continuous ICP monitoring. To avoid bias caused by differences in fluorescent signal detectability, animals were. The tracer was allowed to diffuse throughout the parenchyma for 1h prior to transcardial perfusion at 2w post-sham or CFPI.

Tissue processing

At 2w post-injury, the animals were injected with 150mg/kg euthanasia-III solution (Henry Schein, Dublin, OH), then underwent transcardial perfusion with cold 0.9% saline. Lateral neocortices were dissected and frozen for protein expression and activity assessments (n=36). Animals for histological assessments (n=36) underwent the aforementioned euthanasia process, transcardial perfusion of cold 0.9% saline followed by a switch in transcardial perfusate to 4% paraformaldehyde/ 0.2% glutaraldehyde in Millonig's buffer (136mM sodium phosphate monobasic/109mM sodium hydroxide) to fix the brain for subsequent immunohistochemical processing and analysis. After transcardial perfusion, the brains were removed, post-fixed for 24-48h, then sectioned coronally in 0.1M phosphate buffer with a vibratome (Leica, Banockburn, IL)

at a thickness of 40µm from bregma to 4.0mm posterior to bregma. Sections were collected serially in 12 well-plates and stored in Millonig's buffer at 4°C. A random starting well (wells 1–12) was selected using a random number generator and four serial sections were used for histological analyses. All histological analyses were restricted to layers V and VI of the lateral somatosensory neocortex extending from the area lateral to CA1 to the area lateral to CA3 of the hippocampus (Hernandez et al., 2019).

Quantification of Cathepsin B Activity

Portions of the dissected left and right lateral neocortices and livers of the sham, TBI, and TBI+ICP animals were homogenized in 50 µM citric acid at a pH 6.0, spun at 12,000 xg at 4° C for 10 minutes and the supernatant of the whole homogenate was collected. Protein concentrations were measured using a NanoDrop Lite (Thermo Fisher Scientific, Wilmington, DE) and Cathepsin B activity was measured in a 96-well plate, each well containing 2x Assay Buffer (100mM sodium acetate pH 5.5, 2mM EDTA, 200mM sodium chloride, 8mM DTT), 2µg of neocortex whole homogenate, and Z-Phe-Arg-7-amino-4-(trifluoromethyl) coumarin (ZFR-AMC), a substrate for cysteine proteases that fluoresces upon cleavage by Cathepsin B (Boutté et al., 2020; Hernandez et al., 2022; Hook et al., 2013; Yoon et al., 2021). The plate was read 30- and 60-minutes post-substrate addition at 365/450 nm excitation/emission. Each sample was loaded in triplicate per plate in three independent runs to reduce pipetting and run-to-run variability biasing the results. A positive control well with purified human liver Cathepsin B 5 ng and a negative control well with only assay buffer and substrate were included in every run. The raw arbitrary fluorescent values depicting activity were measured in increased fold compared to the negative control, which was designated as 0-fold activity.

Western blotting

Lateral neocortices of (n = 6/group, 2 samples per animal as brains were dissected at the cerebral fissure into left and right hemispheres) (1) Sham injury with 10% DMSO treatment, (2) Sham injury with CA-074Me treatment, (3) TBI with 10% DMSO treatment, (4) TBI with CA-074 treatment, (5) TBI+ ICP elevation with 10% DMSO, or (6) TBI+ ICP elevation with CA074Me, were homogenized in western lysis buffer (150 mM NaCl, 50 mM Tris pH 8.0, 1% Triton) and protease inhibitor cocktail (AEBSF 10.4mM, Aprotinin 8µM, Bestatin 400µM, E-64 140µM, Leupeptin 8µM, Pepstatin A 150µM, Cat#: P8340, Sigma, Saint Louis, MO) with a motorized pestle. Protein concentrations were measured using a BCA Protein Assay Kit (Pierce Biotechnology, Thermo Fisher Scientific, Rockford, IL, Cat#: 23227). Protein (20 µg for Cathepsin B, 5 µg Bcl-XL, 10 µg Bak and AIF) was boiled for 10min in 50mM dithiothreitol (Cat#: 1610610; Bio-Rad; Hercules, CA), 2x Laemmli loading buffer (Cat#: 1610737; Bio-Rad; Hercules, CA) and run at 200 Volts for 30min on Mini- PROTEAN TGX Stain-Free 4-20% precast polyacrylamide gels (Cat#: 4568096; Bio-Rad, Hercules, CA). Protein was transferred onto 0.45µm PVDF membranes using a Bio-Rad Transblot Turbo transfer system set to the mixed molecular weight manufacturer setting (1.3-2.5 Amps, 25 Volts for 7min). Western blotting was done on an iBind flex apparatus (Invitrogen, Carlsbad, CA) using primary antibodies rabbit anti-Cathepsin B (1:1000; Cat#: 31718S, RRID:AB_2687580), rabbit anti-Bak (1:1000; Cat#: 12105S, RRID:AB_2716685), rabbit anti-Bcl-xl (1:1000; Cat#: 2764S, RRID:AB_2228008) or rabbit anti-AIF (1:1000; Cat#: 5318S, RRID:AB_10634755) (Cell Signaling Technology, Danvers, MA) and anti-rabbit-HRP secondary antibody (1:5000; Cat#: 111- 035-003; Jackson ImmunoResearch Laboratories, West Grove, PA, RRID:AB_2313567). Total protein (Stain Free) and chemiluminescent images were taken on a ChemiDoc imaging system (BioRad). Densitometric analyses of Cathepsin B, AIF, Bak, and Bcl-XL were performed in ImageJ (National Institutes of Health; Bethesda, MD). Cathepsin B, AIF, Bak and Bcl-XL protein bands were normalized to total protein and a naive control. All western blots were run in triplicates on three separate gels to reduce run-to-run variability biasing the results.

Membrane Disruption and Total Cell Count Analysis

Consistent with previous studies, we assessed the potential for neuronal membrane disruption via the utilization of 10kDa dextrans, which are impermeable to cells with intact membranes (Lafrenaye et al., 2014, 2012; Hernandez et al., 2019, 2022). Fluorescently tagged dextran-containing cells, indicative of membrane perturbation, could be visualized via fluorescent microscopy without further processing. Tissue sections from (n= 6/group) (1) Sham injury with 10% DMSO treatment, (2) Sham injury with CA-074Me treatment, (3) TBI with 10% DMSO treatment, (4) TBI with CA-074 treatment, (5) TBI+ ICP elevation with 10% DMSO, or (6) TBI+ ICP elevation with CA074Me were stained with 1:500 dilution of NeuroTrace 435/455 blue fluorescent Nissl Stain (Life Technologies, Eugene, OR, Cat# N21479). The tissue was mounted onto slides using Vectashield Vibrance mounting medium with (Cat#: H-1700; Vector Laboratories, Burlingame, CA). Sections were analyzed by fluorescent optical sectioning microscopy using a Keyence BZ-X800 microscope (Keyence Corporation of America, Itasca, IL, USA). Quantitative analysis was performed as described previously (Lafrenaye et al., 2014b). Briefly, optical sectioning images of the left neocortical region of interest were taken at 40X magnification in a systematically random fashion by a blinded investigator using dextran labeling to verify focus. Image acquisition settings were held constant for comparable regions (layer V or VI) for all groups analyzed. Analyses of neurons exhibiting dextran uptake were performed using the ImageJ cell counting plug-in and verified cellular identity using the NeuroTrace staining. Dextran containing neurons were quantified for each image and averaged for each animal. As for total cell count to assess for cell loss, the NeuroTrace labeled images were placed into the Hybrid Cell Counter function of Keyence BZ-X800 Analyzer software, where the images were set in the simple thresholding tool to have uniform brightness, removed smoothing, auto thresholding, to highlight all Neurotrace positive cells followed by removal of objects smaller than 15 μ m to count cells only.

Cellular Cathepsin B Localization Analysis

Fluorescently tagged dextran-containing cells, indicative of membrane disruption, could be visualized via fluorescent microscopy without further processing. Three tissue sections, 5-6 images /animal from (1) Sham injury with 10% DMSO treatment n=6 animals, 10 non-disrupted and 10 membrane disrupted cells per image, n=372 cells, (2) Sham injury with CA-074Me treatment n=6 animals, 10 non-disrupted and 10 membrane disrupted cells per image, n=424 cells, (3) TBI with 10% DMSO treatment n=6 animals, 10 non-disrupted and 10 membrane disrupted cells per image, n=441 cells, (4) TBI with CA-074Me treatment n=6 animals, 10 non-disrupted and 10 membrane disrupted cells per image, n=480 cells, (5) TBI+ ICP elevation with 10% DMSO n=6 animals, 10 non-disrupted and 10 membrane disrupted cells per image, n=378 cells, or (6) TBI+ ICP elevation with CA-074Me n=6 animals, 10 non-disrupted and 10 membrane disrupted cells per image, n=550 cells, were blocked with 5% normal goat serum (NGS), 2% bovine serum albumin (BSA), and permeabilized with 1.5% triton-X for 2h. This was followed by immunolabeling using primary antibodies rabbit anti- Cathepsin B (1:700; Cat#: 31718; Cell Signaling Technology; Danvers, MA; RRID:AB_2687580) and mouse anti- NeuN (1:500; Cat#: MAB377; MilliporeSigma; Temecula, CA, RRID:AB_2298772). Tissue was incubated in secondary antibodies Alexa-647 conjugated goat anti-mouse(1:700; Cat#: A32728; Life Technologies, Rockford, IL; RRID:AB_10563566) and Alexa-568 conjugated goat anti-rabbit (1:800; Cat#: A11036; Life Technologies, Eugene, OR; RRID:AB_2534102) and the tissue was mounted onto slides using Vectashield hardset mounting medium with 4',6-diamidino-2-phenylindole (DAPI) (Cat#: H-1500; Vector Laboratories, Burlingame, CA). Quantitative analysis was performed as described previously (Hernandez et al., 2019; Lafrenaye et al., 2012a). Briefly, 5 epifluorescent images from the three sections; 3 sections/animal of the left neocortical region of interest were taken at 40X magnification using a Keyence BZ-X800 microscope (Keyence Corporation of America, Itasca, IL, USA) in a systematically random fashion by an investigator blinded to the animal group using the dextran tag to verify images included neurons with and without membrane disruption. Image acquisition settings were held constant for comparable

regions (layer V or VI) and 488-dextran for all groups analyzed. The images including 488-dextran, DAPI, and Cathepsin B were placed into FIJI (Image J). DAPI was used to identify nuclei of cells containing and not containing 488 dextran. Ten cells were identified per category then cells were classified by Cathepsin B appearance of punctate (intra-lysosomal) versus diffuse (extra-lysosomal). A total of ten cells that are non-membrane disrupted and ten cells that are membrane disrupted could not be found for every image. The localization of Cathepsin B was expressed as a percentage of neurons demonstrating punctate (lysosomal) Cathepsin B localization of the total membrane disrupted or non-disruption neuronal population assessed in each experimental group.

Whisker Nuisance Task

Following CFPI, rats demonstrate hypersensitivity in the whisker barrels which can be assessed using the whisker nuisance task (WNT)(Lafrenaye et al., 2014; McNamara et al., 2010; Ryu et al., 2022). Two to three days post arrival in animal facilities, rats were brought from the vivarium up to the lab, into a small room for pre-injury scoring. The post-injury assessment was conducted in the same room the day prior to or the day of sacrifice. Each rat was sat inside a plastic storage container lined with a chux pad and allowed to acclimate to the container for 5 minutes. In each trial, a wooden applicator stick was brushed along the rat's whiskers on each side, for 5 minutes. Meanwhile, the rat was assessed for the following behaviors: movement, body position/stance, breathing, whisker position, whisking response, evading stimulation, response to stick presentation, grooming, ear position, sniffing, fur ruffling, and urination/defecation. Between each trial, rats were given 1-minute periods of rest. Three trials in total were conducted and scored live, by the researcher conducting the behavior. These behaviors were scored on a scale of 0 to 2 (0 = absent, 1 = present (exhibits behaviors 1-2 times), 2 = profound (repetitively shows behavior)), summed per trial, and averaged per animal with a possible maximum score of 24.

Statistics

Data were tested for normality prior to utilizing parametric or non-parametric assessments, which were conducted using SPSS (IBM Corporation, Armonk, NY) software. Animal numbers for each group were determined by an a priori power analysis using effect size and variability previously observed in the lab when assessing pathology between sham and injured groups using the CFPI model, an alpha = 0.05, and a power of 80%. Two-way, one-way, or repeated measures analysis of variance (ANOVA) and Bonferroni post hoc tests were performed for all between-group analyses. Statistical significance was set to $p < 0.05$. Data are reported as mean \pm standard error of the mean (SEM).

Results

Cathepsin B activity was decreased in the left and right cortex 2w post-injury with concurrent CA-074Me administration.

Cathepsin B activity following CFPI has shown no difference between 6 hours to 4 weeks post-injury (Hernandez et al., 2022). For this investigation, we measured the activity of cathepsin B, reported in activity fold change from arbitrary fluorescent units. There was no interaction between the injury group and treatment; $F_{2,93}=0.324$, $p=0.724$. There was a trend toward interaction between injury group and region; $F_{4,93}=2.306$, $p=0.064$. Also, there was an interaction of treatment and region $F_{2,93}=4.299$, $p=0.016$ for Cath B activity. There was a reduction between vehicle and CA-074Me treatment $F_{1,93}=20.469$, $p=1.8 \times 10^{-5}$, and a statistical difference between regions, $F_{2,93}= 40.021$, $p=2.89 \times 10^{-13}$. Bonferroni post-hoc indicated a difference between the left cortex and liver, $p=1.09 \times 10^{-10}$ right cortex and liver, $p=1.49 \times 10^{-8}$ and no difference between left and right cortex $p=0.946$. Even with the additional group of CFPI+ICP elevation added to the comparison, we saw that there was no difference in cathepsin B activity between sham, CFPI,

CFPI+ICP elevation; $F_{2,93}=0.324$, $p=0.724$. However, we did see a drug effect from CA-074Me, causing a significant decrease in activity for both the left and right cortex of brains administered the drug, regardless of injury modality. Moreover, the livers of animals were collected as a positive control for Cathepsin b activity and to also monitor systemic cathepsin b inhibition. The overall assay positive control per every plate was purified human liver Cathepsin B. There was no interaction of injury group, treatment, and region for Cath B activity; $F_{4,93} = 1.013$, $p = 0.405$; Three-way ANOVA: $F_{17,93}= 7.438$, $p=3.63 \times 10^{-11}$ Figure 4.1, Table 1.

Table 1. Cathepsin B Activity Fold Increase				
Injury Group	Treatment	Sample Region	Mean	S.E.M.
sham	10% DMSO n=6	Left Cortex	4.043	0.264
		Right Cortex	4.703	0.317
		Liver	8.332	1.091
	CA-074Me n=6	Left Cortex	1.662	0.601
		Right Cortex	3.125	0.425
		Liver	6.933	0.825
TBI	10% DMSO n=6	Left Cortex	5.810	0.473
		Right Cortex	4.476	0.557
		Liver	6.814	0.720
	CA-074Me n=6	Left Cortex	2.408	0.497
		Right Cortex	3.927	0.414
		Liver	6.873	0.801
TBI+ ICP	10% DMSO n=6	Left Cortex	4.946	0.909
		Right Cortex	3.659	0.951
		Liver	6.578	0.949
	CA-074Me n=6	Left Cortex	2.577	0.622
		Right Cortex	4.016	0.287
		Liver	4.989	0.567

Protein expression of Cathepsin B and other signaling partners; Bak, Bcl-XL, and AIF

The overall expression of Cath B within the lateral neocortex was evaluated for changes following CFPI, in all injury and treatment groups. Western blot analysis revealed that total Cath B protein levels were in mean \pm SD (1) Sham injury with 10% DMSO ($187.84 \pm 50.52\%$), (2) Sham injury with CA-074Me ($222.49 \pm 129.05\%$), (3) TBI with 10% DMSO ($205.16 \pm 66.41\%$), (4) TBI with CA-074 ($213.19 \pm 102.72\%$), (5) TBI+ ICP elevation with 10% DMSO ($226.05 \pm 129.58\%$), or (6) TBI+ ICP elevation with CA074Me ($257.04 \pm 129.58\%$) (Figure 2). There was no interaction

between the injury group and treatment on Cath B protein quantity; two-way ANOVA $F_{2,66}=0.119$, $p=0.888$. There also was no effect on the Cath B protein quantity from the injury type, $F_{2,66}=0.909$, $p=0.408$, or significant effects from inhibitor administration, $F_{1,66}=1.033$, $p=0.313$; two-way ANOVA $F_{5,66}=0.618$, $p=0.687$.

Cath B can participate in various cell damage pathways through downstream proteins such as AIF, Bcl-XL, and Bak. (Chaitanya & Babu, 2008; Chowdhury et al., 2019). (Boya et al., 2003; Oberle et al., 2010) Previously, the protein expression of AIF as well as the expression ratio of the antagonizing proteins Bcl-XL and Bak were also assessed over 6h-4w time course injury and found no difference in these protein quantities after injury compared to sham(Hernandez et al., 2022). However, in this study, it was unknown how TBI+ICP or cathepsin B inhibition would impact such downstream proteins.

As for Bcl-XL protein quantification, 1) Sham injury with 10% DMSO ($100.93 \pm 33.33\%$), (2) Sham injury with CA-074Me ($99.83 \pm 19.76\%$), (3) TBI with 10% DMSO ($93.66 \pm 14.14\%$), (4) TBI with CA-074 ($99.94 \pm 32.84\%$), (5) TBI+ ICP elevation with 10% DMSO($99.63 \pm 32.74\%$), or (6) TBI+ ICP elevation with CA074Me ($97.56 \pm 27.93\%$) mean \pm SD. Two-way ANOVA was performed to compare interactions and effects of injury types and Cath B inhibitor on Bcl-XL protein quantity; $F_{5,66}=0.11$, $p=0.99$. There also was no effect on Bcl-XL protein quantity from the injury type $F_{2,66}=0.100$, $p=0.905$ or inhibitor administration $F_{1,66}=0.025$, $p=0.875$. Two-way ANOVA was performed to compare interactions and effects of injury types and Cath B inhibitor on Bcl-XL protein quantity. There was no interaction between the injury group and treatment; $F_{2,66}=0.162$, $p=0.851$, Figure 4.3.

Bak quantities were measured as such mean \pm SD 1) Sham injury with 10% DMSO ($230.85 \pm 108.21\%$), (2) Sham injury with CA-074Me ($239.82 \pm 126.22\%$), (3) TBI with 10% DMSO ($235.62 \pm 117.75\%$), (4) TBI with CA-074 ($240.35 \pm 144.05\%$), (5) TBI+ ICP elevation with 10% DMSO($223.74 \pm 102.75\%$), or (6) TBI+ ICP elevation with CA074Me ($257.82 \pm 141.87\%$). Injury type did not affect Bak quantities, Figure 4.4. $F_{2,66}=0.010$, $p=0.989$, nor did treatment have an effect in Bak quantities $F_{1,66}=0.295$, $p=0.589$. Interactions were assessed for the effect of injury

types and treatment on Bak protein quantity; no interactions were found between the groups; $F_{2,66}=0.098$, $p=0.907$. Two-way ANOVA $F_{5,66}=0.103$, $p=0.991$.

The quantity of AIF was as such, displayed in mean \pm SD 1) Sham injury with 10% DMSO ($107.83 \pm 10.32\%$), (2) Sham injury with CA-074Me ($102.68 \pm 12.56\%$), (3) TBI with 10% DMSO ($98.25 \pm 15.10\%$), (4) TBI with CA-074 ($104.19 \pm 18.58\%$), (5) TBI+ ICP elevation with 10% DMSO ($102.26 \pm 10.24\%$), or (6) TBI+ ICP elevation with CA074Me ($89.21 \pm 17.02\%$). While no significant difference was seen between the injury groups, there was a trend towards a decrease in AIF protein quantity from the injury type $F_{2,66}=2.671$, $p=0.077$. As the injury group and treatment were assessed for interaction, the two-way ANOVA found a trend toward interaction; $F_{2,66}=2.649$, $p=0.078$. Two-way ANOVA, $F_{5,66}=2.423$, $p=0.044$; Figure 4.5.

Neuronal membrane disruption stays consistent between injury and treatment groups

To determine the effect of CA-074Me on TBI and TBI+ICP 2w post-injury, we infused tagged dextran intracerebroventricularly (ICV) prior to sacrifice at various time points 2w post-CFPI. Cells containing dextran were considered membrane disrupted and were quantified throughout layers V and VI of the lateral neocortex. Within sham animals (Figure 4.6 A & D), membrane disruption was detected ($7.83\% \pm 2.16$ [10% DMSO] and $12.09\% \pm 3.91$ [CA-074Me] total neurons). Rats sustaining TBI (Figure 4.6 B & E) also demonstrated membrane disruption ($6.56\% \pm 1.13$ [10% DMSO] and $10.86\% \pm 3.08$ [CA-074Me] total neurons). At percentages like sham and TBI only, TBI with elevated ICP samples (Figure 4.6 C & F) ($10.72\% \pm 2.60$ [10% DMSO] and $6.34\% \pm 1.28$ [CA-074Me] total neurons) were membrane disrupted (Figure 4.7); two way-ANOVA $F_{2,30}=1.921$ $p=0.164$, with no effects from injury $F_{2,30}=0.187$ $p=0.83$, no effects from drug $F_{5,30}=0.932$ $p=0.474$, nor interactions between injury type and treatment $F_{2,30}=1.921$ $p=0.164$.

Total cell count does not change at 2w post-injury with ICP elevation or administration of CA-074Me

Neurotrace 435 to identify total cell population, specifically of neuronal phenotype in sham, CFPI, or CFPI+ICP elevated animals given either 10%DMSO (vehicle) or CA-074Me Figure. The total population was counted using Keyence software: Sham +10% DMSO (235.60 ± 10.78) [n=6 animals]; injury + 10% DMSO (241.78 ± 13.42) [n=6 animals]; injury with elevated ICP + 10% DMSO (248.61 ± 15.11) [n=6 animals]; sham + CA-074Me (223 ± 17.04); injury + CA-074Me (231.13 ± 17.51) [n=6 animals]; and injury with ICP elevation (245.08 ± 17.79) [n=6 animals] cells per 0.098 mm^2 . Two-way ANOVA $F_{5,30}=0.362$, $p=0.958$ was performed to compare interactions and effects of injury types and Cath B inhibitor, there is no interaction between the injury group and treatment; $F_{2,30}=0.043$, $p=0.958$. There also was no effect on the total cell count from the injury type (Figure 4.6 & 8). $F_{2,30}=0.625$, $p=0.542$ or from inhibitor administration $F_{1,30}=0.473$, $p=0.497$.

Cathepsin B re-localizes from lysosomes to cytosol in disrupted neurons at 2 weeks following central fluid percussion injury

The Cath B re-localization/redistribution has been previously assessed in neuronal membrane disrupted populations following diffuse TBI alone from 6h-4w (Hernandez et al., 2022) and earlier work from our lab demonstrated Cath B relocalization 6h following CFPI with elevated ICP (Lafrenaye et al., 2012). However, the effects of CFPI with elevated ICP on Cath B localization for later timepoints remain nebulous. Cath B inhibitor, CA-074Me, effects on Cath B localization following a later timepoint also is unknown. In order to investigate the effects, localization was determined as punctate (intra-lysosomal) or diffuse (extra-lysosomal) for both membrane disrupted and non-disrupted neurons in each group (sham, TBI, or TBI+ ICP elevation) and (10% DMSO and CA074Me) 2w post-CFPI (Figure 4.9). Cath B was found to be localized within puncta in non-disrupted neurons in Sham injury with 10% DMSO ($62.91 \pm 3.26\%$), Sham injury with CA-074Me ($77.60 \pm 3.15\%$), TBI with 10% DMSO ($68.35 \pm 3.09\%$), TBI with CA074Me ($54.18 \pm 2.87\%$), TBI+ ICP elevation with 10% DMSO ($64.06 \pm 3.23\%$), TBI+ ICP elevation with CA-074Me ($71.80 \pm 2.54\%$), post-CFPI. The majority of Cath B was also localized outside

lysosomal puncta in disrupted neurons at Sham injury with 10% DMSO ($46.54 \pm 3.77\%$), Sham injury with CA-074Me ($28.21 \pm 3.81\%$), TBI with 10% DMSO ($38.73 \pm 3.33\%$), TBI with CA074Me ($38.54 \pm 3.32\%$), TBI+ ICP elevation with 10% DMSO ($58.55 \pm 3.86\%$), TBI+ ICP elevation with CA-074Me ($43.22 \pm 3.37\%$) (Figure 4.10).

The percentages of neurons demonstrating punctate Cath B indicated a significant interaction of membrane disruption, injury type, and treatment; $F_{2,2633}=12.83$, $p=3.00 \times 10^{-6}$. There was a trend of an interaction between treatment and injury type on the percentage of Cath B re-localization $F_{2,2633}=2.50$, $p=0.082$. There were significant interactions between neuronal membrane disruption and injury type ($F_{2,2633}= 4.25$, $p=0.014$) as well as neuronal membrane disruption and treatment ($F_{1,2633}= 11.14$, $p=0.001$) on Cath B localization. There was an effect on Cath B localization from injury ($F_{2,2633} = 10.27$, 3.60×10^{-5}) and membrane disruption ($F_{1,2633}= 141.26$, $p=9.04 \times 10^{-32}$, but not from treatment alone $F_{1,2633}= 2.901$ $p=0.089$). Three-way ANOVA: $F_{1,2633}= 20.69$, $p=1.01 \times 10^{-40}$.

Bonferroni post-hoc multiple comparisons found differences in localization between: membrane disrupted and non-disrupted CA-074Me shams, $p=2.48 \times 10^{-17}$; membrane disrupted and non-disrupted cells 10% DMSO TBI animals, $p=4.37 \times 10^{-9}$; membrane disrupted and non-disrupted cells CA-074Me treated TBI animals, $p=0.025$; membrane disrupted and non-disrupted cells CA-074Me TBI+ICP animals, $p=1.05 \times 10^{-9}$; depicted by *. TBI and sham CA-074Me non-disrupted cells, $p=3.28 \times 10^{-7}$; shown with #. In addition, there were differences in TBI and TBI+ICP elevated animals in 10% DMSO membrane disrupted cells, $p=0.005$; TBI and TBI+ICP elevated animals in CA-074Me non disrupted cells and 10%DMSO membrane disrupted cells, $p=2.96 \times 10^{-4}$; ^. Finally, there were differences found in 10% DMSO and CA-074Me in sham non-disrupted cells, $p=0.021$; 10% DMSO and CA-074Me in TBI non-disrupted cells, $p=0.046$, denoted as \$.

Injury with intracranial pressure increases somatosensory sensitivity that is reduced with CA-074Me

Noted among previous findings from the lab, elevated ICP after TBI led to acute neuronal membrane disruption, chronic neuronal loss within the somatosensory cortex, as well as behavioral sensory hypersensitivity 4w post-injury (Lafrenaye et al., 2014). Therefore, it was of interest to see if there was whisker hypersensitivity 2w post-injury with the added variables of ICP elevation and treatment through the Whisker Nuisance Task (WNT). Pre-injury scores were comparable for each group: Sham injury with 10% DMSO (3.39 ± 0.47) $n=11$, Sham injury with CA-074Me (3.43 ± 0.45) $n=13$, TBI with 10% DMSO (4.63 ± 0.63) $n=12$, TBI with CA074Me (4.30 ± 0.45) $n=13$, TBI+ ICP elevation with 10% DMSO (3.51 ± 0.33) $n=11$, TBI+ ICP elevation with CA-074Me (3.84 ± 0.54) $n=12$. In comparison, the post-injury scores were significantly higher than the pre-injury scoring except for shams given CA-074Me. Sham injury with 10% DMSO (5.06 ± 0.69), Sham injury with CA-074Me (4.20 ± 0.62), TBI with 10% DMSO (6.83 ± 0.89), TBI with CA074Me (6.74 ± 0.49), TBI+ ICP elevation with 10% DMSO (9.15 ± 0.66), TBI+ ICP elevation with CA-074Me (5.81 ± 0.38) Figure 4.11.

The WNT task score was repeated for preinjury and post injury thus, repeated measures ANOVA was conducted; $F_{1,66} = 70.581$ $p=5.07 \times 10^{-12}$. There was an effect between pre and post WNT score from injury type $F_{1,66} = 70.581$ $p=5.07 \times 10^{-12}$. Also, there was a trend towards effects on the pre-post WNT score from treatment $F_{1,66} = 3.891$ $p=0.053$, however no interaction between treatment and injury to affect the pre and post score, $F_{2,66} = 2.335$ $p=0.105$. On the average of the pre/post score there was a significant effect of injury; $F_{2,66} = 8.822$ $p=4.02 \times 10^{-4}$, but not a significant effect of treatment; $F_{1,66} = 2.451$ $p=0.122$ and no indications of interaction of treatment and injury on the score averages, $F_{2,66} = 0.568$ $p=0.569$.

Discussion

Overall, the findings from this study present that CA-074Me, when given as a bolus and continuously via an osmotic pump into the left ventricle, successfully inhibits Cath B activity in the left and right lateral neocortex (Figure 4.1). Cath B activity was not significantly different between injury categories. Next, we found no significant changes in Cath B, Bcl-XL, and Bak protein quantities, yet

we did see a decrease in AIF, though not significant, in the TBI and ICP elevation group that was given CA-074Me (Figure 4.(2,3,4,5)). Our assessment of membrane disruption in the three injury groups had no difference in membrane disruption neither from the treatment. Moreover, there was no cell loss seen between the groups. Cath B was found to be more relocalized in membrane-disrupted neurons, and notably, the Cath B inhibitor CA-074Me does not prevent relocalization in our data. Lastly, with whisker nuisance, we found that behavioral morbidity increased with injury and injury with elevated ICP; Ca-074Me does lower the hypersensitivity in animals given injury with ICP elevation.

Interestingly, the vehicle CFPI, and the vehicle CFPI + ICP demonstrated lower percentage of membrane disrupted neurons we've seen traditionally in our studies. In Lafrenaye 2012, injured Fisher rats had approximately 20% of NeuN+ cells were membrane disrupted and rats with naturally high ICP following injury presented with about 40% membrane disrupted cells of NeuN+ cells (shams had around 3%) 6h post-injury(Lafrenaye et al., 2012). The follow-up study using Sprague-Dawley rats had similar percentages where injured rats had around 25% membrane disrupted NeuN+ neurons and injury with ICP elevation demonstrated 62% membrane disrupted NeuN+ neurons(Lafrenaye et al., 2014). The study evaluating the timeframe of membrane disruption without the study of ICP, 6h post-injury, there was about 52% membrane disruption that dropped to 40% around 1 and 3d, then dropped at 1w to 30% and resurged to 50% at 2 and 4w(Hernandez et al., 2019). These points were all without elevated ICP. So it was surprising to see that the 10% DMSO (vehicle) injured and injury with ICP elevation rats had around 7% and 10% membrane disrupted cells of the total neuronal population, respectively.

However, DMSO has been shown previously to have a neuroprotective effect. In a study conducted by DiGiorgio and colleagues, using the lateral fluid percussion model (LFPI) on rats, they tested drugs alpha-tocopherol and curcumin, with DMSO as their vehicle and had saline controls. While they saw a decrease in Fluoro-Jade staining after LFPI in alpha-tocopherol and curcumin treatments that was also seen with DMSO, but not with saline (Di Giorgio et al., 2008). This is not the first study to demonstrate the neuroprotective effects of this amphipathic molecule, as early

preclinical studies saw a lowering of ICP after intravenous administration of DMSO (de la Torre et al., 1975; Tung et al., 1983). This was also applied in the clinic as a treatment for intractable ICP and led to the rapid reduction of ICP. (Karaca et al., 1991; Marshall et al., 1984; Waller et al., 1983; Wolf & Simon, 1983). However, it was challenging to administer clinically as the DMSO tended to breakdown IV tubing; in addition, DMSO in these patients could lead to hemolysis and hypernatremia/hyperosmolarity, which worked against the effects of lowering mortality via ICP modifications (Marshall et al., 1984; Waller et al., 1983; Wolf & Simon, 1983).

Other biophysical assessments of DMSO on membrane dynamics have demonstrated increased permeability or flexibility. While the full effects of DMSO on cellular membranes is not fully understood, DMSO effects on membranes was initially interrogated using a molecular simulation which initially postulated formation of water pores and increased flexibility of the membrane (Notman et al., 2006) and demonstrated through atomic simulations to also arrive to similar conclusions (Gurtovenko & Anwar, 2007). These simulations were eventually testing in DC-3F Chinese hamster lung fibroblast cells exposed to DMSO at different percentages. Undulations were documented at 10% DMSO, which lead to small blebs at 20% and larger swells at 30% DMSO. Additionally, they measured the Calcium and Yo-Pro-1 uptake in these cells given DMSO and found that above 25% DMSO, the uptake of these molecules began to increase (Ménorval et al., 2012). While we see no differences in membrane disruption in sham animals compared to the other injury groups, perhaps the DMSO is aiding in membrane resealing which could be why we are seeing lower rates of membrane disruption compared to our previous studies (Hernandez et al., 2019; Lafrenaye et al., 2014). In fact, the addition of DMSO to injured guinea pig spinal cord axons even in the presence of 0.5 mM Calcium and at 25 C which this group previously demonstrated, hindered membrane resealing in those axons without DMSO (Shi et al., 2001).

On the other hand, the whisker nuisance task revealed increased sensitivity that we see with injury and injury with ICP elevation, much like our previous studies recapitulating hypersensitivity seen 4w post-CFPI (Lafrenaye et al., 2014). Notably, CA-074Me administration reduces behavioral morbidity to injured levels in injury plus ICP elevation animals; however, has

little effect on injury alone. Earlier studies have also targeted Cath B and saw behavioral deficit rescue. CA-074 given to mice prior to CCI showed a recovery of motor function and spatial learning after CCI with CA-074 (Luo et al., 2010). Another study that knocked out Cath B and/or administered E64d, a cysteine protease inhibitor, after CCI in mice also displayed recovery of motor behavior (Hook et al., 2013). CCI is a focal injury model that produces more severe effects compared to the diffuse nature of CFPI. While Cath B inhibition may not induce recovery from hypersensitivity, the added ICP elevation to injury may result in more severe cell damage mediated through Cath B like in the focal model studies. Herein, this could provide more direction when treating ICP elevation-induced deficits following TBI. Another consideration, the post-sham score for DMSO treated animals is significantly elevated compared to the pre-sham score within those animals. This could possibly be reflective of the increased membrane permeability as mentioned prior. However, CA-074Me treated post sham scores were not different from the pre-injury scores. It is possible that some of the behavior exacerbation may be from the implantation of the cannula and the CA-074Me is aiding in the recovery.

We did not see evident amelioration of membrane disruption with Cath B inhibition. Yet, CA-074Me does not attenuate the relocalization either. Cathepsin B histology highlights more relocalization in the membrane disrupted population, even in sham animals. The protein quantifications for Cath B, Bak, and Bcl-XL also revealed no changes regarding CA-074Me treatment. However, there did seem to be a decrease in the AIF protein expression, particularly in the TBI+ICP group given CA-074Me. This was also the group that saw a reduction in hypersensitivity in the WNT. Cath B inhibition could indicate that sequelae from elevated ICP after TBI is moderated by Cath B cleaving AIF in the mitochondria following relocalization, as Cath B has been shown to cleave AIF (Chaitanya & Babu, 2008; Yuste et al., 2005).

Taken together, these findings highlight the caution of using DMSO as a lone vehicular control and neuroprotective effects, as mentioned by (Di Giorgio et al., 2008). Also, the mechanisms behind membrane disruption seem to be not directly coupled with Cath B. However, Cath B seems to have a role in the TBI with elevated ICP behavioral morbidities, offering a

molecular target in treating the after-effects of elevated ICP following injury.

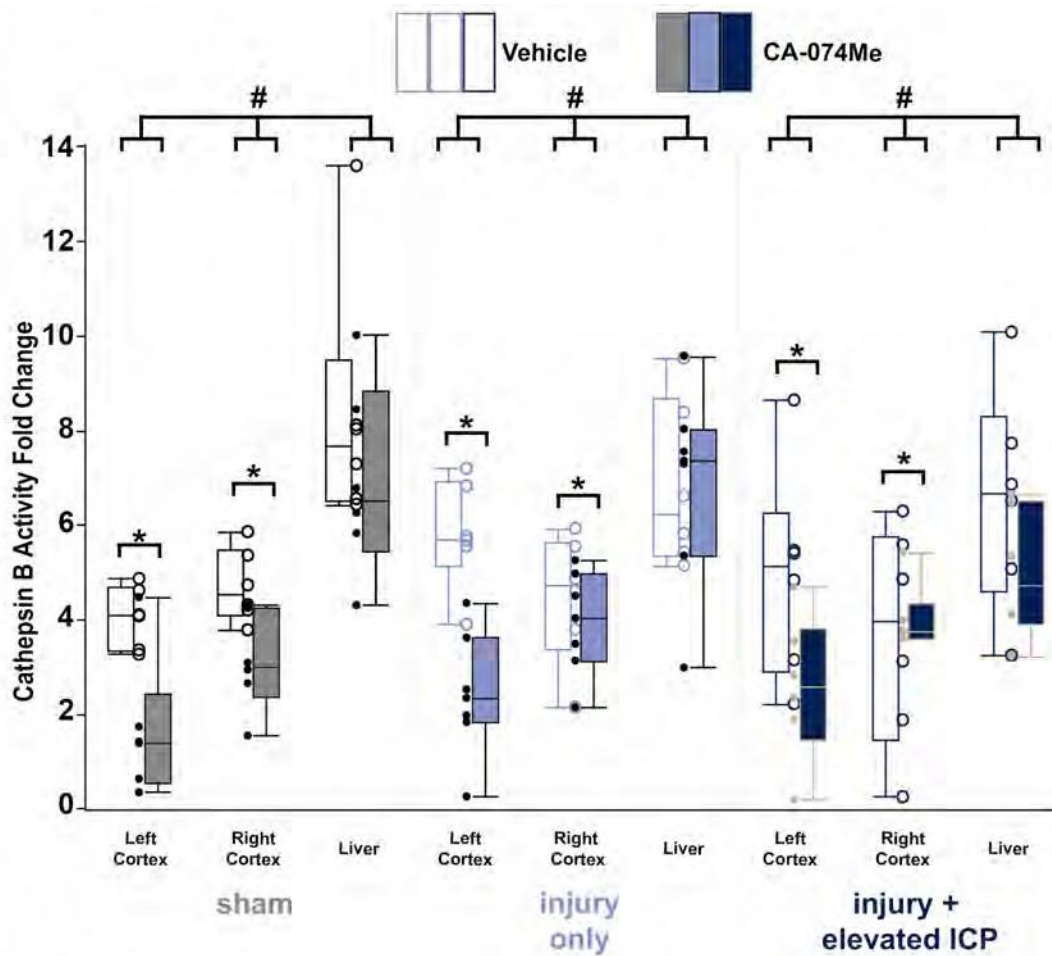


Figure 4.1. Cathepsin B Activity significantly decreases in the left and right lateral neocortex following 2w administration of CA-074Me compared to 10% DMSO (vehicle). Normalized average fluorescent intensity of Cathepsin B in the lateral neocortex and liver: sham-vehicle (n=6 circles) [grey outline] sham-CA-074Me (n=6) [grey fill], TBI only-vehicle (n=6 circles) [light blue outline] TBI only-CA-074Me (n=7) [light blue fill] and TBI+ICP elevation-vehicle (n=6) [dark blue outline] TBI+ICP elevation (n=6) [dark blue fill] depicted in the box and whisker graph. Coordinating dots or circles represent each animal. There were no differences in activity between injury modalities. Mean \pm S.E.M. * $p < 0.05$ compared to injury type-matched vehicle, # $p < 0.05$ compared to injury type-matched liver.

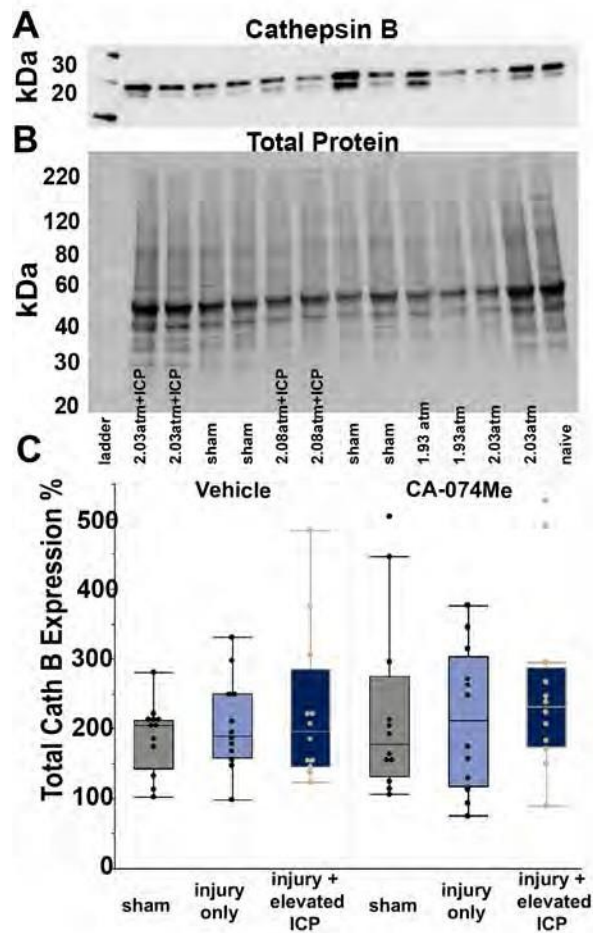


Figure 4.2. Protein quantification in Cathepsin B (Cath B) for (n=6 for each group, with 2 cortical hemispheres, 12 total dots) sham [grey boxes] injury only [light blue boxes] and injury with elevated ICP [dark blue boxes] in both vehicle and CA074Me treatment, respectively, reveals no changes in the injury group or treatment group. (A) is the representative chemiluminescent blot image of the two mature Cath B bands at 24/27 kDa, which was normalized to total protein (B). Graph of expression for all groups (C). Mean \pm S.E.M.

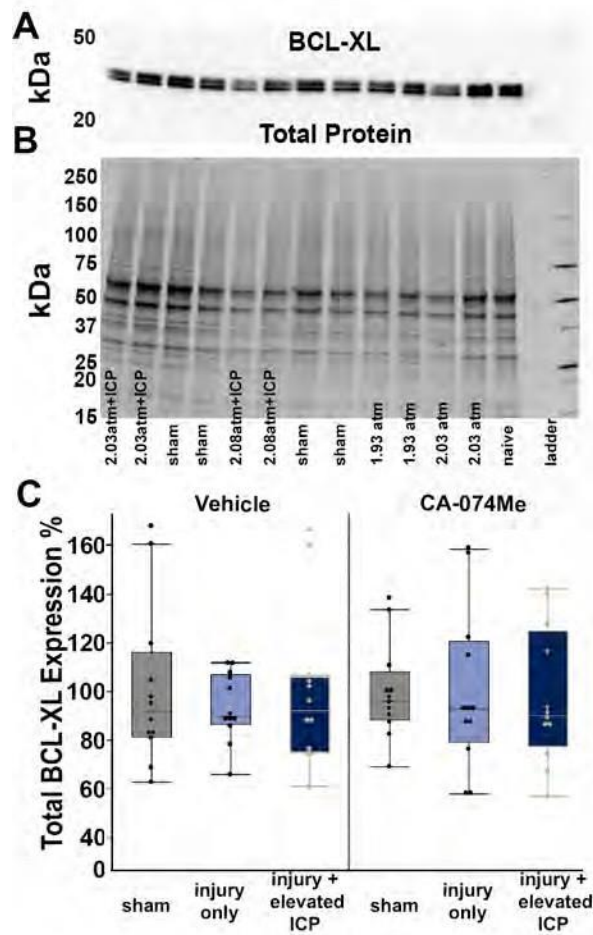


Figure 4.3. Protein quantification of Bcl-XL revealed no differences in the protein quantity regardless of group (n=6 for each group, with 2 cortical hemispheres, 12 total dots). (A) is the representative chemiluminescent blot image of the two Bcl-XL bands at 30 kDa, normalized to the total protein lanes (B). Graph (C) depicts sham [grey boxes] injury only [light blue boxes] and injury with elevated ICP [dark blue boxes] in both vehicle and CA074Me treatment, respectively. Mean \pm S.E.M.

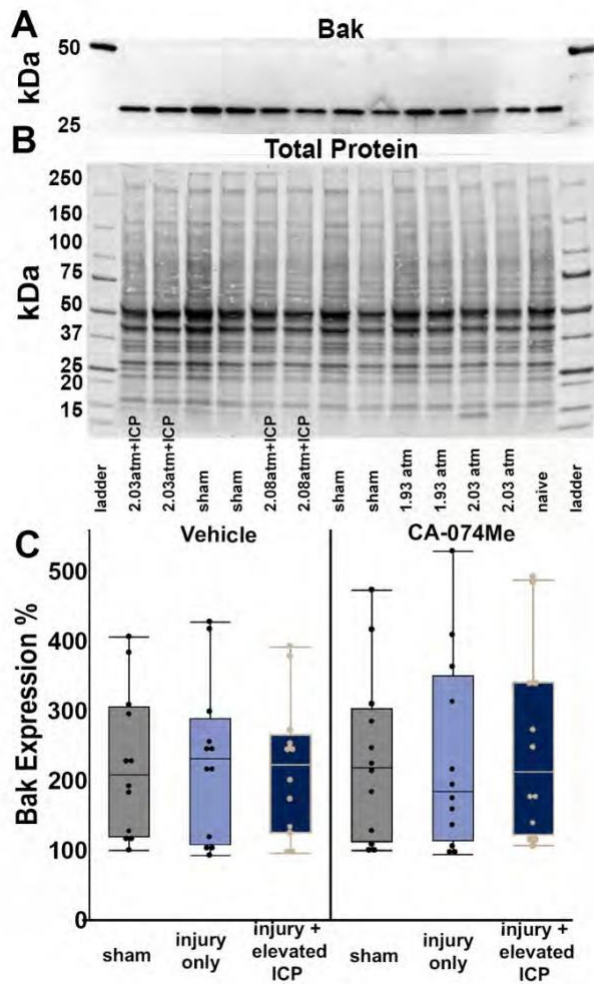


Figure 4.4. Bak protein levels were unchanged regardless of injury or treatment group. (n=6 for each group, with 2 cortical hemispheres, 12 total dots). (A) is the representative chemiluminescent blot image of the Bak band at 25kDa, normalized to the total protein lanes (B). Graph (C) depicts sham [grey boxes] injury only [light blue boxes] and injury with elevated ICP [dark blue boxes] in both vehicle and CA074Me treatment, respectively. Mean \pm S.E.M.

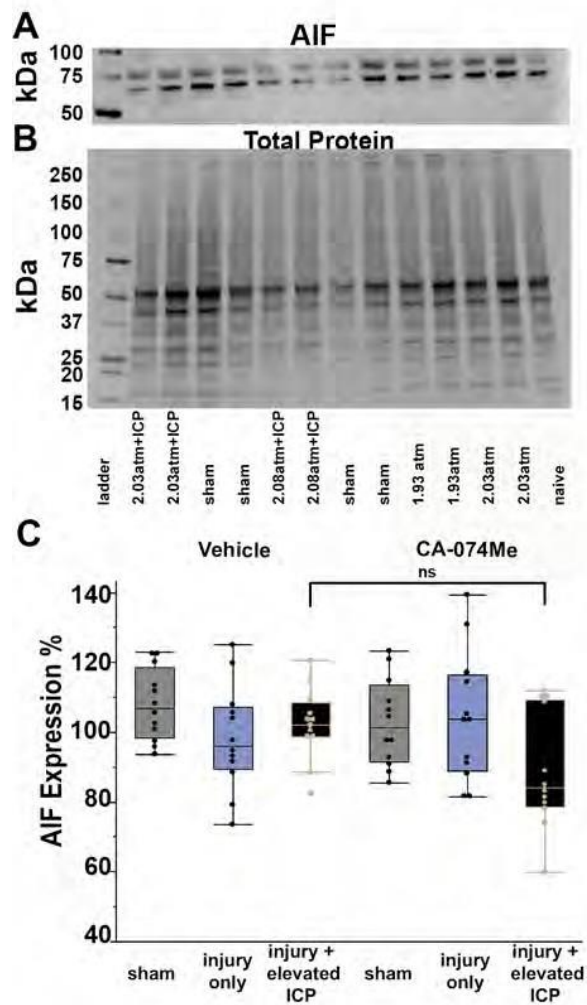


Figure 4.5. There were no alterations of the protein quantity in AIF for the injury groups or treatment groups ($n=6$ for each group, with 2 cortical hemispheres, 12 total dots). (A) is the representative chemiluminescent blot image of the two AIF bands at ~67 kDa; (B) is the total protein lane image to which the protein bands were normalized. AIF expression graphed in (C) follows sham [grey boxes], injury only [light blue boxes], and injury with elevated ICP [dark blue boxes] in both vehicle and CA074Me treatment, respectively. Mean \pm S.E.M. ns $p=0.078$ for interaction between treatment and injury

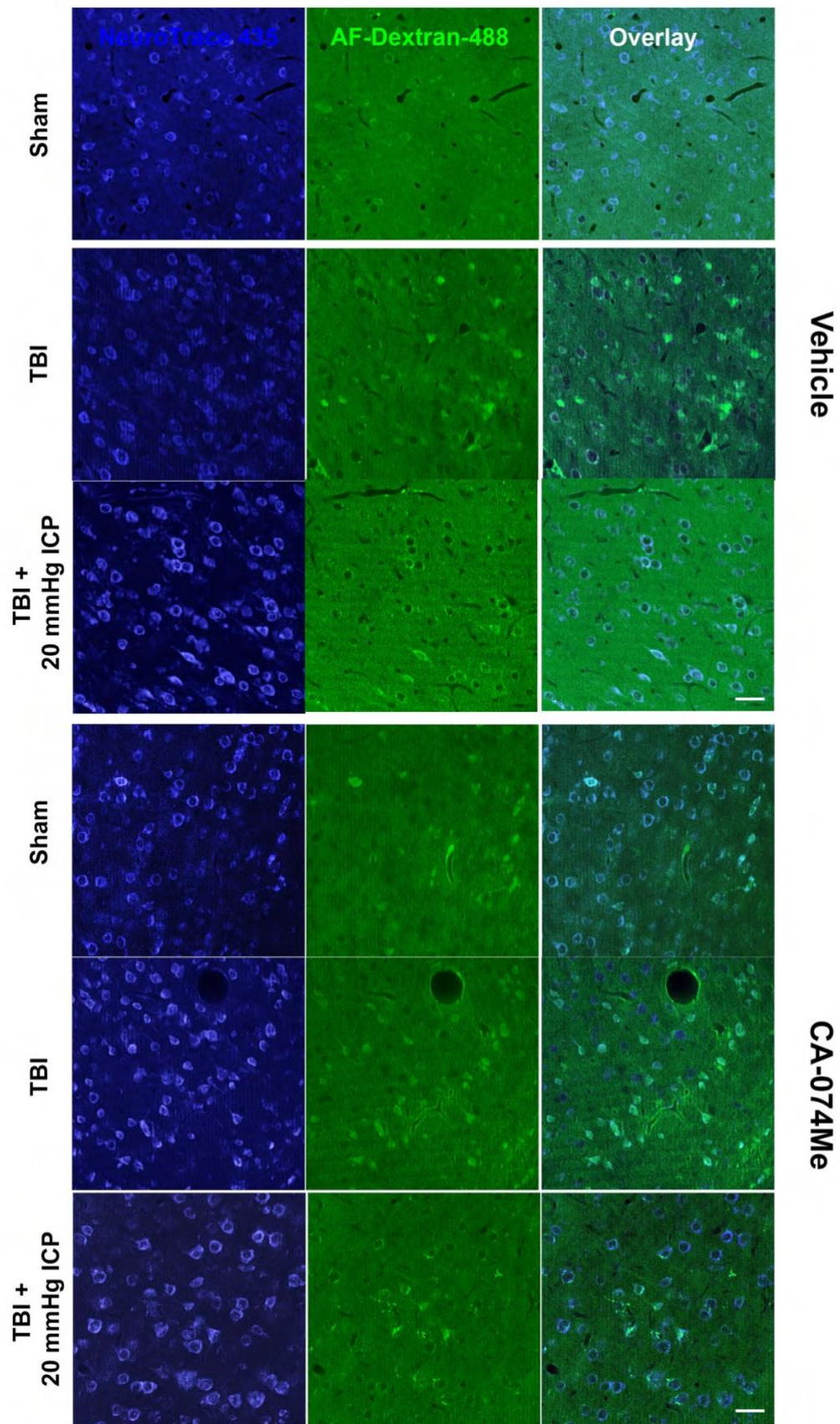


Figure 4.6. Representative images of membrane disruption after sham, TBI, or TBI+ 20 mmHg ICP elevation with 10% DMSO (vehicle) or CA-074Me (Cath B inhibitor). The left panel in blue are Neurotrace positive cells, and the middle panel are images of cells containing dextran (membrane disruption). The right panel is the overlay of the NeuroTrace and membrane disrupted dextran images. Scale bar 20 μ m.

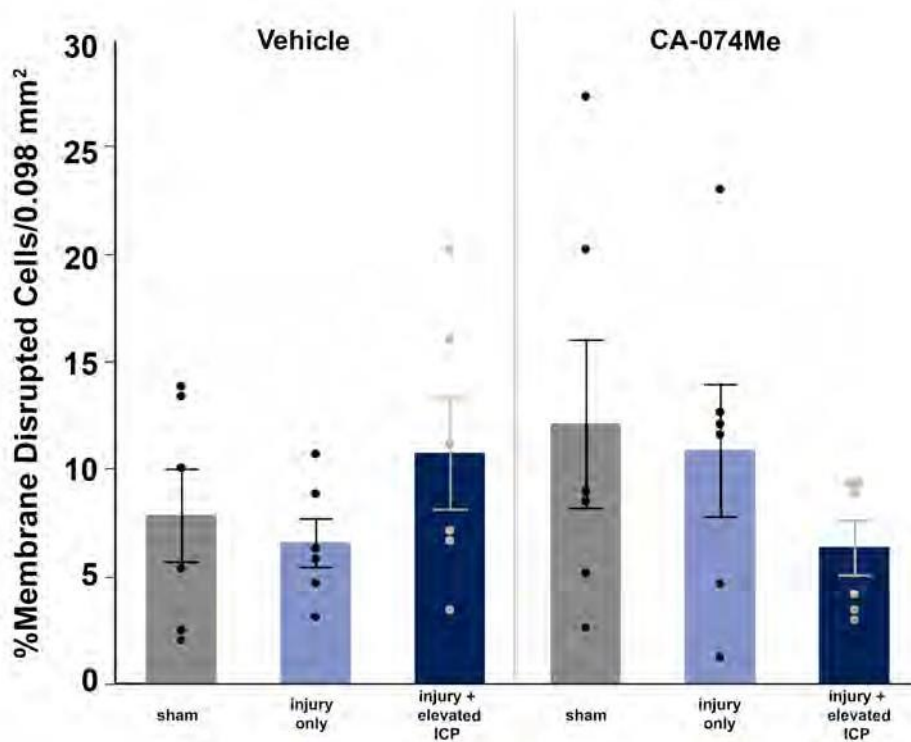


Figure 4.7. There are no significant changes in membrane disruption between injury and treatment groups. The bar graph highlights a consistent membrane disrupted population in the presence of the vehicle (10% DMSO) or CA-074Me, in the varying injury modalities, sham (n=6 10% DMSO; n=6 CA-074Me) [grey bars], injury only (n=6 10% DMSO; n=6 CA-074Me) [light blue bars], injury with elevated ICP (n=6 10% DMSO; n=6 CA-074Me)[dark blue bars]. Coordinating dots or circles represent each animal. Data as mean \pm S.E.M.

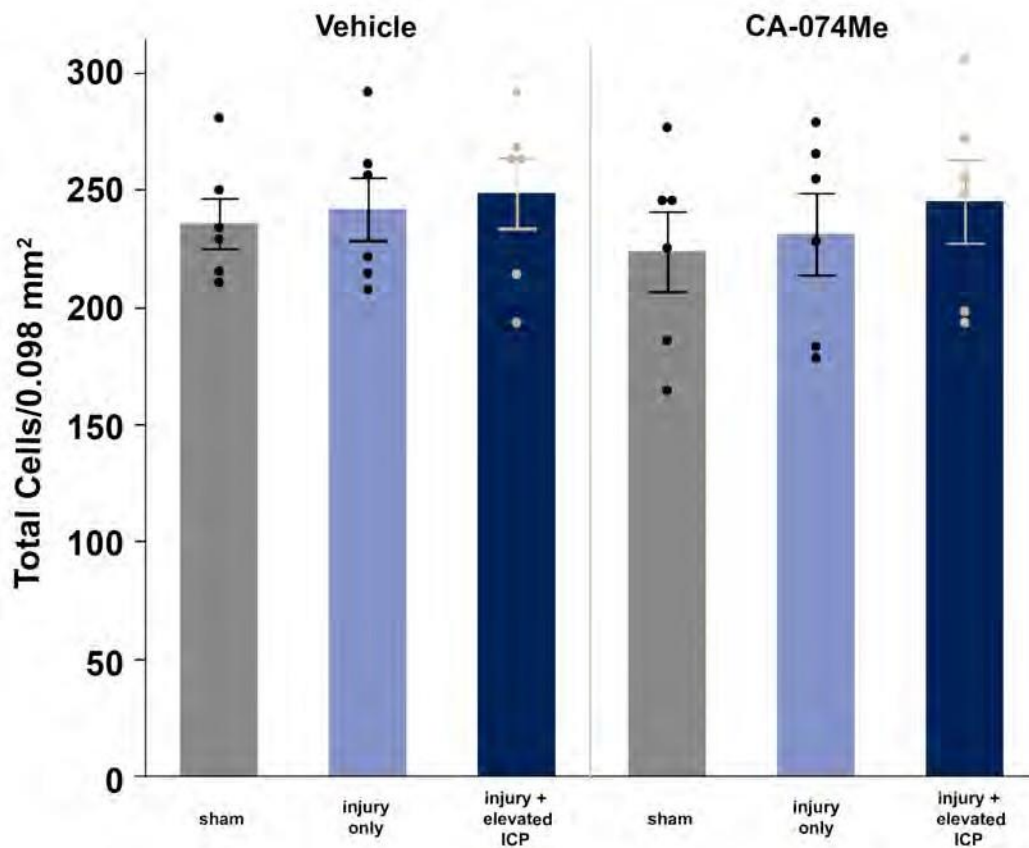


Figure 4.8. The total number of cells not affected by injury manipulation, even with ICP elevation and treatment in the lateral neocortex layers V and VI. The mean number of cells were quantified per unit area (0.098 mm^2) and averaged per animal. Sham animals ($n=6$ 10% DMSO; $n=6$ CA-074Me) [grey bars] were compared to injury only ($n=6$ 10% DMSO; $n=6$ CA-074Me) [light blue bars] and injury with elevated ICP ($n=6$ 10% DMSO; $n=6$ CA-074Me) [dark blue bars]. Coordinating dots or circles represent each animal. Data presented in mean \pm S.E.M.

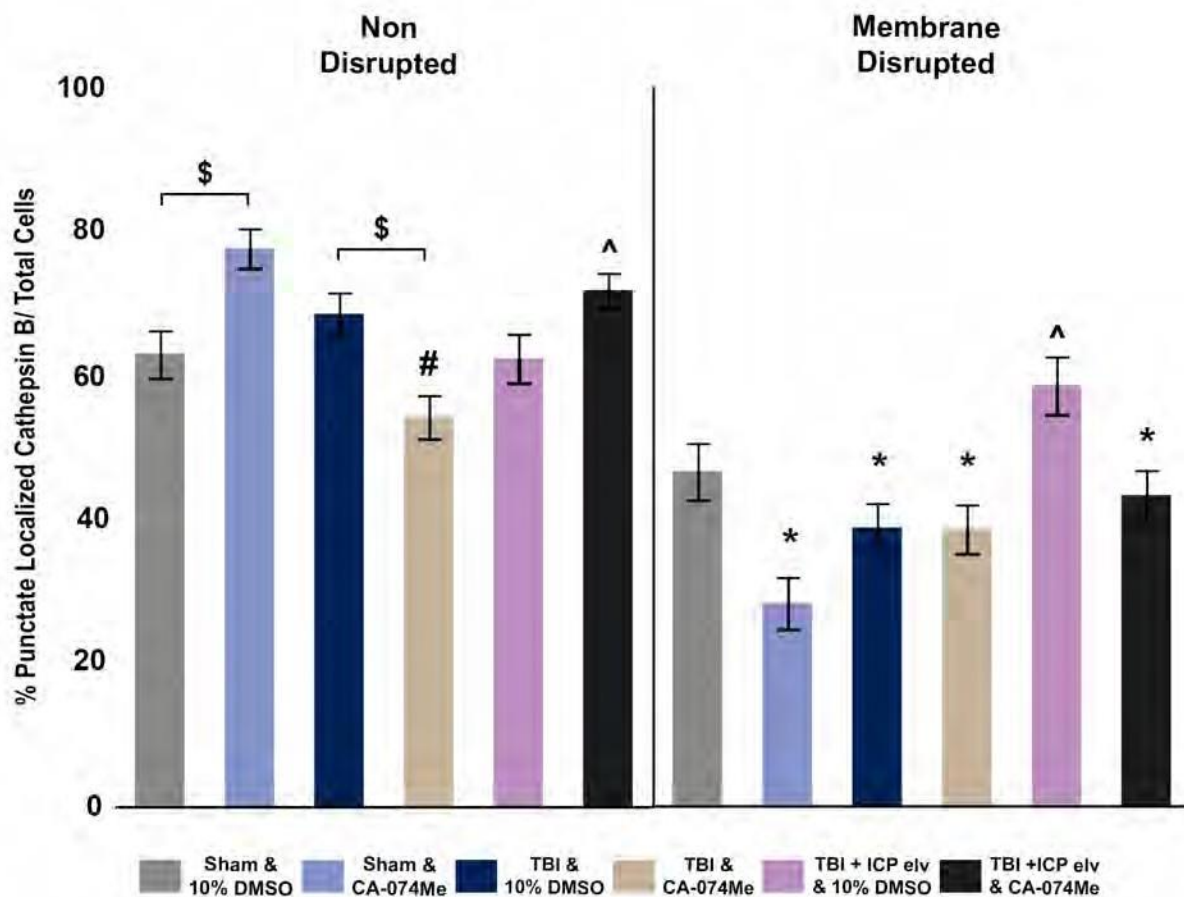


Figure 4.10. Percentage (%) of Punctate Cathepsin B presented in a bar graph. Neurons were identified as membrane disrupted and non-disrupted based upon dextran uptake. Then neurons were evaluated for Cath B inside lysosomes (punctate/ 100% localized) or outside lysosomes (diffuse 0% localized). Cathepsin B is frequently localized in lysosomes in non-disrupted neurons when given CA-074Me, except in TBI only animals. As for disrupted neurons, CA-074Me appears not positively to affect Cath B localization in lysosomes. Sham & 10% DMSO (n=372 cells) [grey bars] Sham & CA-074Me (n=424 cells) [light blue bars] were compared to TBI & 10% DMSO (n=441 cells) [dark blue bars], TBI & CA-074Me (n= 480 cells) [tan bars] and TBI+ICP elevation & 10% DMSO (n=378 cells) [pink bars] and TBI+ICP elevation & CA-074Me (n=550 cells) [black bars] and were depicted in mean \pm S.E.M. * p<0.05 compared to non-disrupted counterpart, #p<0.05 compared to sham & CA-074Me, \$ p<0.05 compared to vehicle-treated counterpart. ^p<0.05 compared to non-ICP elevated counterpart.

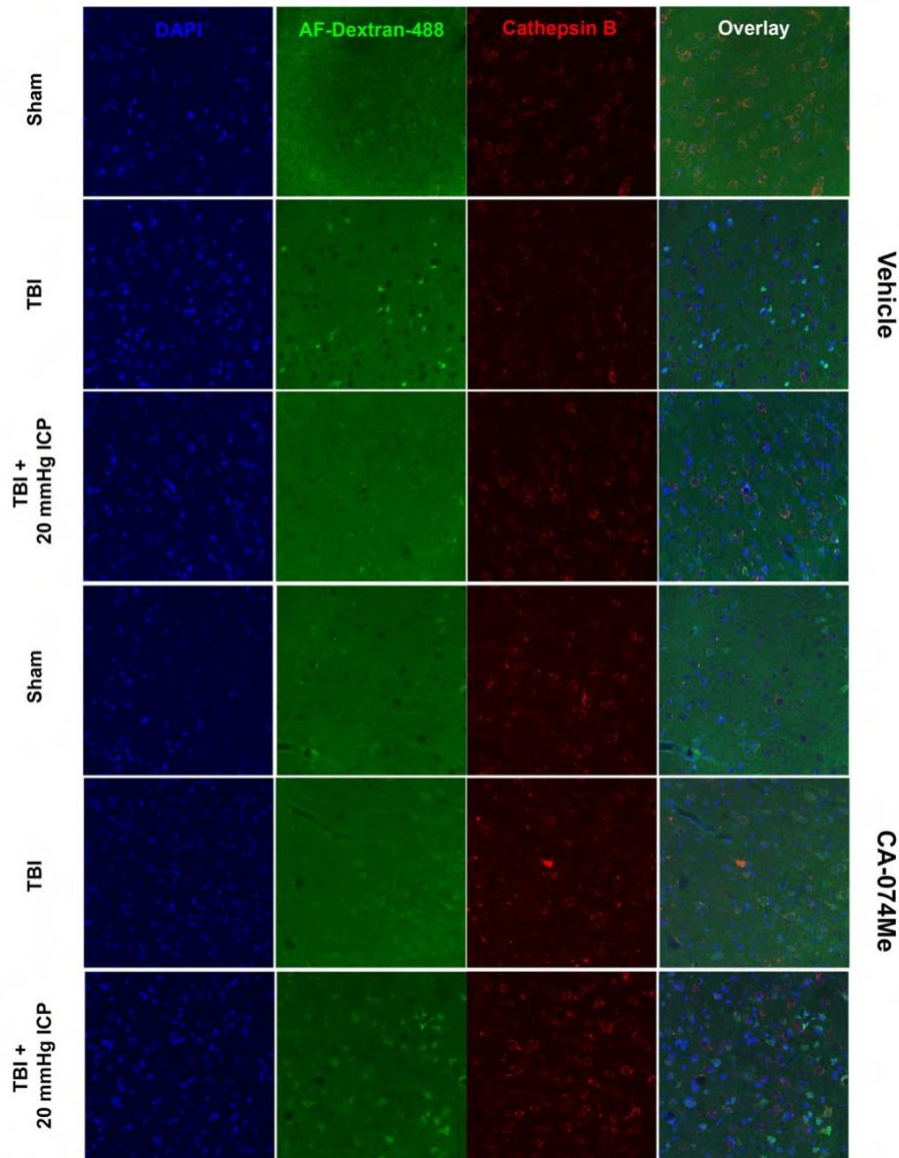


Figure 4.9. Representative fluorescent images of injured (sham, TBI, TBI +20mmHg ICP) and treatment groups (10% DMSO (vehicle) and CA074Me). Left most panel contains DAPI labeled nuclei (blue), then the second panel contains images of membrane disrupted neurons filled with Alexa-Fluor 488 Dextran (green), and the third panel is of Cathepsin B containing cells.

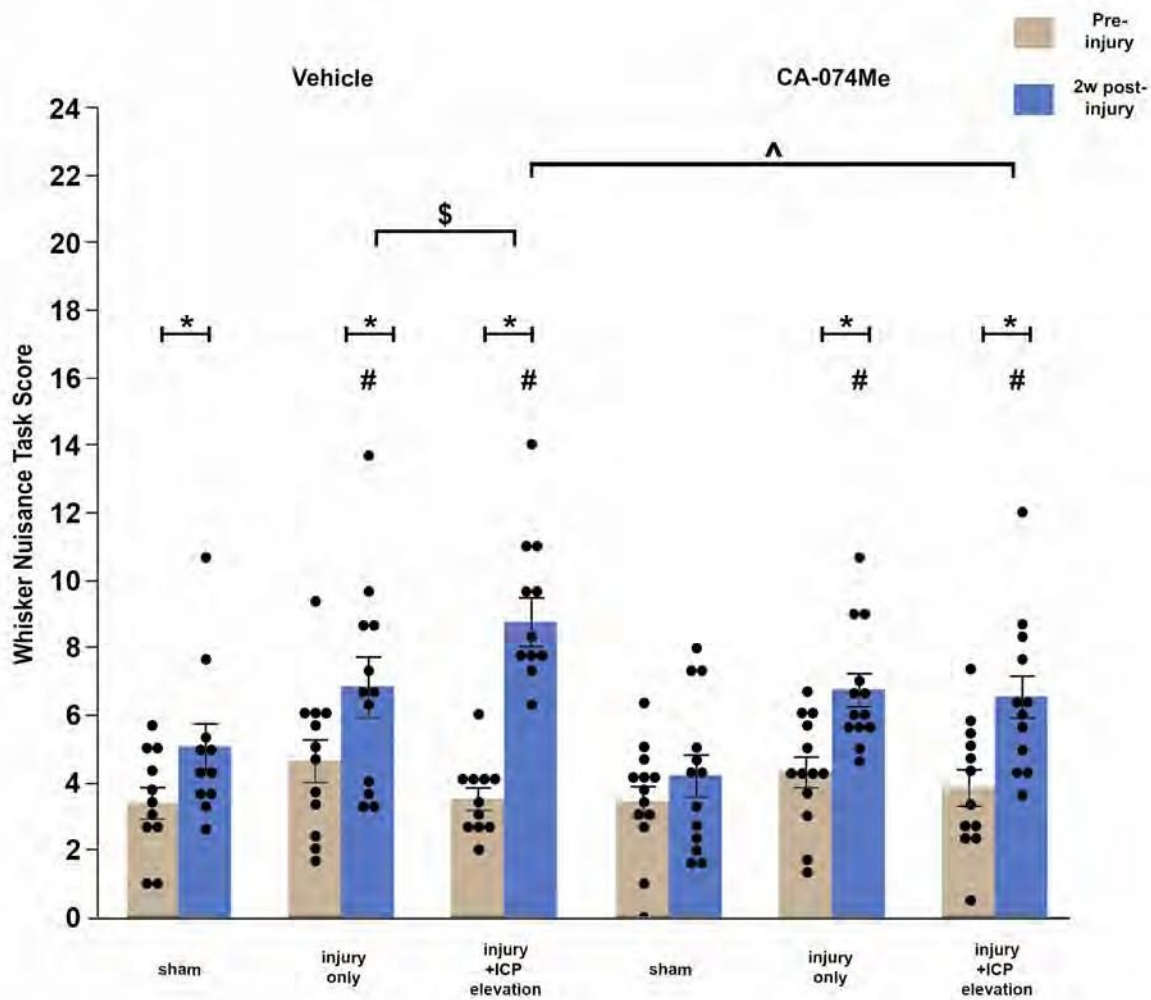


Figure 4.11. Somatosensory sensitivity was affected by injury and further with secondary ICP elevation. Cathepsin B inhibitor CA-074Me reduces sensitivity, specifically in injury with secondary ICP elevation. Bar graph of animals' whisker nuisance scores pre-injury (tan bars) and at 2w post- (sham/injury/ injury+ICP elevation) (blue bars) in (groups treated with vehicle (10% DMSO) or CA-074Me. Sham-Vehicle n=11, injury-vehicle n=12, injury+ICP elevation-vehicle n=11, sham-CA074Me n=13, injury-CA074Me n=13, injury+ICP elevation-CA074Me n=12 Mean ± SEM. # p<0.05 compared to sham, * p<0.05 compared pre-injury, \$ p=0.053 compared to injury-vehicle, ^ p<0.05 compared to vehicle

Discussion

Two Phases of Membrane Disruption; Potential for Resealing?

From this body of work, we can conclude that following central fluid percussion injury in male Sprague Dawley rats, there is sub-acute (6h-3d) membrane disruption that recedes at 1w and returns at a late period (2w and 4w post-injury). Figure 1.1 (Chapter 1). This shift in the membrane disrupted population could represent resealing, followed by a secondary pathology re-inducing membrane disruption. Therefore, there is an opportunity for intervention following injury right before more pathological processes occur.

Importantly, a subset of membrane disrupted neurons was found to reseal their plasmalemma following injury by multiple groups. Using shear injury in vitro, the LaPlaca group found that some mechanoporated neurons were no longer permeable minutes post-injury (Cullen et al., 2011; Geddes et al., 2003). In vivo studies also found a subset of neurons containing only the pre-injury administered dextran, indicating that they had resealed their membranes. This was seen using 10 kDa dextran conjugated to green and red fluorophores were infused into the lateral ventricle pre- and post-injury in Sprague Dawley rats (Farkas et al., 2006; Lafrenaye et al., 2014). Further studies also found that not only were mechanoporated neurons capable of membrane resealing, but there was also a delayed membrane disrupted population of neurons that only contained the post-injury administered dextran and some neurons that displayed enduring membrane disruption, in which they contained both pre- and post-injury administered dextran (Lafrenaye et al., 2014). Such findings demonstrate that, while some mechanoporated neurons continued to demonstrate membrane disruption, other neuronal membranes could reseal following injury. Moreover, acute resealing of mechanoporated rat neurons is Ca^{2+} regulated in which resealing was found to be significantly reduced either without extracellular calcium or when intracellular calcium was chelated (Prado & LaPlaca, 2020). This link between membrane

resealing, or lack thereof, and recovery or cell death following injury could provide opportunities for therapies that leverage these resealing potentials in those injured neurons. Furthermore, they looked at the dynamics of mechanoporation and membrane re-sealing. The initial sets of cultures received a pre-injury administration of ethidium homodimers (EthD-1); other cultures were designated for pre- and post-injury administration of Ethidium homodimers. While initially, there was membrane disruption that could be primarily due to mechanical perturbation, the cells present evidence of resealing.

When holes are introduced into artificial liposomes, they have been shown in simple biochemical experiments to re-seal themselves simply through the shifting of its phospholipids to repair the gap. However, for a cell, this is no simple feat as there are intramembrane proteins and protein networks, such as the cytoskeleton, impeding a response. So, the cell has additional responses to compensate for the intricate structures, leading to variation in repair time. The mechanism from what follows mechanoporation is not well known, especially in neurons. In addition, it seems like the plasma membrane damage is a target of rapid counteraction from cellular repair mechanisms (Hendricks & Shi, 2014). When looking at cell membrane repair in studies, the first step established in many cell types is the initial surge of calcium. This calcium surge induces additional signaling the recruitment of a variety of proteins, lipids, and membrane-bound organelles. While some of these processes are helpful to the cell, others may actually delay repair.

Membrane repair seems to be a chronological and balanced process. Following membrane disruption, there is a stark increase in intracellular calcium thought to arise from interference with the electrochemical gradient that is maintained by the cell membrane. Early mechanoporation in neurites induces a rise in calcium within one second of high-strain cell shear injury in vitro (LaPlaca & Thibault, 1997, 1998). Without external calcium, there was still a rise in intracellular calcium following injury, but the increase was much lower. This group's findings

highlighted that additional intracellular calcium was from NMDA signaling in this particular study (LaPlaca & Thibault, 1998). Calcium was determined as a necessary component in membrane resealing with 3T3 fibroblasts and sea urchin embryos which underwent micropuncture. The calcium was traced using Fura-2, which is normally impermeable to cell membranes. When calcium was removed or antagonized by magnesium, membrane restoration was not completed in the injured embryos (Steinhardt et al., 1994). The drastic rise in cytosolic calcium triggers the release of proteases which cleave proteins needed to move vesicles and endosomes to the membrane surface for repair. This mimics similarly to what is seen with vesicle release for neurotransmission (Bi et al., 1995; Steinhardt et al., 1994). These proteins include the SNAREs, SNAP-25, synaptobrevin. (Bi et al., 1995; Detrait et al., 2000; Reddy et al., 2001; Steinhardt et al., 1994). These are used to move vesicles from the Golgi apparatus, lysosomes, or other endosomes to areas of membrane disparity (Reddy et al., 2001). The work done so far to comprehend cellular membrane repair has resulted in a few held styles. There is the initial packing around the area of permeability with various organelles, vesicles, and proteins (Christ et al., 2017; Draeger et al., 2014; Miyake et al., 2001; Miyake & McNeil, 2003). Early studies on how invertebrate neurons repaired their axons following transection by using non-ionic and ionic tracers to track membrane repair. Using ultrastructure from electron microscopy, it demonstrated that the invertebrate neurons used membrane-bound organelles to help seal areas of permeability (Eddleman et al., 1998). Mitochondria also have been shown to gather near sites of membrane disruption in axons following injury (Kilinc et al., 2008). Lysosomes, in particular, were shown to pack in areas of membrane permeability in mouse fibroblast cells (Jaiswal et al., 2002).

Lysosomes are also said to play a role membrane repair (Jaiswal et al., 2002; Reddy et al., 2001). Beyond serving as an endpoint for cellular debris, lysosomes are integral components in membrane repair. Lysosomes can be recruited to the membrane as if it were to be involved in exocytosis and have been shown gathering alongside the membrane gap. At this point, it is

hypothesized that lysosomes will bind allowing for the removal of the damaged portion of the membrane and distribute some of its membrane to reseal (Gatta & Carlton, 2019; Jaiswal et al., 2002; Togo et al., 1999; Wollert et al., 2009). Membrane bound components in mammalian PC12 and B104 cell culture lines grown to neurites were shown to seal in the presence of calcium using calcein-AM and fluorescein-dextran (Yoo et al., 2003). Those cell line grown neurites were subjected to transection and were labeled and quantified for syntaxin and synpatotagmin, which assist in membrane interactions.

Another piece in consideration should be in relation to rise in intracellular calcium is the release of phosphatidylinositol 4,5-bisphosphate (PIP₂) and diacylglycerol (DAG) from phosphatidylinositol. However, this is more favorable in the presence of DAG lipid-concentrated regions. PIP₂ is also crucial in the maintenance of the cytoskeletal and membrane interactions (Raucher et al., 2000). DAG is released after cleaving of phosphatidylinositol and has been shown to be involved in individual cell repair (Vaughan et al., 2014). Using *Xenopus* oocytes and stab wound assay, inhibition of DAG formation blocks recruitment of Cdc42 and Rho which actively play a role in cytoskeleton and wound repair. DAG works with these proteins through protein kinase C (PKC). In addition, DAG suppression in general slows wound healings as DAG is important to recruit phosphatidylserine (PS), phosphatidic acid(PA) , phosphatidylinositol (3,4,5)-triphosphate (PIP₃) and PIP₂ (Vaughan et al., 2014).

Lipid dynamics are crucial in membrane repair. With artificial liposomes, any disruption to the membrane induces thermodynamically favorable resealing, instantly. Within in a cell such as a fibroblast, cell membrane repair following injury occurs within mere minutes (Miyake & McNeil, 2003). Additionally, the rise in calcium from membrane disruption activates another group of proteins, annexins to bind to phosphatidylserine, which becomes exposed following membrane disruption (Bouter et al., 2015). Annexins are calcium-sensitive proteins which bind to phospholipids and other annexins to form a complex (Babiychuk et al., 2008; Bouter et al., 2011,

2015; Draeger et al., 2011, 2014; Togo, 2006). Annexin V in particular has been shown to be crucial as when laser-injured mouse perivascular cells have null annexin V compared to wild-type cells; Annexin V was shown to bind to the injured plasma membrane in wild-type cells which lead to quicker sealing of the membrane (Bouter et al., 2011). When simulated in an artificial membrane made of lipids, annexin demonstrated the same binding properties as (Bouter et al., 2011). Annexins have not been approached in neuronal membrane injury models, but warrants further investigation in regards to membrane repair.

Future Directions

Next steps to evaluate membrane resealing would be to employ a surfactant such as Poloxamer 188 and evaluate the membrane disrupted populations at later time points. Another component to study the membrane disrupted population would be to use GCAMP transgenic rats with head-mounted scopes to look at calcium dynamics and perhaps also look at dextran mobility live following injury.

Guess Who? (NeuN Negative Membrane Disrupted Subpopulation)

In addition to finding multiple temporal waves of membrane disruption, Hernandez et al. also observed a subset of membrane disrupted neurons that lacked expression of the pan-neuronal marker, Neuronal Nuclei (NeuN) (Hernandez et al., 2019). NeuN was identified in 1992 and was described as a mature neuronal marker owing to its ubiquitous expression pattern within neurons throughout the brain (Mullen et al., 1992). Some neuronal populations, however, including Purkinje cells in the cerebellum, olfactory mitral cells, retinal photoreceptors, subsets of interneurons, and inner granule cells, typically do not express NeuN, demonstrating that not all neurons are also NeuN+ (Cannon & Greenamyre, 2009; Morin et al., 2011; Mullen et al., 1992; Weyer & Schilling, 2003). It was further found that NeuN, which is coded by the Rbfox3 gene, is an RNA-binding protein, homolog of Fox-1(feminizing on X), a protein

found in *C. elegans* that functions in alternative splicing of various proteins (K. K. Kim et al., 2009). One of those proteins is Numb, which is important for neuronal development and differentiation, leading to the notion that NeuN could be involved in neuronal development (K. K. Kim et al., 2013).

Following injury, glial cells, such as astrocytes, have demonstrated susceptibility to membrane disruption *in vitro* and following spinal cord injury (Halford et al., 2017; Levine et al., 2016). As glial cells do not express NeuN, it was postulated that the NeuN negative (NeuN-) membrane disrupted cells could be glia. Therefore, traditional markers of the primary glial cell types, glial fibrillary acidic protein (GFAP) for astrocytes, adenomatous polyposis coli (APC/CC-1) for oligodendrocytes, ionized calcium-binding adaptor molecule 1 (Iba-1) for microglia, and neuron-glia antigen 2 (NG2) for NG2 cells, were immunofluorescently assessed for signs of membrane disruption at all time points following CFPI. However, none of the glial cell types demonstrated signs of membrane disruption, indicating that the NeuN- membrane disrupted population was unlikely to be glial in nature (Hernandez et al., 2019). This finding differs from the glial-positive results in the Wanner group's study of astrocytic membrane disruption, which could be in part due to differences in injury modality and time discrepancies (Levine et al., 2016). As previous studies also demonstrated, TUNEL and H&E staining did not reveal significant cell death or cell loss at any post-injury time point out to 4w post-CFPI, suggesting that the NeuN- population was not associated with subsequent cell death or loss following TBI (Hernandez et al., 2019; Lafrenaye et al., 2014).

Upon investigation, a NeuN- membrane disrupted population of neurons was observed to be present at all post-injury time points and were found to be significantly increased at 2w post-CFPI (Hernandez et al., 2019). However, protein assessments did not reveal differences in NeuN expression in the lateral neocortex at any time following injury. This result indicates that the changes in NeuN could be occurring within a small subpopulation that would not be discernable

with an evaluation of overall NeuN expression within the cortex. To interrogate this possibility, immunohistochemistry paired with hematoxylin and eosin counterstaining was used to quantify the percentage of NeuN expressing neurons within layers V and VI of the lateral neocortex. Interestingly, a NeuN- subpopulation of neurons was consistently observed in both sham and injured animals regardless of time points. This suggests there is a consistent subpopulation of NeuN- neurons within the lateral neocortex, a finding not previously reported, and that these populations may be more vulnerable to late-phase membrane disruption following TBI. These were explored in chapter 2 of this work. Tissue from the time course study was labeled via immunohistochemistry for doublecortin, which is found to be upregulated in immature neurons, then downregulated in mature neurons when NeuN expression peaks (Zimatkin & Karnyushko, 2017). Early publications of neuronal membrane disruption indicate that c-Fos, an immediate early gene is found to be upregulated in membrane disrupted cells (Grembowicz et al., 1999). Therefore, simultaneous double labels with NeuN and doublecortin or c-fos were analyzed with the fluorescent dextran in order to elucidate the identity of the NeuN- membrane disrupted cells in a quantitative fashion.

Our immunoblotting indicated no change in doublecortin protein amounts in sham animals compared to 1d, 1w, 2w post-CFPI. Additionally, there was no difference in the amount of NeuN positive/DCX positive cells or the NeuN negative/DCX positive cells between the sham and injured animals. Membrane disrupted neurons could also still be reverting to a more mature phenotype that does not involve the expression of doublecortin.

However, there is also the possibility that membrane disrupted neurons that did not label with NeuN may not be reverting to an immature phenotype. The NeuN A60 antibody, which was used in this study, requires at least one phosphorylation on the N-terminus of NeuN to properly

label (Lind et al., 2005; Maxeiner et al., 2014; Won et al., 2016). Alterations in the phosphorylation state of NeuN in various neuronal subpopulations within the cortex may also explain the consistently present NeuN- subpopulation found by Hernandez et al. (2019), however, for the binding of the A60 epitope from the NeuN antibody, that action is phosphorylation independent (Kim et al., 2009; Lind et al., 2005; Maxeiner et al., 2014). As NeuN is involved in mRNA splicing, this decreased presentation of NeuN could possibly serve as an indicator of neuronal protein expression activity, and perhaps is slowing to allocate resources to protective mechanisms in opposition to carrying out the pre-injury function. This would be supported by the cFos positivity equally overlapping with NeuN positivity (Figure 2.4.)

Additionally, as mentioned above, there are neuronal subtypes, such as subsets of interneurons, that do not express NeuN, which could also represent this NeuN- subpopulation ((Cai et al., 2009; Duan et al., 2016; Varea et al., 2011; Weyer & Schilling, 2003; Xiong et al., 2008). Perhaps the transience NeuN is vital to the nature of interneurons which produce oscillations to promote functional connectivity. Mutations of Rbfox3 (NeuN) have been shown to produce Rolandic epilepsy and has also been shown to mediate seizures via GABAergic interneurons, such as Neuropeptide Y (NPY) cells, as well as determined to play an important role in hippocampal circuitry as well (Huang et al., 2022; Lal et al., 2013; Wang et al., 2015). Perhaps decreasing/ceasing in protein expression of NeuN/Rbfox3 after TBI could lead to the development of post-traumatic epilepsy.

Future Directions

The next steps into investigating the membrane disrupted population would be to use other markers of astrocytes, and co-label with DCX and NeuN to see if that is indeed the NeuN- membrane disrupted population that remains unaccounted. Also, perhaps it would be of value to label for Rbfox3 (NeuN) RNAscope in situ hybridization to see if the message is distributed

differently among different populations of neurons, therefore resulting in a NeuN- population. This could also be completed with single cell RNAseq to identify other possible markers or mRNA profiles of these cells.

Mechanisms in membrane disruption: Cathepsin B or not to be?

Many proteases have been implicated in leading the pathological cascade in CNS injury. Previous work from 2012 looking at 6h post-CFPI with intracranial pressure elevation highlighted that Cath B relocates from the lysosomal compartments into the cytosol in membrane disrupted neurons (Lafrenaye et al., 2012). This was based on confocal and electron microscopy that show the re-distribution of Cathepsin B, out of lysosomes into the cytosol. The neurons with Cathepsin B outside the lysosome appear abnormal (Lafrenaye et al., 2012).

In Hernandez et al 2022, the relocalization of Cathepsin B is associated with membrane disruption at the later time points, as demonstrated in the immunofluorescent data of our study. As we see, Cath B is leaving the lysosomes in ultrastructure, this could be a result of lysosomal membrane permeabilization (LMP), considering the plasma membrane is enduring a similar perturbation. TBI has been previously associated with membrane permeabilization of lysosomes and mitochondria, involving the Cath B pathway (C.-L. Luo et al., 2013; C.-L. L. Luo et al., 2010; Oberle et al., 2010; Windelborn & Lipton, 2008). Studies looking at Cath B in TBI, focusing on autophagy, present that cPLA2 (cytosolic phospholipase A2) after CCI in mice is directly involved in LMP with sequelae such as the release of lysosomal enzymes like Cath B. (Sarkar et al., 2020) In addition, Cath B has been shown in vitro to remodel neurites through lysosomal membrane trafficking. Disruption of the lysosomes or Cath B with Cath L impedes neurite outgrowth. Perhaps the release of Cath B deregulates membrane remodeling through disruption of lysosomal function thus could be why membrane disruption is evident at later time points. (Jiang et al., 2020)

TBI studies seem to point to Cathepsin B signaling in a cell death-related manner (Luo et al., 2010; Hook et al., 2013). However, these studies are conducted in contusion models, while the study in inquiry uses a diffuse injury model. Diffuse pathologies may have different pathological inductions and conclusions, than focal pathologies, especially with protein changes. As mentioned in the introduction, diffuse pathologies reflect the widespread sporadic damage that occurs throughout the brain and not just in a focus. Conversely, a group investigating membrane disruption showed that Cathepsin B was beneficial in membrane resealing, since inhibition of cathepsin B decreased resealing and that it was Cathepsin D, a lysosomal aspartyl protease, inhibition that allowed for resealing (Castro-Gomes et al., 2016). On the other hand, Cathepsin B, unlike Cathepsin D, has been documented to retain its catalytic properties in the cytosol, in which Cathepsin D is less likely to favor less acidic environments. More work would need to be done to see if Cathepsin B is actually initiating secondary membrane disruption or helping reseal injured neurons or playing a hand in both. Cathepsin B in the role of injury through further inhibitor studies may provide additional information in membrane repair following TBI.

The focus of Chapter 4 was deliberately using a Cathepsin B inhibitor, CA-074Me, following injury for 2 weeks to gauge the role of Cath B further. CA-074Me is the methyl ester-conjugated version of Cath B selective inhibitor, L-3- *trans*-(Propylcarbamoyl)oxirane-2-carbonyl]-L-isoleucyl-L-Proline (CA-074), developed to allow passive diffusion of the molecule through plasma membranes. We conducted a dose-response study to determine which drug, comparing E64c, a epoxysuccinyl cysteine protease inhibitor, CA-074 and its methyl ester, CA-074Me, at 10µg in 15µl bolus (0.67µg/µL). Initially, we administered one of these three drugs alongside 20% DMSO controls, and these naïve rats were survived for 6h and then their activity was measured. It was found that there was not much inhibition of activity from each drug at that dose: 10% inhibition for CA-074, 20% CA-074Me, and no inhibition for E64c (Figure S.1). Therefore, to get a better approximation of the following dose to try, we inhibited the homogenates in vitro, using 1mM

(3.834 $\mu\text{g}/\mu\text{L}$) CA-074 to determine how much more fold of the drug was needed. With this amount of drug in the plate added to inhibit 80% activity, we needed approximately a 6-fold increase in our dose (Figure S.2). We then increased our maximum dose to 100 μg in a 10 μL bolus (10 $\mu\text{g}/\mu\text{L}$), which achieved 50% inhibition after 6h in a naïve rat with CA-074Me compared to 10% inhibition with E64c. Next, we implanted pumps into the naïve 6h animals following 100 μg bolus where they received 1 $\mu\text{g}/\mu\text{L}$ infusion of CA-074Me from an osmotic pump with a catheter and cannula into the left ventricle. The pump infusion rate was 2.5 $\mu\text{L}/\text{hour}$, for a total of 15 μg infused in addition to the 100 μg bolus. As we planned to have the animals sustain the osmotic pump to two weeks and to meet adequate inhibition as cath B turnover rate is every 15 hours. We changed the dose to adequately inhibit over 2 weeks, to 5 $\mu\text{g}/\mu\text{L}$, infused over 2w. We achieved around 50% inhibition, so we moved on to adding injury to the animals to verify, and we doubled the dose for 10 $\mu\text{g}/\mu\text{L}$, however, only saw 60% ipsilateral inhibition (Figure S.3), leading to the evaluation of both sides of the brain during protein assessments. After conducting the experiments for Chapter 4, I found there were no protein differences between the left and right cortex regarding inhibition, even though CA-074Me was only infused through the left ventricle.

Cath B is unique compared to other cathepsins as it functions as an endopeptidase (cleaves internal amino acids) and an exopeptidase (cleaving internal amino acids). In the lysosome, the exopeptidase structures are exposed due to the acidity of the environment, encouraging the formation of the salt bridge that forms an occluding loop (Nägler et al., 1997). When Cath B enters higher pH environments like the cytosol, that occluding loop changes conformations in turn revealing the endopeptidase site. In recent years, the Hook lab thoroughly investigated how efficient Cath B inhibitors are in different pH settings, where it can work in both lysosomal and the cytosolic environments (Yoon et al., 2021, 2022). Cath B does not have as much activity reduction across all pHs with CA-074. It works best around pH 5.6 at nM concentrations; however, this excludes the cytosol conformation since the inhibitor of the low pH

active site is hidden. unless the drug is administered in a high enough concentration (Yoon et al., 2021, 2022). Thus, we could have been missing a specific type of inhibition, however, we used a high enough dose of CA-074Me (~25.2 mM) to inhibit both lysosomal and cytosolic cath B.

While there were no significant differences in Cathepsin B protein quantities between the injury groups or treatment, it was noted that there was a more pronounced mature product doublet. Other investigators have indicated a single chain whole mature protein and the heavy chain portion cleaved from the light chain that cannot be detected by antibodies, as the epitope is on the heavy chain(Cavallo-Medved et al., 2011; Meyer et al., 2021; Mort & Buttle, 1997; Poreba et al., 2019; Wu et al., 2015). When Cath B is going through the secretory pathway forming its mature peptide form, it has the mannose 6 phosphate signal when it's going from the ER to the Golgi(Katunuma, 2010). There have been experiments studying the artificial truncation of Cath B of the heavy chain of mature Cath B that signal for the mitochondria or the nucleus. However, those were associated with cell death (Bestvater et al., 2005). However, it seems more likely there is an accumulation of single chain and heavy chain Cathepsin B as we are not seeing cell loss (Figure 4.8).

Recalling the protein quantifications for total Cath B, Bak, and Bcl-XL, there were no changes regarding CA-074Me treatment or injury type. However, there was a decrease in the AIF protein expression, particularly in the TBI+ICP group given CA-074Me. While it did not show a significant change, there was a trend toward decreasing AIF. We also saw a decrease in behavioral hypersensitivity to whisker stimulation from CA-074Me given to these TBI+ICP animals and not in sham or injury-only animals. The mechanism following ICP elevation could be using AIF and Bid pathway, however, no increase was seen in AIF for TBI+ICP animals.

However, there is a lot less Cath B lysosomal localization in the non-disrupted population, specifically in the TBI and CA-074Me group. This could also be as a result of DMSO-induced

membrane permeabilization, mentioned in chapter 4 as 5% DMSO in cultured astrocytes have disrupted mitochondrial membranes (Yuan et al., 2014). As previously mentioned, there was no cell loss seen across all groups, hinting that membrane permeability may not be as negative as previously thought. In a dietary manipulation study from the Cullen Group, they showed that rats receiving sham injury and given fish oil had increased membrane permeability, but overall brain lesions recovered better with a high saturated fat and cholesterol diet (Keating et al., 2021).

Future Directions

The next directions for this study would be to compare animals (sham, TBI, and TBI+ICP) given saline and DMSO as two different to fully investigate that DMSO is altering membrane disrupted properties. The role of cytosolic Cathepsin B can be further evaluated by using a pH selective Cathepsin B inhibitor and using a pH specific substrate in activity assays.(Yoon et al., 2021, 2023) Other ways to study the lysosomal perturbations that could be followed would be to use histochemical stainings to look at pH changes in lysosomes and cytosol of those cells using the Beta galactoside assays which are used for senescence but have shown potential to look at lysosomal dysfunction(Bleeker et al., 2000; de Mera-Rodríguez et al., 2021). Moreover, the data generated from the above studies and those proposed can be used to do more ultrastructural analyses of lysosomes following Cath B inhibitors to specifically look at Cath B. DMSO effects could also be studied ultrastructurally to see if there are any membrane deformities as seen in other studies and how other membranous structures within the cell withstand DMSO treatment.

Taken all together, neuronal membrane disruption is not the “dead end” for the cell based on the time course evaluations (Ch1) and DMSO (Ch4) administration. However, the role of Cathepsin B remains elusive in regard to membrane disruption.

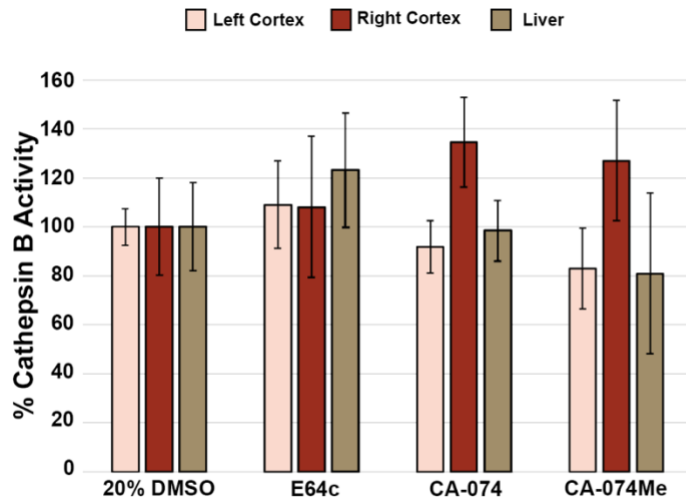


Figure S.1. Cathepsin B activity is reduced in naïve animals (n=2 per treatment group) given CA-074 and CA-074Me. The amount of E64c, CA-074, and CA-074Me infused ventricularly into each animal was 10µg/15µL. Normalized average fluorescence intensity (normalized to naïve given vehicle of 20% DMSO) of Cathepsin B activity within left [pink bars] and right [red bars] homogenates of the lateral neocortex and liver [tan bars] is reported in the bar graph.

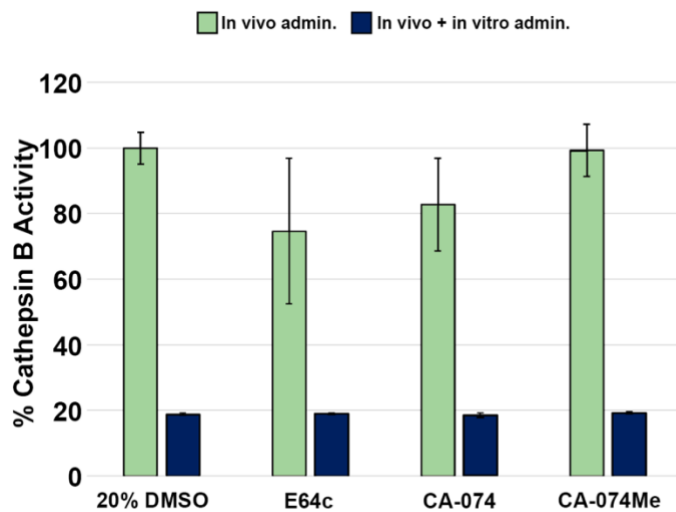


Figure S.2. Cathepsin B activity is reduced to 20% in naïve animals (n=2 per treatment

group) when adding CA-074 *in vitro* at 3.834 $\mu\text{g}/\mu\text{L}$. Normalized average fluorescence intensity (normalized to naïve given vehicle of 20% DMSO) of Cathepsin B activity within *in vivo* treated left homogenates [green bars] and *in vivo+in vitro* [blue bars] homogenates of the lateral neocortex is reported in the bar graph.

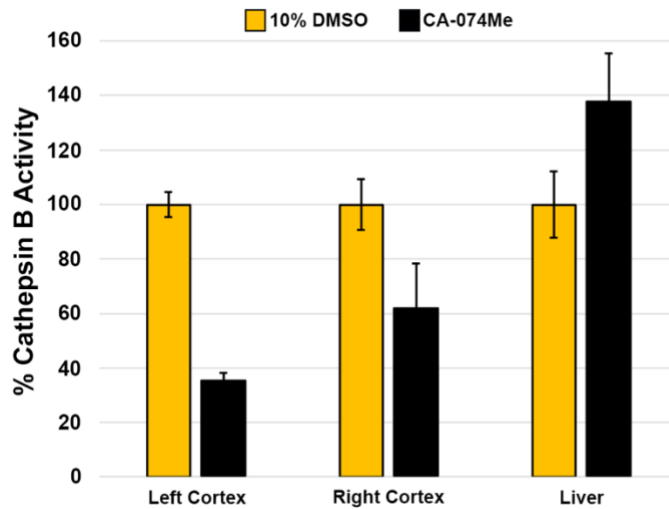


Figure S.1. Cathepsin B activity is reduced in injured animals survived for 2w (n=3 per treatment group) given 10% DMSO [yellow bars] or CA-074Me [black bars] via bolus and osmotic pump infusion into the left lateral ventricle (bolus: 100 $\mu\text{g}/10\mu\text{L}$, osmotic pump: 10 $\mu\text{g}/\mu\text{L}$, at 0.5 $\mu\text{L}/\text{h}$ for 2w). Normalized average fluorescence intensity (normalized to injured animal given vehicle of 10% DMSO bolus and osmotic pump infusion) of Cathepsin B activity within left and right homogenates of the lateral neocortex and liver is reported in the bar graph.

1. Abu Hamdeh, S., Shevchenko, G., Mi, J., Musunuri, S., Bergquist, J., & Marklund, N. (2018). Proteomic differences between focal and diffuse traumatic brain injury in human brain tissue. *Scientific Reports*, 8(1), 6807. <https://doi.org/10.1038/s41598-018-25060-0>
2. Ahmadi, S., Sarveazad, A., Babahajian, A., Ahmadzadeh, K., & Yousefifard, M. (2022). Comparison of Glasgow Coma Scale and Full Outline of UnResponsiveness score for prediction of in-hospital mortality in traumatic brain injury patients: A systematic review and meta-analysis. *European Journal of Trauma and Emergency Surgery*. <https://doi.org/10.1007/s00068-022-02111-w>
3. Amritraj, A., Peake, K., Kodam, A., Salio, C., Merighi, A., Vance, J. E., & Kar, S. (2009). Increased Activity and Altered Subcellular Distribution of Lysosomal Enzymes Determine Neuronal Vulnerability in Niemann-Pick Type C1-Deficient Mice. *The American Journal of Pathology*, 175(6), 2540–2556. <https://doi.org/10.2353/ajpath.2009.081096>
4. Andriessen, T. M. J. C., Jacobs, B., & Vos, P. E. (2010a). Clinical characteristics and pathophysiological mechanisms of focal and diffuse traumatic brain injury. *Journal of Cellular and Molecular Medicine*, 14(10), 2381–2392. <https://doi.org/10.1111/j.1582-4934.2010.01164.x>
5. Babiychuk, E. B., Monastyrskaya, K., & Draeger, A. (2008). Fluorescent annexin A1 reveals dynamics of ceramide platforms in living cells. *Traffic*, 9(10), 1757–1775. <https://doi.org/10.1111/j.1600-0854.2008.00800.x>
6. Benchoua, A., Braudeau, J., Reis, A., Couriaud, C., & Onténiente, B. (2004). Activation of proinflammatory caspases by cathepsin B in focal cerebral ischemia. *Journal of Cerebral Blood Flow and Metabolism*, 24(11), 1272–1279. <https://doi.org/10.1097/01.WCB.0000140272.54583.FB>
7. Bestvater, F., Dallner, C., & Spiess, E. (2005). The C-terminal subunit of artificially truncated human cathepsin B mediates its nuclear targeting and contributes to cell viability. *BMC Cell Biology*, 6(1), 16. <https://doi.org/10.1186/1471-2121-6-16>
8. Bi, G. Q., Alderton, J. M., & Steinhardt, R. A. (1995). Calcium-regulated exocytosis is required for cell membrane resealing. *Journal of Cell Biology*, 131(6 II), 1747–1758. <https://doi.org/10.1083/jcb.131.6.1747>
9. Bleeker, F. E., Hazen, L. G. M., Köhler, A., & Van Noorden, C. J. F. (2000). Direct comparison of the sensitivity of enzyme histochemical and immunohistochemical methods: Cathepsin B expression in human colorectal mucosa. *Acta Histochemica*, 102(3), 247–257. [https://doi.org/10.1078/S0065-1281\(04\)70033-1](https://doi.org/10.1078/S0065-1281(04)70033-1)

10. Bouter, A., Carmeille, R., Gounou, C., Bouvet, F., Degrelle, S. A., Evain-Brion, D., & Brisson, A. R. (2015). Review: Annexin-A5 and cell membrane repair. *Placenta*, 36(S1), S43–S49. <https://doi.org/10.1016/j.placenta.2015.01.193>
11. Bouter, A., Gounou, C., Bérat, R., Tan, S., Gallois, B., Granier, T., D'Estaintot, B. L., Pöschl, E., Brachvogel, B., & Brisson, A. R. (2011). Annexin-A5 assembled into two-dimensional arrays promotes cell membrane repair. *Nature Communications*, 2(1). <https://doi.org/10.1038/ncomms1270>
12. Boutté, A. M., Hook, V., Thangavelu, B., Sarkis, G. A., Abbatiello, B. N., Hook, G., Jacobsen, J. S., Robertson, C. S., Gilsdorf, J., Yang, Z., Wang, K. K. W., & Shear, D. A. (2020). Penetrating Traumatic Brain Injury Triggers Dysregulation of Cathepsin B Protein Levels Independent of Cysteine Protease Activity in Brain and Cerebral Spinal Fluid. *Journal of Neurotrauma*, 37(13), 1574–1586. <https://doi.org/10.1089/neu.2019.6537>
13. Boya, P., Andreau, K., Poncet, D., Zamzami, N., Perfettini, J. L., Metivier, D., Ojcius, D. M., Jäättelä, M., & Kroemer, G. (2003). Lysosomal membrane permeabilization induces cell death in a mitochondrion-dependent fashion. *Journal of Experimental Medicine*, 197(10), 1323–1334. <https://doi.org/10.1084/jem.20021952>
14. Bratton, S. L., Chestnut, R. M., Ghajar, J., Hammond, F. F. M., Harris, O. A., Hartl, R., Manley, G. T., Nemecek, A., Newell, D. W., Rosenthal, G., Schouten, J., Shutter, L., Timmons, S. D., Ullman, J. S., Videtta, W., Wilberger, J. E., & Wright, D. W. (2007). VIII. Intracranial Pressure Thresholds. *Journal of Neurotrauma*, 24. <https://doi.org/10.1089/neu.2007.9988>
15. Cai, Y., Xiong, K., Chu, Y., Luo, D. W., Luo, X. G., Yuan, X. Y., Struble, R. G., Clough, R. W., Spencer, D. D., Williamson, A., Kordower, J. H., Patrylo, P. R., & Yan, X. X. (2009). Doublecortin expression in adult cat and primate cerebral cortex relates to immature neurons that develop into GABAergic subgroups. *Experimental Neurology*, 216(2), 342–356. <https://doi.org/10.1016/j.expneurol.2008.12.008>
16. Cannon, J. R., & Greenamyre, J. T. (2009). NeuN is not a reliable marker of dopamine neurons in rat substantia nigra. *Neuroscience Letters*, 464(1), 14–17. <https://doi.org/10.1016/j.neulet.2009.08.023>
17. Cavallo-Medved, D., Moin, K., & Sloane, B. (2011). Cathepsin B: Basis Sequence: Mouse. *The AFCS-Nature Molecule Pages*, 2011. <http://www.ncbi.nlm.nih.gov/pubmed/28781583%0Ahttp://www.pubmedcentral.nih.gov/articlerender.fcgi?artid=PMC5541861>

18. Chaitanya, G. V., & Babu, P. P. (2008). Multiple apoptogenic proteins are involved in the nuclear translocation of Apoptosis Inducing Factor during transient focal cerebral ischemia in rat. *Brain Research*, 1246, 178–190.
<https://doi.org/10.1016/j.brainres.2008.09.075>
19. Choo, A. M., Liu, J., Lam, C. K., Dvorak, M., Tetzlaff, W., & Oxland, T. R. (2007). Contusion, dislocation, and distraction: Primary hemorrhage and membrane permeability in distinct mechanisms of spinal cord injury. *Journal of Neurosurgery. Spine*, 6(3), 255–266. <https://doi.org/10.3171/spi.2007.6.3.255>
20. Chowdhury, K. D., Sarkar, A., Chatterjee, S., Patra, D., Sengupta, D., Banerjee, S., Chakraborty, P., & Sadhukhan, G. C. (2019). Cathepsin B mediated scramblase activation triggers cytotoxicity and cell cycle arrest by andrographolide to overcome cellular resistance in cisplatin resistant human hepatocellular carcinoma HepG2 cells. *Environmental Toxicology and Pharmacology*, 68, 120–132.
<https://doi.org/10.1016/j.etap.2019.03.003>
21. Christ, L., Raiborg, C., Wenzel, E. M., Campsteijn, C., & Stenmark, H. (2017). Cellular Functions and Molecular Mechanisms of the ESCRT Membrane-Scission Machinery. *Trends in Biochemical Sciences*, 42(1), 42–56. <https://doi.org/10.1016/j.tibs.2016.08.016>
22. Coomans, C., Saaltink, D.-J., Deboer, T., Tersteeg, M., Lanooij, S., Schneider, A. F., Mulder, A., van Minnen, J., Jost, C., Koster, A. J., & Vreugdenhil, E. (2021). Doublecortin-like expressing astrocytes of the suprachiasmatic nucleus are implicated in the biosynthesis of vasopressin and influences circadian rhythms. *Glia*, 69(11), 2752–2766. <https://doi.org/10.1002/glia.24069>
23. Cullen, D. K., Vernekar, V. N., & LaPlaca, M. C. (2011a). Trauma-induced plasmalemma disruptions in three-dimensional neural cultures are dependent on strain modality and rate. *Journal of Neurotrauma*, 28(11), 2219–2233. <https://doi.org/10.1089/neu.2011.1841>
24. Dams-O'Connor, K., Juengst, S. B., Bogner, J., Chiaravalloti, N. D., Corrigan, J. D., Giacino, J. T., Harrison-Felix, C. L., Hoffman, J. M., Ketchum, J. M., Lequerica, A. H., Marwitz, J. H., Miller, A. C., Nakase-Richardson, R., Rabinowitz, A. R., Sander, A. M., Zafonte, R., & Hammond, F. M. (2023). Traumatic brain injury as a chronic disease: Insights from the United States Traumatic Brain Injury Model Systems Research Program. *The Lancet. Neurology*, 22(6), 517–528. [https://doi.org/10.1016/S1474-4422\(23\)00065-0](https://doi.org/10.1016/S1474-4422(23)00065-0)
25. Darlot, F., Vinit, S., Matarazzo, V., & Kastner, A. (2017a). Sustained cell body reactivity and loss of NeuN in a subset of axotomized bulbospinal neurons after a chronic high cervical spinal cord injury. *European Journal of Neuroscience*, 46(11), 2729–2745.
<https://doi.org/10.1111/ejn.13737>

26. de Castro, M., Bunt, G., & Wouters, F. (2016). Cathepsin B launches an apoptotic exit effort upon cell death-associated disruption of lysosomes. *Cell Death Discovery*, 2(1), 16012. <https://doi.org/10.1038/cddiscovery.2016.12>
27. de la Torre, J. C., Kawanaga, H. M., Rowed, D. W., Johnson, C. M., Goode, D. J., Kajihara, K., & Mullan, S. (1975). Dimethyl Sulfoxide in Central Nervous System Trauma. *Annals of the New York Academy of Sciences*, 243(1), 362–389. <https://doi.org/10.1111/j.1749-6632.1975.tb25377.x>
28. de Mera-Rodríguez, J. A., Álvarez-Hernán, G., Gañán, Y., Martín-Partido, G., Rodríguez-León, J., & Francisco-Morcillo, J. (2021). Is Senescence-Associated β -Galactosidase a Reliable in vivo Marker of Cellular Senescence During Embryonic Development? *Frontiers in Cell and Developmental Biology*, 9. <https://www.frontiersin.org/articles/10.3389/fcell.2021.623175>
29. Dextrat, E. R., Yoo, S., Eddleman, C. S., Fukuda, M., Bittner, G. D., & Fishman, H. M. (2000). Plasmalemmal repair of severed neurites of PC12 cells requires Ca^{2+} and synaptotagmin. *Journal of Neuroscience Research*. [https://doi.org/10.1002/1097-4547\(20001115\)62:4<566::AID-JNR11>3.0.CO;2-4](https://doi.org/10.1002/1097-4547(20001115)62:4<566::AID-JNR11>3.0.CO;2-4)
30. Di Giorgio, A. M., Hou, Y., Zhao, X., Zhang, B., Lyeth, B. G., & Russell, M. J. (2008). Dimethyl sulfoxide provides neuroprotection in a traumatic brain injury model. *Restorative Neurology and Neuroscience*, 26(6), 501–507.
31. Dixon, C. E., Lyeth, B. G., Povlishock, J. T., Findling, R. L., Hamm, R. J., Marmarou, A., Young, H. F., & Hayes, R. L. (1987a). A fluid percussion model of experimental brain injury in the rat. *Journal of Neurosurgery*, 67(1), 110–119. <https://doi.org/10.3171/jns.1987.67.1.0110>
32. Draeger, A., Monastyrskaya, K., & Babiychuk, E. B. (2011). Plasma membrane repair and cellular damage control: The annexin survival kit. *Biochemical Pharmacology*. <https://doi.org/10.1016/j.bcp.2010.12.027>
33. Draeger, A., Schoenauer, R., Atanassoff, A. P., Wolfmeier, H., & Babiychuk, E. B. (2014). Dealing with damage: Plasma membrane repair mechanisms. *Biochimie*. <https://doi.org/10.1016/j.biochi.2014.08.008>
34. Duan, W., Zhang, Y. P., Hou, Z., Huang, C., Zhu, H., Zhang, C. Q., & Yin, Q. (2016). Novel Insights into NeuN: from Neuronal Marker to Splicing Regulator. *Molecular Neurobiology*, 53(3), 1637–1647. <https://doi.org/10.1007/s12035-015-9122-5>

35. Eddleman, C. S., Ballinger, M. L., Smyers, M. E., Fishman, H. M., & Bittner, G. D. (1998). Endocytotic Formation of Vesicles and Other Membranous Structures Induced by Ca²⁺ and Axolemmal Injury. *The Journal of Neuroscience*, 18(11), 4029–4041. <https://doi.org/10.1523/jneurosci.18-11-04029.1998>
36. Ellis, R. C., O'Steen, W. A., Hayes, R. L., Nick, H. S., Wang, K. K. W., & Anderson, D. K. (2005). Cellular localization and enzymatic activity of cathepsin B after spinal cord injury in the rat. *Experimental Neurology*, 193(1), 19–28. <https://doi.org/10.1016/j.expneurol.2004.11.034>
37. Escartin, C., Galea, E., Lakatos, A., O'Callaghan, J. P., Petzold, G. C., Serrano-Pozo, A., Steinhäuser, C., Volterra, A., Carmignoto, G., Agarwal, A., Allen, N. J., Araque, A., Barbeito, L., Barzilai, A., Bergles, D. E., Bonvento, G., Butt, A. M., Chen, W.-T., Cohen-Salmon, M., ... Verkhratsky, A. (2021). Reactive astrocyte nomenclature, definitions, and future directions. *Nature Neuroscience*, 24(3), 312–325. <https://doi.org/10.1038/s41593-020-00783-4>
38. Farahvar, A., Gerber, L. M., Chiu, Y.-L., Carney, N., Härtl, R., & Ghajar, J. (2012). Increased mortality in patients with severe traumatic brain injury treated without intracranial pressure monitoring. *Journal of Neurosurgery*, 117(4), 729–734. <https://doi.org/10.3171/2012.7.JNS111816>
39. Farkas, O., Lifshitz, J., & Povlishock, J. T. (2006a). Mechanoporation Induced by Diffuse Traumatic Brain Injury: An Irreversible or Reversible Response to Injury? *Journal of Neuroscience*, 26(12), 3130–3140. <https://doi.org/10.1523/JNEUROSCI.5119-05.2006>
40. Feldstein, A. E., Werneburg, N. W., Canbay, A., Guicciardi, M. E., Bronk, S. F., Rydzewski, R., Burgart, L. J., & Gores, G. J. (2004). Free fatty acids promote hepatic lipotoxicity by stimulating TNF- α expression via a lysosomal pathway. *Hepatology*, 40(1), 185–194. <https://doi.org/10.1002/hep.20283>
41. Foghsgaard, L., Wissing, D., Mauch, D., Lademann, U., Bastholm, L., Boes, M., Elling, F., Leist, M., & Jäätelä, M. (2001). Cathepsin B Acts as a Dominant Execution Protease in Tumor Cell Apoptosis Induced by Tumor Necrosis Factor. *Journal of Cell Biology*, 153(5), 999–1010. <https://doi.org/10.1083/jcb.153.5.999>
42. Gatta, A. T., & Carlton, J. G. (2019). The ESCRT-machinery: Closing holes and expanding roles. *Current Opinion in Cell Biology*, 59, 121–132. <https://doi.org/10.1016/j.ceb.2019.04.005>

43. Geddes, D. M., Cargill, R. S., & LaPlaca, M. C. (2003a). Mechanical Stretch to Neurons Results in a Strain Rate and Magnitude-Dependent Increase in Plasma Membrane Permeability. *Journal of Neurotrauma*, 20(10), 1039–1049. <https://doi.org/10.1089/089771503770195885>
44. Geddes, D. M., LaPlaca, M. C., & Cargill, R. S. (2003b). Susceptibility of hippocampal neurons to mechanically induced injury. *Experimental Neurology*, 184(1), 420–427. [https://doi.org/10.1016/S0014-4886\(03\)00254-1](https://doi.org/10.1016/S0014-4886(03)00254-1)
45. Giannaris, E. L., & Rosene, D. L. (2012). A stereological study of the numbers of neurons and glia in the primary visual cortex across the lifespan of male and female rhesus monkeys. *Journal of Comparative Neurology*, 520(15), 3492–3508. <https://doi.org/10.1002/cne.23101>
46. Gonzales, B. J., Mukherjee, D., Ashwal-Fluss, R., Loewenstein, Y., & Citri, A. (2020). Subregion-specific rules govern the distribution of neuronal immediate-early gene induction. *Proceedings of the National Academy of Sciences*, 117(38), 23304–23310. <https://doi.org/10.1073/pnas.1913658116>
47. Gorse, K. M., & Lafrenaye, A. D. (2018). The Importance of Inter-Species Variation in Traumatic Brain Injury-Induced Alterations of Microglial-Axonal Interactions. *Frontiers in Neurology*, 9, 778. <https://doi.org/10.3389/fneur.2018.00778>
48. Granacher, R. P. (2007). The Epidemiology and Pathophysiology of Traumatic Brain Injury. In *Traumatic Brain Injury: Methods for Clinical and Forensic Neuropsychiatric Assessment, Second Edition* (pp. 1–7). CRC Press. <https://books.google.com/books?id=xt1YFydzXKQC>
49. Greer, J. E., McGinn, M. J., & Povlishock, J. T. (2011a). Diffuse Traumatic Axonal Injury in the Mouse Induces Atrophy, c-Jun Activation, and Axonal Outgrowth in the Axotomized Neuronal Population. *Journal of Neuroscience*, 31(13), 5089–5105. <https://doi.org/10.1523/JNEUROSCI.5103-10.2011>
50. Guicciardi, M. E., Deussing, J., Miyoshi, H., Bronk, S. F., Svingen, P. A., Peters, C., Kaufmann, S. H., & Gores, G. J. (2000). Cathepsin B contributes to TNF- α -mediated hepatocyte apoptosis by promoting mitochondrial release of cytochrome c. *Journal of Clinical Investigation*, 106(9), 1127–1137. <https://doi.org/10.1172/JCI9914>
51. Gurtovenko, A. A., & Anwar, J. (2007). Modulating the Structure and Properties of Cell Membranes: The Molecular Mechanism of Action of Dimethyl Sulfoxide. *The Journal of Physical Chemistry B*, 111(35), 10453–10460. <https://doi.org/10.1021/jp073113e>

52. Gusel'nikova, V. V., B, Г. B., Korzhevskiy, D. E., & Э, К. Д. (2015). NeuN As a Neuronal Nuclear Antigen and Neuron Differentiation Marker. *Acta Naturae*, 7(2), Article 2. <https://doi.org/10.32607/20758251-2015-7-2-42-47>
53. Hahn, Y. K., Masvekar, R. R., Xu, R., & Knapp, K. F. H. and P. E. (2015). Chronic HIV-1 Tat and HIV Reduce Rbfox3/NeuN: Evidence for Sex- Related Effects. In *Current HIV Research* (Vol. 13, Issue 1, pp. 10–20). <http://dx.doi.org/10.2174/1570162X13666150311163733>
54. Halford, J., Shen, S., Itamura, K., Levine, J., Chong, A. C., Czerwieniec, G., Glenn, T. C., Hovda, D. A., Vespa, P., Bullock, R., Dietrich, W. D., Mondello, S., Loo, J. A., & Wanner, I.-B. (2017). New astroglial injury-defined biomarkers for neurotrauma assessment. *Journal of Cerebral Blood Flow & Metabolism*, 37(10), 3278–3299. <https://doi.org/10.1177/0271678X17724681>
55. Harris, J. P., Mietus, C. J., Browne, K. D., Wofford, K. L., Keating, C. E., Brown, D. P., Johnson, B. N., Wolf, J. A., Smith, D. H., Cohen, A. S., Duda, J. E., & Cullen, D. K. (2023). Neuronal somatic plasmalemmal permeability and dendritic beading caused by head rotational traumatic brain injury in pigs—An exploratory study. *Frontiers in Cellular Neuroscience*, 17. <https://www.frontiersin.org/articles/10.3389/fncel.2023.1055455>
56. Hawthorne, C., & Piper, I. (2014). Monitoring of Intracranial Pressure in Patients with Traumatic Brain Injury. *Frontiers in Neurology*, 5. <https://www.frontiersin.org/articles/10.3389/fneur.2014.00121>
57. Heald, R., & Cohen-Fix, O. (2014). Morphology and Function of Membrane-bound Organelles. *Current Opinion in Cell Biology*, 0, 79–86. <https://doi.org/10.1016/j.ceb.2013.10.006>
58. Hendricks, B. K., & Shi, R. (2014). Mechanisms of neuronal membrane sealing following mechanical trauma. *Neuroscience Bulletin*, 30(4), 627–644. <https://doi.org/10.1007/s12264-013-1446-4>
59. Hernandez, M. L., Chatlos, T., Gorse, K. M., & Lafrenaye, A. D. (2019). Neuronal Membrane Disruption Occurs Late Following Diffuse Brain Trauma in Rats and Involves a Subpopulation of NeuN Negative Cortical Neurons. *Frontiers in Neurology*, 10. <https://doi.org/10.3389/fneur.2019.01238>
60. Hernandez, M. L., Marone, M., Gorse, K. M., & Lafrenaye, A. D. (2022). Cathepsin B Relocalization in Late Membrane Disrupted Neurons Following Diffuse Brain Injury in Rats. *ASN Neuro*, 14, 17590914221099112. <https://doi.org/10.1177/17590914221099112>

61. Hook, G. R., Yu, J., Sipes, N., Pierschbacher, M. D., Hook, V., & Kindy, M. S. (2013). The Cysteine Protease Cathepsin B Is a Key Drug Target and Cysteine Protease Inhibitors Are Potential Therapeutics for Traumatic Brain Injury. *Journal of Neurotrauma*, 31(5), 515–529. <https://doi.org/10.1089/neu.2013.2944>
62. Jacko, M., Weyn-Vanhentenryck, S. M., Smerdon, J. W., Yan, R., Feng, H., Williams, D. J., Pai, J., Xu, K., Wichterle, H., & Zhang, C. (2018). Rbfox Splicing Factors Promote Neuronal Maturation and Axon Initial Segment Assembly. *Neuron*, 97(4), 853-868.e6. <https://doi.org/10.1016/j.neuron.2018.01.020>
63. Jaiswal, J. K., Andrews, N. W., & Simon, S. M. (2002). Membrane proximal lysosomes are the major vesicles responsible for calcium-dependent exocytosis in nonsecretory cells. *Journal of Cell Biology*, 159(4), 625–635. <https://doi.org/10.1083/jcb.200208154>
64. James, S. L., Theadom, A., Ellenbogen, R. G., Bannick, M. S., Montjoy-Venning, W., Lucchesi, L. R., Abbasi, N., Abdulkader, R., Abraha, H. N., Adsuar, J. C., Afarideh, M., Agrawal, S., Ahmadi, A., Ahmed, M. B., Aichour, A. N., Aichour, I., Aichour, M. T. E., Akinyemi, R. O., Akseer, N., ... Murray, C. J. L. (2019). Global, regional, and national burden of traumatic brain injury and spinal cord injury, 1990–2016: A systematic analysis for the Global Burden of Disease Study 2016. *The Lancet Neurology*, 18(1), 56–87. [https://doi.org/10.1016/S1474-4422\(18\)30415-0](https://doi.org/10.1016/S1474-4422(18)30415-0)
65. Jiang, M., Meng, J., Zeng, F., Qing, H., Hook, G., Hook, V., Wu, Z., & Ni, J. (2020). Cathepsin B inhibition blocks neurite outgrowth in cultured neurons by regulating lysosomal trafficking and remodeling. *Journal of Neurochemistry*, 155(3), 300–312. <https://doi.org/10.1111/jnc.15032>
66. Jin, Y., Suzuki, H., Maegawa, S., Endo, H., Sugano, S., Hashimoto, K., Yasuda, K., & Inoue, K. (2003). A vertebrate RNA-binding protein Fox-1 regulates tissue-specific splicing via the pentanucleotide GCAUG. *The EMBO Journal*, 22(4), 905–912. <https://doi.org/10.1093/emboj/cdg089>
67. Karaca, M., Bilgin, U. Y., Akar, M., & de la Torre, J. C. (1991). Dimethyl sulphoxide lowers ICP after closed head trauma. *European Journal of Clinical Pharmacology*, 40(1), 113–114. <https://doi.org/10.1007/BF00315149>
68. Katunuma, N. (2010). Posttranslational Processing and Modification of Cathepsins and Cystatins. *Journal of Signal Transduction*, 2010, 1–8. <https://doi.org/10.1155/2010/375345>
69. Kay, T., Harrington, D. E., Adams, R., Anderson, T., Berrol, S., Cicerone, K., Dahlberg, C., Gerber, D., Goka, R., Harley, P., Hilt, J., Horn, L., Lehmkuhl, D., & Malec, J. (1993). American Congress of Rehabilitation Medicine: Definition of Mild Traumatic Brain Injury. *Journal of Head Trauma Rehabilitation*, 8(3), 86–87.

70. Keating, C. E., Browne, K. D., & Cullen, D. K. (2021). Dietary manipulation of vulnerability to traumatic brain injury-induced neuronal plasma membrane permeability. *Experimental Neurology*, 340, 113649. <https://doi.org/10.1016/j.expneurol.2021.113649>
71. Keating, C. E., Browne, K. D., Duda, J. E., & Cullen, D. K. (2020). Neurons in Subcortical Oculomotor Regions Are Vulnerable to Plasma Membrane Damage after Repetitive Diffuse Traumatic Brain Injury in Swine. *Journal of Neurotrauma*, 37(17), 1918–1932. <https://doi.org/10.1089/neu.2019.6738>
72. Khouri, H. E., Plouffe, C., Hasnain, S., Hiram, T., Storer, A. C., & Ménard, R. (1991). A model to explain the pH-dependent specificity of cathepsin B-catalysed hydrolyses. *Biochemical Journal*, 275(3), 751–757. <https://doi.org/10.1042/bj2750751>
73. Kilinc, D., Gallo, G., & Barbee, K. A. (2008a). Mechanically-induced membrane poration causes axonal beading and localized cytoskeletal damage. *Experimental Neurology*, 212(2), 422–430. <https://doi.org/10.1016/j.expneurol.2008.04.025>
74. Kilinc, D., Gallo, G., & Barbee, K. A. (2008b). Mechanically-induced membrane poration causes axonal beading and localized cytoskeletal damage. *Experimental Neurology*, 212(2), 422–430. <https://doi.org/10.1016/j.expneurol.2008.04.025>
75. Kilinc, M., Gürsoy-Özdemir, Y., Gürer, G., Erdener, S. E., Erdemli, E., Can, A., & Dalkara, T. (2010). Lysosomal rupture, necroapoptotic interactions and potential crosstalk between cysteine proteases in neurons shortly after focal ischemia. *Neurobiology of Disease*, 40(1), 293–302. <https://doi.org/10.1016/j.nbd.2010.06.003>
76. Kim, K. K., Adelstein, R. S., & Kawamoto, S. (2009a). Identification of Neuronal Nuclei (NeuN) as Fox-3, a New Member of the Fox-1 Gene Family of Splicing Factors. *Journal of Biological Chemistry*, 284(45), 31052–31061. <https://doi.org/10.1074/jbc.M109.052969>
77. Kim, K. K., Adelstein, R. S., & Kawamoto, S. (2009b). Identification of Neuronal Nuclei (NeuN) as Fox-3, a New Member of the Fox-1 Gene Family of Splicing Factors. *Journal of Biological Chemistry*, 284(45), 31052–31061. <https://doi.org/10.1074/jbc.M109.052969>
78. Kim, K. K., Kim, Y. C., Adelstein, R. S., & Kawamoto, S. (2011). Fox-3 and PSF interact to activate neural cell-specific alternative splicing. *Nucleic Acids Research*, 39(8), 3064–3078. <https://doi.org/10.1093/nar/gkq1221>
79. Kim, K. K., Nam, J., Mukoyama, Y. S., & Kawamoto, S. (2013a). Rbfox3-regulated alternative splicing of Numb promotes neuronal differentiation during development. *Journal of Cell Biology*, 200(4), 443–458. <https://doi.org/10.1083/jcb.201206146>

80. Kim, S., Kim, H., & Um, J. W. (2018). Synapse development organized by neuronal activity-regulated immediate-early genes. *Experimental & Molecular Medicine*, 50(4), Article 4. <https://doi.org/10.1038/s12276-018-0025-1>
81. Kochanek, P. M., Clark, R. S., & Jenkins, L. W. (2013). Pathobiology of secondary brain injury. In *Brain Injury Medicine: Principles and Practice* (2nd ed., pp. 148–161). Demos Medical Publishing, 2012.
82. Lafrenaye, A. D., Krahe, T. E., & Povlishock, J. T. (2014a). Moderately Elevated Intracranial Pressure after Diffuse Traumatic Brain Injury is Associated with Exacerbated Neuronal Pathology and Behavioral Morbidity in the Rat. *Journal of Cerebral Blood Flow & Metabolism*, 34(10), 1628–1636. <https://doi.org/10.1038/jcbfm.2014.122>
83. Lafrenaye, A. D., McGinn, M. J., & Povlishock, J. T. (2012a). Increased Intracranial Pressure after Diffuse Traumatic Brain Injury Exacerbates Neuronal Somatic Membrane Poration but not Axonal Injury: Evidence for Primary Intracranial Pressure-Induced Neuronal Perturbation. *Journal of Cerebral Blood Flow & Metabolism*, 32(10), 1919–1932. <https://doi.org/10.1038/jcbfm.2012.95>
84. Langlois, J. A., Rutland-Brown, W., & Wald, M. M. (2006a). The Epidemiology and Impact of Traumatic Brain Injury. *Journal of Head Trauma Rehabilitation*, 21(5), 375–378. <https://doi.org/10.1097/00001199-200609000-00001>
85. LaPlaca, M. C., Lee, V. M.-Y., & Thibault, L. E. (1997). An In Vitro Model of Traumatic Neuronal Injury: Loading Rate-Dependent Changes in Acute Cytosolic Calcium and Lactate Dehydrogenase Release. *Journal of Neurotrauma*, 14(6), 355–368. <https://doi.org/10.1089/neu.1997.14.355>
86. LaPlaca, M. C., Lessing, M. C., Prado, G. R., Zhou, R., Tate, C. C., Geddes-Klein, D., Meaney, D. F., & Zhang, L. (2019a). Mechanoporation is a potential indicator of tissue strain and subsequent degeneration following experimental traumatic brain injury. *Clinical Biomechanics*, 64, 2–13. <https://doi.org/10.1016/j.clinbiomech.2018.05.016>
87. LaPlaca, M. C., & Prado, G. R. (2010). Neural mechanobiology and neuronal vulnerability to traumatic loading. *Journal of Biomechanics*, 43(1), 71–78. <https://doi.org/10.1016/j.jbiomech.2009.09.011>
88. LaPlaca, M. C., Prado, G. R., Cullen, D., & Simon, C. M. (2009). Plasma membrane damage as a marker of neuronal injury. *Conference Proceedings : ... Annual International Conference of the IEEE Engineering in Medicine and Biology Society. IEEE Engineering in Medicine and Biology Society. Conference, 2009*, 1113–1116. <https://doi.org/10.1109/IEMBS.2009.5334457>

89. LaPlaca, M. C., & Thibault, L. E. (1997). An in vitro traumatic injury model to examine the response of neurons to a hydrodynamically-induced deformation. *Annals of Biomedical Engineering*, 25(4), 665–677. <https://doi.org/10.1007/BF02684844>
90. LaPlaca, M. C., & Thibault, L. E. (1998a). Dynamic mechanical deformation of neurons triggers an acute calcium response and cell injury involving the N-methyl-D-aspartate glutamate receptor. *Journal of Neuroscience Research*, 52(2), 220–229.
91. LaPlaca, M. C., & Thibault, L. E. (1998b). Dynamic mechanical deformation of neurons triggers an acute calcium response and cell injury involving the N-methyl-D-Aspartate glutamate receptor. *Journal of Neuroscience Research*, 52(2), 220–229. [https://doi.org/10.1002/\(SICI\)1097-4547\(19980415\)52:2<220::AID-JNR10>3.0.CO;2-B](https://doi.org/10.1002/(SICI)1097-4547(19980415)52:2<220::AID-JNR10>3.0.CO;2-B)
92. Lavezzi, A. M., Corna, M. F., & Matturri, L. (2013). Neuronal nuclear antigen (NeuN): A useful marker of neuronal immaturity in sudden unexplained perinatal death. *Journal of the Neurological Sciences*, 329(1–2), 45–50. <https://doi.org/10.1016/j.jns.2013.03.012>
93. Lee, J. C. M., Simonyi, A., Sun, A. Y., & Sun, G. Y. (2011). Phospholipases A2 and neural membrane dynamics: Implications for Alzheimer's disease. *Journal of Neurochemistry*, 116(5), 813–819. <https://doi.org/10.1111/j.1471-4159.2010.07033.x>
94. Levine, J., Kwon, E., Paez, P., Yan, W., Czerwieniec, G., Loo, J. A., Sofroniew, M. V., & Wanner, I.-B. (2016a). Traumatically injured astrocytes release a proteomic signature modulated by STAT3-dependent cell survival. *Glia*, 64(5), 668–694. <https://doi.org/10.1002/glia.22953>
95. Li, Y., Jones, J. W., M. C. Choi, H., Sarkar, C., Kane, M. A., Koh, E. Y., Lipinski, M. M., & Wu, J. (2019). CPLA2 activation contributes to lysosomal defects leading to impairment of autophagy after spinal cord injury. *Cell Death & Disease*, 10(7), 531. <https://doi.org/10.1038/s41419-019-1764-1>
96. Lifshitz, J., Kelley, B. J., & Povlishock, J. T. (2007a). Perisomatic thalamic axotomy after diffuse traumatic brain injury is associated with atrophy rather than cell death. *J Neuropathol Exp Neurol*, 66(3), 218–229. <https://doi.org/10.1097/01.jnen.0000248558.75950.4d00005072-200703000-00006> [pii]
97. Lind, D., Franken, S., Kappler, J., Jankowski, J., & Schilling, K. (2005). Characterization of the neuronal marker NeuN as a multiply phosphorylated antigen with discrete subcellular localization. *Journal of Neuroscience Research*, 79(3), 295–302. <https://doi.org/10.1002/jnr.20354>

98. Luo, C.-L., Chen, X.-P., Li, L.-L., Li, Q.-Q., Li, B.-X., Xue, A.-M., Xu, H.-F., Dai, D.-K., Shen, Y.-W., Tao, L.-Y., & Zhao, Z.-Q. (2013). Poloxamer 188 Attenuates in vitro Traumatic Brain Injury-Induced Mitochondrial and Lysosomal Membrane Permeabilization Damage in Cultured Primary Neurons. *Journal of Neurotrauma*, 30(7), 597–607. <https://doi.org/10.1089/neu.2012.2425>
99. Luo, C.-L., Chen, X.-P., Yang, R., Sun, Y.-X., Li, Q.-Q., Bao, H.-J., Cao, Q.-Q., Ni, H., Qin, Z.-H., & Tao, L.-Y. (2010). Cathepsin B contributes to traumatic brain injury-induced cell death through a mitochondria-mediated apoptotic pathway. *Journal of Neuroscience Research*, 88(13), 2847–2858. <https://doi.org/10.1002/jnr.22453>
100. Lusardi, T. A., Wolf, J. A., Putt, M. E., Smith, D. H., & Meaney, D. F. (2004). Effect of Acute Calcium Influx after Mechanical Stretch Injury In Vitro on the Viability of Hippocampal Neurons. *Journal of Neurotrauma*, 21(1). <https://doi.org/10.1089/089771504772695959>
101. Ma, V. Y., Chan, L., & Carruthers, K. J. (2014). Incidence, prevalence, costs, and impact on disability of common conditions requiring rehabilitation in the united states: Stroke, spinal cord injury, traumatic brain injury, multiple sclerosis, osteoarthritis, rheumatoid arthritis, limb loss, and back pa. *Archives of Physical Medicine and Rehabilitation*, 95(5), 986–995. <https://doi.org/10.1016/j.apmr.2013.10.032>
102. Maas, A. I. R., Menon, D. K., Manley, G. T., Abrams, M., Åkerlund, C., Andelic, N., Aries, M., Bashford, T., Bell, M. J., Bodien, Y. G., Brett, B. L., Büki, A., Chesnut, R. M., Citerio, G., Clark, D., Clasby, B., Cooper, D. J., Czeiter, E., Czosnyka, M., ... Zemek, R. (2022). Traumatic brain injury: Progress and challenges in prevention, clinical care, and research. *The Lancet Neurology*, 21(11), 1004–1060. [https://doi.org/10.1016/S1474-4422\(22\)00309-X](https://doi.org/10.1016/S1474-4422(22)00309-X)
103. Macovei, A., Faè, M., Biggiogera, M., de Sousa Araújo, S., Carbonera, D., & Balestrazzi, A. (2018). Ultrastructural and Molecular Analyses Reveal Enhanced Nucleolar Activity in Medicago truncatula Cells Overexpressing the MtTdp2α Gene. *Frontiers in Plant Science*, 9, 596. <https://doi.org/10.3389/fpls.2018.00596>
104. Marin, J. R., Weaver, M. D., & Mannix, R. C. (2017). Burden of USA hospital charges for traumatic brain injury. *Brain Injury*, 31(1), 24–31. <https://doi.org/10.1080/02699052.2016.1217351>
105. Marmarou, A., Signoretti, S., Aygok, G., Fatouros, P., & Portella, G. (2006). Traumatic brain edema in diffuse and focal injury: Cellular or vasogenic? *Acta Neurochirurgica*, 96, 24–29. <https://doi.org/10.1016/j.pcad.2015.11.006>
106. Marshall, L. F., Camp, P. E., & Bowers, S. (1984). Dimethyl Sulfoxide for the Treatment of Intracranial Hypertension: A Preliminary Trial. *Neurosurgery*, 14(6), 659–663.

107. Maxeiner, S., Glassmann, A., Kao, H. T., & Schilling, K. (2014). The molecular basis of the specificity and cross-reactivity of the NeuN epitope of the neuron-specific splicing regulator, Rbfox3. *Histochemistry and Cell Biology*, 141(1), 43–55. <https://doi.org/10.1007/s00418-013-1159-9>
108. Mbye, L. H., Keles, E., Tao, L., Zhang, J., Chung, J., Larvie, M., Koppula, R., Lo, E. H., & Whalen, M. J. (2012). Kollidon VA64, a membrane-resealing agent, reduces histopathology and improves functional outcome after controlled cortical impact in mice. *Journal of Cerebral Blood Flow and Metabolism : Official Journal of the International Society of Cerebral Blood Flow and Metabolism*, 32(3), 515–524. <https://doi.org/10.1038/jcbfm.2011.158>
109. McLean, A., Dikmen, S., Temkin, N., Wyler, A. R., & Gale, J. L. (1984). Psychosocial functioning at 1 month after head injury. *Neurosurgery*, 14(4), 393–399. <https://doi.org/10.1227/00006123-198404000-00001>
110. McMahon, P., Hricik, A., Yue, J. K., Puccio, A. M., Inoue, T., Lingsma, H. F., Beers, S. R., Gordon, W. A., Valadka, A. B., Manley, G. T., Okonkwo, D. O., Casey, S. S., Cooper, S. R., Dams-O'Connor, K., Menon, D. K., Sorani, M. D., Yuh, E. L., Mukherjee, P., Schnyer, D. M., & Vassar, M. J. (2014). Symptomatology and functional outcome in mild traumatic brain injury: Results from the prospective TRACK-TBI study. *Journal of Neurotrauma*, 31(1), 26–33. <https://doi.org/10.1089/neu.2013.2984>
111. McNeil, P. L., & Steinhardt, R. A. (2003). Plasma Membrane Disruption: Repair, Prevention, Adaptation. *Annual Review of Cell and Developmental Biology*, 19(1), 697–731. <https://doi.org/10.1146/annurev.cellbio.19.111301.140101>
112. McPhail, L. T., McBride, C. B., McGraw, J., Steeves, J. D., & Tetzlaff, W. (2004). Axotomy abolishes NeuN expression in facial but not rubrospinal neurons. *Experimental Neurology*, 185(1), 182–190. <https://doi.org/10.1016/j.expneurol.2003.10.001>
113. Ménorval, M.-A. de, Mir, L. M., Fernández, M. L., & Reigada, R. (2012). Effects of Dimethyl Sulfoxide in Cholesterol-Containing Lipid Membranes: A Comparative Study of Experiments In Silico and with Cells. *PLOS ONE*, 7(7), e41733. <https://doi.org/10.1371/journal.pone.0041733>
114. Meyer, N., Henkel, L., Linder, B., Zielke, S., Tascher, G., Trautmann, S., Geisslinger, G., Münch, C., Fulda, S., Tegeder, I., & Kögel, D. (2021). Autophagy activation, lipotoxicity and lysosomal membrane permeabilization synergize to promote pimozone- and loperamide-induced glioma cell death. *Autophagy*, 17(11), 3424–3443. <https://doi.org/10.1080/15548627.2021.1874208>

115. Miller, J. D., Becker, D. P., Ward, J. D., Sullivan, H. G., Adams, W. E., & Rosner, M. J. (1977). Significance of intracranial hypertension in severe head injury. *Journal of Neurosurgery*, 47(4), 503–516. <https://doi.org/10.3171/jns.1977.47.4.0503>
116. Miyake, K., & McNeil, P. L. (2003). Mechanical injury and repair of cells. *Critical Care Medicine*, 31(Supplement), S496–S501. <https://doi.org/10.1097/01.ccm.0000081432.72812.16>
117. Miyake, K., McNeil, P. L., Suzuki, K., Tsunoda, R., & Sugai, N. (2001). An actin barrier to resealing. *Journal of Cell Science*, 114(Pt 19), 3487–3494.
118. Mizunoe, Y., Kobayashi, M., Hoshino, S., Tagawa, R., Itagawa, R., Hoshino, A., Okita, N., Sudo, Y., Nakagawa, Y., Shimano, H., & Higami, Y. (2020). Cathepsin B overexpression induces degradation of perilipin 1 to cause lipid metabolism dysfunction in adipocytes. *Scientific Reports*, 10(1). <https://doi.org/10.1038/s41598-020-57428-6>
119. Moles, A., Tarrats, N., Fernández-Checa, J. C., & Marí, M. (2012). Cathepsin B overexpression due to acid sphingomyelinase ablation promotes liver fibrosis in Niemann-Pick disease. *Journal of Biological Chemistry*, 287(2), 1178–1188. <https://doi.org/10.1074/jbc.M111.272393>
120. Mollan, S. P., Ali, F., Hassan-Smith, G., Botfield, H., Friedman, D. I., & Sinclair, A. J. (2016). Evolving evidence in adult idiopathic intracranial hypertension: Pathophysiology and management. *Journal of Neurology, Neurosurgery and Psychiatry*, 87(9), 982–992. <https://doi.org/10.1136/jnnp-2015-311302>
121. Morin, L. P., Hefton, S., & Studholme, K. M. (2011). Neurons identified by NeuN/Fox-3 immunoreactivity have a novel distribution in the hamster and mouse suprachiasmatic nucleus. *Brain Research*, 1421, 44–51. <https://doi.org/10.1016/j.brainres.2011.09.015>
122. Mort, J. S., & Buttle, D. J. (1997). MOLECULES IN FOCUS Cathepsin B. In *International Journal of Biochemistry and Cell Biology* (Vol. 29, Issue 29, pp. 715–720).
123. Mullen, R. J., Buck, C. R., & Smith, A. M. (1992a). NeuN, a neuronal specific nuclear protein in vertebrates. *Development (Cambridge, England)*, 116(1), 201–211. <https://doi.org/VL - 116>
124. Nagakannan, P., Islam, I., Conrad, M., Eftekharpour, E., Islam, M. I., Conrad, M., & Eftekharpour, E. (2021). Cathepsin B is an executioner of ferroptosis. *BBA - Molecular Cell Research*, 1868(3), 118928. <https://doi.org/10.1016/j.bbamcr.2020.118928>

125. Ngler, D. K., Storer, A. C., Portaro, F. C. V., Carmona, E., Juliano, L., & Mnard, R. (1997). Major increase in endopeptidase activity of human cathepsin B upon removal of occluding loop contacts. *Biochemistry*, 36(41), 12608–12615. <https://doi.org/10.1021/bi971264+>
126. Notman, R., Noro, M., O'Malley, B., & Anwar, J. (2006). Molecular Basis for Dimethylsulfoxide (DMSO) Action on Lipid Membranes. *Journal of the American Chemical Society*, 128(43), 13982–13983. <https://doi.org/10.1021/ja063363t>
127. Oberle, C., Huai, J., Reinheckel, T., Tacke, M., Rassner, M., Ekert, P. G., Buellbach, J., & Borner, C. (2010). Lysosomal membrane permeabilization and cathepsin release is a Bax/Bak-dependent, amplifying event of apoptosis in fibroblasts and monocytes. *Cell Death and Differentiation*, 17(7), 1167–1178. <https://doi.org/10.1038/cdd.2009.214>
128. Pettus, E. H., Christman, C. W., Giebel, M. L., & Povlishock, J. T. (1994a). Traumatically Induced Altered Membrane Permeability: Its Relationship to Traumatically Induced Reactive Axonal Change. *Journal of Neurotrauma*, 11(5), 507–522. <https://doi.org/10.1089/neu.1994.11.507>
129. Poreba, M., Groborz, K., Vizovisek, M., Maruggi, M., Turk, D., Turk, B., Powis, G., Drag, M., & S. Salvesen, G. (2019). Fluorescent probes towards selective cathepsin B detection and visualization in cancer cells and patient samples. *Chemical Science*, 10(36), 8461–8477. <https://doi.org/10.1039/C9SC00997C>
130. Prado, G. R., & LaPlaca, M. C. (2020). Neuronal Plasma Membrane Integrity is Transiently Disturbed by Traumatic Loading. *Neuroscience Insights*, 15, 263310552094609. <https://doi.org/10.1177/2633105520946090>
131. Pratt, M. R., Sekedat, M. D., Chiang, K. P., & Muir, T. W. (2009). Direct Measurement of Cathepsin B Activity in the Cytosol of Apoptotic Cells by an Activity-Based Probe. *Chemistry & Biology*, 16(9), 1001–1012. <https://doi.org/10.1016/j.chembiol.2009.07.011>
132. Raucher, D., Stauffer, T., Chen, W., Shen, K., Guo, S., York, J. D., Sheetz, M. P., & Meyer, T. (2000). Phosphatidylinositol 4,5-bisphosphate functions as a second messenger that regulates cytoskeleton-plasma membrane adhesion. *Cell*, 100(2), 221–228. [https://doi.org/10.1016/S0092-8674\(00\)81560-3](https://doi.org/10.1016/S0092-8674(00)81560-3)
133. Reddy, A., Caler, E. V., & Andrews, N. W. (2001). Plasma membrane repair is mediated by Ca²⁺-regulated exocytosis of lysosomes. *Cell*, 106(2), 157–169. [https://doi.org/10.1016/S0092-8674\(01\)00421-4](https://doi.org/10.1016/S0092-8674(01)00421-4)

134. Rodríguez-Muela, N., Hernández-Pinto, A. M., Serrano-Puebla, A., García-Ledo, L., Latorre, S. H., De La Rosa, E. J., & Boya, P. (2015). Lysosomal membrane permeabilization and autophagy blockade contribute to photoreceptor cell death in a mouse model of retinitis pigmentosa. *Cell Death and Differentiation*, 22(3), 476–487. <https://doi.org/10.1038/cdd.2014.203>
135. Ruzza, P., Quintieri, L., Osler, A., Calderan, A., Biondi, B., Floreani, M., Guiotto, A., & Borin, G. (2006). Fluorescent, internally quenched, peptides for exploring the pH-dependent substrate specificity of cathepsin B. *Journal of Peptide Science*, 12(7), 455–461. <https://doi.org/10.1002/psc.748>
136. Ryu, J., Jeizan, P., Ahmed, S., Ehsan, S., Jose, J., Regan, S., Gorse, K., Kelliher, C., & Lafrenaye, A. (2022). Post-Injury Buprenorphine Administration Is Associated with Long-Term Region-Specific Glial Alterations in Rats. *Pharmaceutics*, 14(10), 2068. <https://doi.org/10.3390/pharmaceutics14102068>
137. Ryu, J., Stone, P., Lee, S., Payne, B., Gorse, K., & Lafrenaye, A. (2021a). Buprenorphine alters microglia and astrocytes acutely following diffuse traumatic brain injury. *Scientific Reports*, 11, 8620. <https://doi.org/10.1038/s41598-021-88030-z>
138. Sarkar, C., Jones, J. W., Hegdekar, N., Thayer, J. A., Kumar, A., Faden, A. I., Kane, M. A., & Lipinski, M. M. (2020). PLA2G4A/cPLA2-mediated lysosomal membrane damage leads to inhibition of autophagy and neurodegeneration after brain trauma. *Autophagy*, 16(3), 466–485. <https://doi.org/10.1080/15548627.2019.1628538>
139. Sedmak, G., & Judaš, M. (2019). The total number of white matter interstitial neurons in the human brain. *Journal of Anatomy*. <https://doi.org/10.1111/joa.13018>
140. Shandra, O., Winemiller, A. R., Heithoff, B. P., Munoz-Ballester, C., George, K. K., Benko, M. J., Zuidhoek, I. A., Besser, M. N., Curley, D. E., Edwards, G. F., Mey, A., Harrington, A. N., Kitchen, J. P., & Robel, S. (2019). Repetitive Diffuse Mild Traumatic Brain Injury Causes an Atypical Astrocyte Response and Spontaneous Recurrent Seizures. *The Journal of Neuroscience*, 39(10), 1944–1963. <https://doi.org/10.1523/JNEUROSCI.1067-18.2018>
141. Shi, R., Qiao, X., Emerson, N., & Malcom, A. (2001). Dimethylsulfoxide Enhances CNS Neuronal plasma membrane resealing after injury in low temperature or low calcium. *Journal of Neurocytology*, 30, 829–839. <https://doi.org/10.1023/a:1019645505848>
142. Shim, Y., Kim, J., Kim, H. S., Oh, J., Lee, S., & Ha, E. J. (2023). Intracranial Pressure Monitoring for Acute Brain Injured Patients: When, How, What Should We Monitor. *Korean Journal of Neurotrauma*, 19(2), 149–161. <https://doi.org/10.13004/kjnt.2023.19.e32>

143. Singleton, R. H., & Povlishock, J. T. (2004a). Identification and Characterization of Heterogeneous Neuronal Injury and Death in Regions of Diffuse Brain Injury: Evidence for Multiple Independent Injury Phenotypes. *Journal of Neuroscience*, 24(14), 3543–3553. <https://doi.org/10.1523/JNEUROSCI.5048-03.2004>
144. Singleton, R. H., Zhu, J., Stone, J. R., & Povlishock, J. T. (2002). Traumatically Induced Axotomy Adjacent to the Soma Does Not Result in Acute Neuronal Death. *The Journal of Neuroscience*, 22(3), 791 LP – 802. <https://doi.org/10.1523/JNEUROSCI.22-03-00791.2002>
145. Steinhardt, R. A., Bi, G., & Alderton, J. M. (1994). Cell Membrane Resealing by a Vesicular Mechanism Similar to Neurotransmitter Release. *Science*, 263(5145), 390–393.
146. Stocchetti, N., & Maas, A. I. R. (2014). Traumatic Intracranial Hypertension. *New England Journal of Medicine*, 370(22), 2121–2130. <https://doi.org/10.1056/nejmra1208708>
147. Stocchetti, N., Zoerle, T., & Carbonara, M. (2017). Intracranial pressure management in patients with traumatic brain injury: An update. *Current Opinion in Critical Care*, 23(2), 110–114. <https://doi.org/10.1097/MCC.0000000000000393>
148. Sugawara, T., Leśn, A., Noshita, N., Gasche, Y., & Chan, P. H. (2002). Effects of global ischemia duration on neuronal, astroglial, oligodendroglial, and microglial reactions in the vulnerable hippocampal CA1 subregion in rats. *Journal of Neurotrauma*, 19(1), 85–98. <https://doi.org/10.1089/089771502753460268>
149. Sullivan, H. G., Martinez, J., Becker, D. P., Miller, J. D., Griffith, R., & Wist, A. O. (1976). Fluid-percussion model of mechanical brain injury in the cat. *Journal of Neurosurgery*, 45(5), 521–534.
150. Taylor, C. A., Bell, J. M., Breiding, M. J., & Xu, L. (2017a). Traumatic Brain Injury–Related Emergency Department Visits, Hospitalizations, and Deaths—United States, 2007 and 2013. *MMWR. Surveillance Summaries*, 66(9), 1–16. <https://doi.org/10.15585/mmwr.ss6609a1>
151. Teasdale, G., & Jennett, B. (1974). ASSESSMENT OF COMA AND IMPAIRED CONSCIOUSNESS: A Practical Scale. *The Lancet*, 304(7872), 81–84. [https://doi.org/10.1016/S0140-6736\(74\)91639-0](https://doi.org/10.1016/S0140-6736(74)91639-0)
152. Thomas, T. C., Ogle, S. B., Rumney, B. M., May, H. G., Adelson, P. D., & Lifshitz, J. (2018). Does time heal all wounds? Experimental diffuse traumatic brain injury results in persisting histopathology in the thalamus. *Behavioural Brain Research*, 340, 137–146. <https://doi.org/10.1016/j.bbr.2016.12.038>

153. Togo, T. (2006). Disruption of the plasma membrane stimulates rearrangement of microtubules and lipid traffic toward the wound site. *Journal of Cell Science*. <https://doi.org/10.1242/jcs.03006>
154. Togo, T., Alderton, J. M., Bi, G. Q., & Steinhardt, R. A. (1999). The mechanism of facilitated cell membrane resealing. *Journal of Cell Science*.
155. Tung, H., James, H. E., Laurin, R., & Marshall, L. F. (1983). Modification of the effect of dimethyl sulfoxide on intracranial pressure, brain water, and electrolyte content by indomethacin. *Acta Neurochirurgica*, 68(1–2), 101–110. <https://doi.org/10.1007/BF01406206>
156. Ünal-Çevik, I. I., Kiliç, M., Gürsoy-Özdemir, Y., Gurer, G., Dalkara, T., Kiliç, M., Gürsoy-Özdemir, Y., Gurer, G., Dalkara, T., Kiliç, M., Gürsoy-Özdemir, Y., Gurer, G., & Dalkara, T. (2004). Loss of NeuN immunoreactivity after cerebral ischemia does not indicate neuronal cell loss: A cautionary note. *Brain Research*, 1015(1–2), 169–174. <https://doi.org/10.1016/j.brainres.2004.04.032>
157. Vaughan, E. M., You, J.-S., Elsie Yu, H.-Y., Lasek, A., Vitale, N., Hornberger, T. A., & Bement, W. M. (2014). Lipid domain-dependent regulation of single-cell wound repair. *Molecular Biology of the Cell*, 25(12), 1867–1876. <https://doi.org/10.1091/mbc.e14-03-0839>
158. Verwer, R. W. H., Sluiter, A. A., Balesar, R. A., Baayen, J. C., Noske, D. P., Dirven, C. M. F., Wouda, J., van Dam, A. M., Lucassen, P. J., & Swaab, D. F. (2007). Mature astrocytes in the adult human neocortex express the early neuronal marker doublecortin. *Brain*, 130(12), 3321–3335. <https://doi.org/10.1093/brain/awm264>
159. Waller, F. T., Tanabe, C. T., & Paxton, H. D. (1983). Treatment of Elevated Intracranial Pressure with Dimethyl Sulfoxide. *Annals of the New York Academy of Sciences*, 411(1), 286–292. <https://doi.org/10.1111/j.1749-6632.1983.tb47310.x>
160. Wang, J., Wang, L., Zhang, X., Xu, Y., Chen, L., Zhang, W., Liu, E., Xiao, C., & Kou, Q. (2021). Cathepsin B aggravates acute pancreatitis by activating the NLRP3 inflammasome and promoting the caspase-1-induced pyroptosis. *International Immunopharmacology*, 94, 107496. <https://doi.org/10.1016/j.intimp.2021.107496>
161. Wen, Y. D., Sheng, R., Zhang, L. S., Han, R., Zhang, X., Zhang, X. D., Han, F., Fukunaga, K., & Qin, Z. H. (2008). Neuronal injury in rat model of permanent focal cerebral ischemia is associated with activation of autophagic and lysosomal pathways. *Autophagy*, 4(6), 762–769. <https://doi.org/10.4161/auto.6412>

162. Werner, C., & Engelhard, K. (2007). Pathophysiology of Traumatic Brain Injury. *British Journal of Anesthesia*, 99(1), 4–9. <https://doi.org/10.1093/bja/aem131>
163. Weyer, A., & Schilling, K. (2003). Developmental and cell type-specific expression of the neuronal marker NeuN in the murine cerebellum. *Journal of Neuroscience Research*, 73(3), 400–409. <https://doi.org/10.1002/jnr.10655>
164. Whalen, M. J., Dalkara, T., You, Z., Qiu, J., Bermpohl, D., Mehta, N., Suter, B., Bhide, P. G., Lo, E. H., Ericsson, M., & Moskowitz, M. A. (2008a). Acute Plasmalemma Permeability and Protracted Clearance of Injured Cells after Controlled Cortical Impact in Mice. *Journal of Cerebral Blood Flow & Metabolism*, 28(3), 490–505. <https://doi.org/10.1038/sj.jcbfm.9600544>
165. Williams, J. M., Gomes, F., Drudge, O. W., & Kessler, M. (1984). Predicting outcome from closed head injury by early assessment of trauma severity. *Journal of Neurosurgery*, 61(3), 581–585. <https://doi.org/10.3171/jns.1984.61.3.0581>
166. Wilson, L., Stewart, W., Dams-O'Connor, K., Diaz-Arrastia, R., Horton, L., Menon, D. K., & Polinder, S. (2017). The chronic and evolving neurological consequences of traumatic brain injury. In *The Lancet Neurology* (Vol. 16, Issue 10, pp. 813–825). [https://doi.org/10.1016/S1474-4422\(17\)30279-X](https://doi.org/10.1016/S1474-4422(17)30279-X)
167. Windelborn, J. A., & Lipton, P. (2008). Lysosomal release of cathepsins causes ischemic damage in the rat hippocampal slice and depends on NMDA-mediated calcium influx, arachidonic acid metabolism, and free radical production. *Journal of Neurochemistry*, 106(1), 56–69.
168. Witcher, K. G., Bray, C. E., Dziabis, J. E., McKim, D. B., Benner, B. N., Rowe, R. K., Kokiko-Cochran, O. N., Popovich, P. G., Lifshitz, J., Eiferman, D. S., & Godbout, J. P. (2018). Traumatic brain injury-induced neuronal damage in the somatosensory cortex causes formation of rod-shaped microglia that promote astrogliosis and persistent neuroinflammation. *Glia*, 66(12), 2719–2736. <https://doi.org/10.1002/glia.23523>
169. Wofford, K. L., Harris, J. P., Browne, K. D., Brown, D. P., Grovola, M. R., Mietus, C. J., Wolf, J. A., Duda, J. E., Putt, M. E., Spiller, K. L., & Cullen, D. K. (2017). Rapid neuroinflammatory response localized to injured neurons after diffuse traumatic brain injury in swine. *Experimental Neurology*, 290, 85–94. <https://doi.org/10.1016/j.expneurol.2017.01.004>
170. Wolf, H. K., Buslei, R., Schmidt-Kastner, R., Schmidt-Kastner, P. K., Pietsch, T., Wiestler, O. D., & Blümcke, I. (1996). NeuN: A useful neuronal marker for diagnostic histopathology. *Journal of Histochemistry and Cytochemistry*, 44(10), 1167–1171. <https://doi.org/10.1177/44.10.8813082>

171. Wolf, P., & Simon, M. (1983). Dimethyl sulfoxide (DMSO) induced serum hyperosmolality. *Clinical Biochemistry*, 16(4), 261–262. [https://doi.org/10.1016/S0009-9120\(83\)90168-6](https://doi.org/10.1016/S0009-9120(83)90168-6)
172. Wollert, T., Wunder, C., Lippincott-Schwartz, J., & Hurley, J. H. (2009). Membrane scission by the ESCRT-III complex. *Nature*, 458(7235), 172–177. <https://doi.org/10.1038/nature07836>
173. Won, M., Lee, S., Choi, S., Ro, H., Kim, K.-J., Kim, J.-H., Kim, K. E., & Kim, K. K. (2016). Identification and characterization of the RNA-binding protein Rbfox3 in zebrafish embryo. *Biochemical and Biophysical Research Communications*, 472(2), 373–378. <https://doi.org/10.1016/j.bbrc.2016.03.005>
174. Wu, Q.-Q., Xu, M., Yuan, Y., Li, F.-F., Yang, Z., Liu, Y., Zhou, M.-Q., Bian, Z.-Y., Deng, W., Gao, L., Li, H., & Tang, Q.-Z. (2015). Cathepsin B deficiency attenuates cardiac remodeling in response to pressure overload via TNF- α /ASK1/JNK pathway. *American Journal of Physiology-Heart and Circulatory Physiology*, 308(9), H1143–H1154. <https://doi.org/10.1152/ajpheart.00601.2014>
175. Yoo, S., Nguyen, M. P., Fukuda, M., Bittner, G. D., & Fishman, H. M. (2003). Plasmalemmal Sealing of Transected Mammalian Neurites Is a Gradual Process Mediated by Ca²⁺-Regulated Proteins. *Journal of Neuroscience Research*, 74(4), 541–551. <https://doi.org/10.1002/jnr.10771>
176. Yoon, M. C., Christy, M. P., Phan, V. V., Gerwick, W. H., Hook, G., O'Donoghue, A. J., & Hook, V. (2022). Molecular Features of CA-074 pH-Dependent Inhibition of Cathepsin B. *Biochemistry*, 61(4), 228–238. <https://doi.org/10.1021/acs.biochem.1c00684>
177. Yoon, M. C., Phan, V., Podvin, S., Mosier, C., O'Donoghue, A. J., & Hook, V. (2023). Distinct Cleavage Properties of Cathepsin B Compared to Cysteine Cathepsins Enable the Design and Validation of a Specific Substrate for Cathepsin B over a Broad pH Range. *Biochemistry*. <https://doi.org/10.1021/acs.biochem.3c00139>
178. Yoon, M. C., Solania, A., Jiang, Z., Christy, M. P., Podvin, S., Mosier, C., Lietz, C. B., Ito, G., Gerwick, W. H., Wolan, D. W., Hook, G., O'Donoghue, A. J., & Hook, V. (2021). Selective Neutral pH Inhibitor of Cathepsin B Designed Based on Cleavage Preferences at Cytosolic and Lysosomal pH Conditions. *ACS Chemical Biology*, 16(9), 1628–1643. <https://doi.org/10.1021/acscchembio.1c00138>

179. Yuan, C., Gao, J., Guo, J., Bai, L., Marshall, C., Cai, Z., Wang, L., & Xiao, M. (2014). Dimethyl Sulfoxide Damages Mitochondrial Integrity and Membrane Potential in Cultured Astrocytes. *PLOS ONE*, 9(9), e107447. <https://doi.org/10.1371/journal.pone.0107447>
180. Yuste, V. J., Moubarak, R. S., Delettre, C., Bras, M., Sancho, P., Robert, N., d'Alayer, J., & Susin, S. A. (2005). Cysteine protease inhibition prevents mitochondrial apoptosis-inducing factor (AIF) release. *Cell Death & Differentiation*, 12(11), Article 11. <https://doi.org/10.1038/sj.cdd.4401687>
181. Zhu, X., Tao, L., Tejima-Mandeville, E., Qiu, J., Park, J., Garber, K., Ericsson, M., Lo, E. H., & Whalen, M. J. (2012). Plasmalemma permeability and necrotic cell death phenotypes after intracerebral hemorrhage in mice. *Stroke; a Journal of Cerebral Circulation*, 43(2), 524–531. <https://doi.org/10.1161/STROKEAHA.111.635672>
182. Zimatkin, S. M., & Karnyushko, O. A. (2017). Expression of Doublecortin and NeuN in Developing Neurons in the Rat Cerebellum. *Neuroscience and Behavioral Physiology*, 47(2), 122–126. <https://doi.org/10.1007/s11055-016-0374-y>

VITA

Martina Laura Hernandez (she/they) was born August 29, 1996, in Halifax County, Virginia, to Diana L. Tripodi and Carlos H. Hernandez. They moved to Suffolk County, New York in 1998 and resided there until 2008, moving back to Halifax County. She graduated from Halifax County High School in 2014, simultaneously with an Associate of Arts and Science from Southside Virginia Community College. She continued her higher education at Virginia Commonwealth University, Richmond, Virginia where she completed a Bachelor of Science in Chemistry; concentration in Biochemistry in 2017.